การแปรผันของโอโซนในบรรยากาศชั้นโทรโพสเฟียร์ตามฤดูกาลระหว่างปี พ.ศ. 2550 – 2552 ณ สถานีวิจัยในชั้นบรรยากาศ อำเภอพิมาย จังหวัดนครราชสีมา

นายสุภัทรชัย ศักดิ์สกุลไกร

วิทยานิพนธ์นี้เป็นส่วนหนึ่งของการศึกษาตามหลักสูตรปริญญาวิทยาศาสตรมหาบัณฑิต
สาขาวิชาโลกศาสตร์ ภาควิชาธรณีวิทยา
คณะวิทยาศาสตร์ จุฬาลงกรณ์มหาวิทยาลัย
ปีการศึกษา 2556

SEASONAL VARIATION OF TROPOSPHERIC OZONE DURING 2007 – 2009 AT "THE OBSERVATORY FOR ATMOSPHERIC RESEARCH AT PHIMAI", CHANGWAT NAKHONRATCHASIMA

Mr. Supattarachai Saksakulkrai

A Thesis Submitted in Partial Fulfillment of the Requirements
for the Degree of Master of Science Program in Earth Sciences
Department of Geology
Faculty of Science
Chulalongkorn University
Academic Year 2013

Thesis Title	SEASONAL VARIATION OF TROPOSPHERIC OZONE DURING 2007 – 2009 AT "THE OBSERVATORY FOR ATMOSPHERIC RESEARCH AT PHIMAI", CHANGWAT NAKHONRATCHASIMA
By	Mr. Supattarachai Saksakulkrai
Field of Study	Earth Sciences
Thesis Advisor	Sathon Vijarnwannaluk, Ph.D.

Accepted by the Faculty of Science, Chulalongkorn University in Partial Fulfillment of the Requirements for the Master's Degree

.....Dean of the Faculty of Science

(Professor Supot Hannongbua, Dr.rer.nat.)

THESIS COMMITTEE

.....Chairman

(Assistant Professor Sombat Yumuang, Ph.D.)

.....Thesis Advisor

(Sathon Vijarnwannaluk, Ph.D.)

.....Examiner

(Assistant Professor Srilert Chotpantarat, Ph.D.)

.....External Examiner

(Assistant Professor Pakpong Pochanart, Ph.D.)

สุภัทรชัย ศักดิ์สกุลไกร : การแปรผันของโอโซนในบรรยากาศชั้นโทรโพสเฟียร์ตามฤดูกาลระหว่างปี พ.ศ. 2550 – 2552 ณ สถานีวิจัยในชั้นบรรยากาศ อำเภอพิมาย จังหวัดนครราชสีมา. (SEASONAL VARIATION OF TROPOSPHERIC OZONE DURING 2007 – 2009 AT "THE OBSERVATORY FOR ATMOSPHERIC RESEARCH AT PHIMAI", CHANGWAT NAKHONRATCHASIMA) อ.ที่ปรึกษาวิทยานิพนธ์หลัก: ดร. สธน วิจารณ์วรรณลักษณ์, ๑๒๐ หน้า.

โอโซนในชั้นบรรยากาศโทรโพสเฟียร์ (O_3) ถูกตรวจวัดด้วยเครื่องมือ UV-photometric continuous ozone monitor ณ สถานีวิจัยในชั้นบรรยากาศ อำเภอพิมาย ระหว่างกันยายน 2550 – สิงหาคม 2552 เพื่อศึกษาและอธิบายการเปลี่ยนแปลงตามฤดูกาลและปัจจัยที่ส่งผล ได้แก่ ก๊าซคาร์บอนมอนออกไซด์ (CO) ความชื้นสัมพัทธ์ (RH) และ รังสีตรง การแปรผันของโอโซนตามฤดูกาลพบว่ามีค่าสูงสุดในช่วงฤดูร้อน (มีนาคม ถึง เมษายน) และมีค่าต่ำสุดในช่วงฤดูฝน (มิถุนายน ถึง ตุลาคม) ความเข้มข้นของโอโซนเฉลี่ยรายวันสุดสูงและต่ำสุด คือ 63.77 และ 9.00 ppb ในวันที่ 5 มีนาคม 2551 และ 19 มิถุนายน 2552 ตามลำดับ ค่าเฉลี่ยรายเดือนสูงสุดและต่ำสุด คือ 45.7 และ 15.8 ppb ในเดือนมกราคม 2552 และ กรกฎาคม 2552 ตามลำดับ การแปรผันของโอโซนในหนึ่งวันมีการเพิ่มขึ้นในช่วงกลางวันและลดลงในช่วงกลางคืน ในฤดูแล้งพบว่ามีการแปรผันในหนึ่งวันของโอโซนสูงกว่าฤดูฝน การวิเคราะห์ทิศทางละอองลอยแบบย้อนกลับ (backward trajectory analysis) ด้วยโปรแกรม HYSPLT เพื่อวิเคราะห์ผลจากการเคลื่อนที่ในระยะไกลของมวลอากาศ โดยมวลอากาศถูกจำแนกออกเป็น Northeast Continental (NE-C) Northeast/East Continental and Marine (NEE-CM) Northeast/East/South Marine (NEES-M) และ Southwest Marine (SW-M) ความเข้มข้นของโอโซนสูงสุด 39.3 ppb ถูกพบในมวลอากาศชนิด NE-C ระหว่างฤดูหนาว (พฤศจิกายน ถึง กุมภาพันธ์) อันเนื่องมาจากการเคลื่อนที่ในระยะไกลของก๊าซก่อโอโซนจากบริเวณตอนเหนือของเอเชีย ส่วนมวลอากาศชนิด NEE-CM เกิดในช่วงเวลาเดียวกับ NE-C แต่พบความเข้มข้นของโอโซนต่ำกว่าเพราะได้รับอิทธิพลจากอากาศบริสุทธิ์จากมหาสมุทรแปซิฟิก ส่วนมวลอากาศที่มีต้นกำเนิดจากมหาสมุทรแปซิฟิก คือ NEES-M มักเกิดในช่วงฤดูร้อน (มีนาคม ถึง เมษายน) และพบความเข้มข้นของโอโซนต่ำกว่าในมวลอากาศที่กำเนิดจากพื้นทวีป (NE-C และ NEE-CM) แต่พบปฏิกิริยาเคมีแสงในการสร้างโอโซนสูงอันเนื่องมาจากการเผาไหม้ชีวมวลที่มีมากในช่วงดังกล่าวทั่วพื้นทวีปเอเชียตะวันออกเฉียงใต้ ค่าเฉลี่ยโอโซนต่ำสุด (22.1 ppb) พบในมวลอากาศ SW-M โดยอิทธิพลการเคลื่อนที่ในระยะไกลของมวลอากาศบริสุทธิ์จากมหาสมุทรอินเดีย สัมประสิทธิ์สหสัมพันธ์ระหว่าง O_3 และ CO มีค่าสูงสุดทางบวกในมวลอากาศ NEES-M และต่ำสุดใน SW-M สัมประสิทธิ์สหสัมพันธ์ระหว่าง O_3 และ RH มีค่าสูงสุดทางลบในมวลอากาศ SW-M ส่วน O_3 และรังสีตรง พบความสัมพันธ์ในระดับต่ำ หรือไม่มีความสัมพันธ์อย่างมีนัยสำคัญ

ภาควิชา ธรณีวิทยา ลายมือชื่อนิสิต .....

สาขาวิชา โลกศาสตร์ ลายมือชื่อ อ.ที่ปรึกษาวิทยานิพนธ์หลัก .....

ปีการศึกษา 2556

5372367923 : MAJOR EARTH SCIENCES
KEYWORDS: TROPOSPHERIC OZONE / BACKWARD TRAJECTORY ANALYSIS / BIOMASS BURNING

SUPATTARACHAI SAKSAKULKRAI: SEASONAL VARIATION OF TROPOSPHERIC OZONE DURING 2007 – 2009 AT "THE OBSERVATORY FOR ATMOSPHERIC RESEARCH AT PHIMAI", CHANGWAT NAKHONRATCHASIMA. ADVISOR: SATHON VIJARNWANNALUK, Ph.D., 120 pp.

Tropospheric ozone (O_3) has been measured at The Observatory for Atmospheric Research at Phimai by UV-photometric continuous ozone monitor during September 2007 – August 2009 in order to investigate the seasonal behaviors and relations between O_3 and factors comprising of carbon monoxide (CO), relative humidity (RH), and direct radiation. Seasonal variations of O_3 show dry season maximum in local summer (March to April) and wet season minimum (June to October). The highest and lowest daily O_3 concentrations were 63.77 and 9.00 ppb in 5 March 2008 and 19 June 2009, respectively. The maximum and minimum of O_3 monthly average were 45.7 ppb in January 2009 and 15.8 ppb in July 2009. O_3 diurnal variations increase during day time and decrease during nighttime. Higher diurnal cycles were found in dry season, while, lower diurnal cycles were found in wet season. In order to investigate the effect of long-range transport, air masses were categorized by the backward trajectory analysis on HYSPLT program into four types, Northeast Continental (NE-C), Northeast/East Continental and Marine (NEE-CM), Northeast/East/South Marine (NEES-M), and Southeast Marine (SW-M). Highest O_3 concentration at 39.3 ppb found in NE-C during local winter (November – February) due to long-range transport of O_3 precursors from North Asia. NEE-CM occurred in the same period as NE-C but with lower O_3 than NE-C by influence of cleaner air in Pacific. NEES-M prevailed during local summer (March – April), O_3 was found lower than continental originated air masses (NE-C and NEE-CM). However, the strong O_3 photochemical production was found in NEES-M due to heavy biomass burning in Southeast Asia continent. The lowest O_3 of 22.1 ppb was found with air mass originated in Indian Ocean, SW-M, due to long-range transport of clean marine air mass. Correlation coefficients (R^2) between O_3 and CO show highest positive relation in NEES-M and lowest in SW-M. R^2 between O_3 and RH show highest negative relation in marine originated, NEES-M and SW-M. R^2 between O_3 and direct radiation was found very low or no significant correlation.

Department: Geology Student's Signature .....

Field of Study: Earth Sciences Advisor's Signature .....

Academic Year: 2013

ACKNOWLEDGEMENTS

I sincerely thank my Advisor, Dr. Sathon Vijanwannaluk, Department of Physic, Faculty of Science, Chulalongkorn University for their supports, encouragements, critically advises and reviews of thesis.

I would like to thank Miss Boossarasiri Thana, Department of Geology, Faculty of Sciences, Chulalongkorn University for their valuable suggestion and support, opportunity for working at the observatory for atmospheric research at Phimai. Furthermore, I would like to thank Professor Kita Kazuyuki, Faculty of Science, Ibaraki University for establishing and maintaining the CO and ozone instruments at the study site, Assistant Professor Dr. Pakpong Pochanart, School of social and environmental development, National Institute of Development Administration (NIDA) for their suggestion and advising.

I thank to my entire friends in Earth science program for their support throughout my thesis with their valuable suggestions.

Finally, I would like to thank my parents for their support and encouragement throughout my study.

CONTENTS

Page

Page

Page

LIST OF TABLES

PAGE

LIST OF FIGURES

PAGE

CHAPTER I
INTRODUCTION

1.1 Overview

The climate change is the important problem for the earth's atmosphere. The earth's sphere not only consists of the atmosphere, but also consists of the hydrosphere, biosphere, and lithosphere. There are relations between each sphere. Therefore, the climate change on the atmosphere also impacts other sphere as well.

For a few decades, we realized that the climate change is the global problem and must to be resolved. There are many researches aimed to investigate these problems. The Intergovernmental Panel on Climate Change (IPCC) forth assessment report revealed that the global land-surface air temperature has risen since 1850 to 2005 (Fig 1.1). The major cause of climate change is Greenhouse gases (GHGs) from anthropogenic emission, e.g. biomass burning, farm waste burning, industrial emission. Anthropogenic emission causes the global GHGs over 20% e.g. Carbon monoxide (CO), Carbon dioxide (CO_2), Nonmethane hydrocarbons (NMHCs), Chloromethane (CH_3Cl), and Hydrogen (H_2) (Andreae et al., 1992).

GHGs affect the radiative forcing (RF) in the atmosphere. The sunlight energy reaches into the earth's surface as the shortwave radiation which is absorbed by the ground, then, the ground reradiates as longwave radiation. Some of longwave radiation is trapped on the top of troposphere by the existing GHGs and reradiatied as longwave radiation back to the earth's surface like that happen in a green house. Therefore, this process can retain the air temperature condition under the top of troposphere. However, the rising GHGs concentrations affect the shortwave/longwave radiation balance and trap more longwave radiation resulting in the raised air temperature (IPCC, 2007).

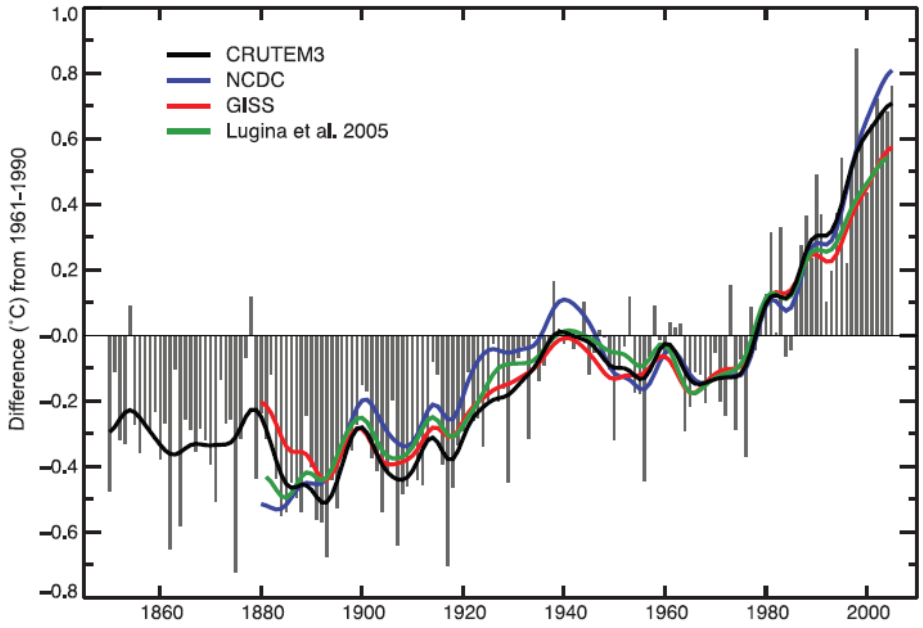

Figure 1.1 Annual anomalies of global land-surface air temperature (°C), 1850 to 2005 (IPCC, 2007).

Figure from the IPCC forth assessment report (IPCC, 2007) presenting below, show causes of the radiative forcing changes. The primary causes of positive RF change are long-lived GHGs including ozone (O_3).

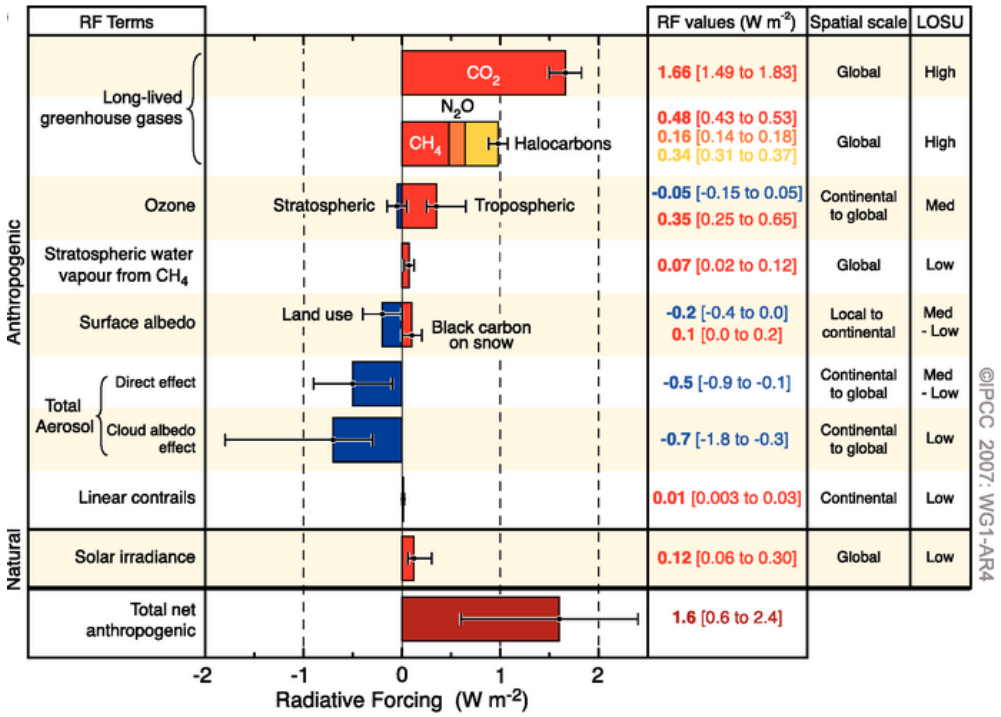

Figure 1.2 Radiative forcing (IPCC, 2007)

Why the tropospheric ozone so important?

There are two types of ozone; stratospheric ozone and tropospheric ozone. Most of global ozone content is stratospheric ozone existing in the stratosphere and absorbing the ultraviolet radiation, thus, some of radiation cannot penetrate this layer to the troposphere layer. This action leads to negative RF and decreases air temperature in the troposphere layer. Existing tropospheric ozone in the troposphere also absorbs the ultraviolet radiation as stratospheric ozone. The radiative adsorption by tropospheric ozone leads to the positive RF and increase of air temperature in the troposphere layer. Moreover, the high concentration of tropospheric ozone causes the photochemical smog in the urban or high polluted area. Ozone is an oxidant in photochemical smog exerting harmful effects on living organism especially respiratory system and plants.

Tropospheric ozone is a secondary air pollutant which is formed by primary air pollutants reaction in the atmosphere. There are many processes involving in reaction of primary air pollutants, one of these is the photolysis reaction which is the key of the tropospheric ozone production process. Therefore, the uncommonly high tropospheric ozone level implies the high primary air pollutants level in the troposphere. The substrates of tropospheric ozone called “ozone precursors” are Nitrogen oxide (NO_x), Carbon monoxide (CO), Volatile organic compounds (VOCs), and Methane (CH_4). Most of these ozone precursors are produced by human activities, especially vehicles and factory biomass burning.

The transportation of pollutant has been forced by the seasonal winds called monsoon. This carries pollutants from local to regional and global scale. Moreover, monsoon winds have the alternating directions in each season which has occurred annually. This phenomenon provides the different sources of pollutants including ozone precursors.

Thailand is in the center part of South-east Asia and has been affected by monsoon. This is interesting issue that how does the monsoon could affect the air pollution, especially tropospheric ozone and its precursors.

1.2 Study area

Figure 1.3 The observatory for atmospheric research at Phimai

This study has been undertaken at The Observatory for Atmospheric at Phimai, Changwat Nakhon Ratchasima (Fig. 1.3) and the regional representative which is located at 212 meters above mean sea level on sub rural/urban area at the center of Southeast Asia continent which surrounded by agricultural activities. Phimai site is under influence of two monsoon winds, northeast and southwest monsoons, which affect the pollutants from North Asia, Bangkok metropolis. More importantly, during dry season, Phimai is the center of agricultural biomass burning which creates tremendous amount of pollutants.

1.3 Statement of problem

Nowadays, the air pollution problem issue is rather ignored. The studies regarding to this issue in Thailand is very limited. Therefore, research study is an important reason in order to completely fulfill the missing piece of knowledge.

As mentioned above in section 1.1, tropospheric ozone is the main of this study. The monsoons and their trajectories are used to reveal how tropospheric ozone change as well as long-range transport of ozone and its precursors.

Thailand located in the areas affected by monsoon regularly. Therefore, the researching about relations between monsoon and pollutants are necessary. Moreover, the long-range transboundary air pollutions from social and industry developments in many countries become the international problem. The results of this study will reveal the pathway of pollutants and seasonal ozone variations. These would be informational base for the future research and for those who are interested. In addition, these could be a capable tool to relieve/prevent the current/future air pollution problem.

1.4 Objective

To study and understand the seasonal variation of tropospheric ozone and related factors at The Observatory for Atmospheric Research at Phimai, Nakhon Ratchasima province during September 2007 – August 2009.

1.5 Scope of investigation

The long-term automatic continuous measurement of tropospheric ozone and other parameters have been installed at The Observatory for Atmospheric Research at Phimai. Due to the most complete O_3 data is found during September 2007 to August 2009, therefore, data of tropospheric ozone (O_3), carbon monoxide (CO), direct radiation, and relative humidity (RH) in such period were used for analyses of the tropospheric ozone variations and relations between ozone and factors. These will be explained again in Chapter III.

In addition, the HYSPLIT 4 model was used in order to investigate the influence of long-range transport of air masses by backward trajectory analysis. More details are also illustrated in Chapter III.

1.6 Expected results

1. To reveal the seasonal variations of tropospheric ozone on the study area and explain the relations between tropospheric ozone and affective factors.

2. To understand the path way of pollutants affected the tropospheric ozone content.

3. To indicate the transboundary problem from other areas that affects pollutants at Phimai site.

CHAPTER II

THEORY AND LITERATURE REVIEWS

The pollutants have been emitted since the middle ages and became the important global problem since industrial revolution era for more than two centuries. Many researches have been done in several areas; these reveal the completely agreeable results that those pollutant emissions especially anthropogenic emissions led to destruction of the atmosphere.

In this study, we interested in the tropospheric ozone which is a secondary pollutant produced by a primary pollutant gases called the ozone precursors. In this chapter, theories of O_3, precursor or another implicated knowledge are explained. Besides, the previous research literatures are also reviewed.

2.1 Tropospheric ozone

Ozone was first discovered in 1839 by German scientist Christian Friedrich Schonbein. The name of ozone is derived from a Greek word meaning "to smell". When we talk about ozone, most well knowing is regarding stratospheric ozone which is a key factor of ozone's hole problem.

As shown in the Fig. 2.1 below, ozone exists at very high altitude over 20 to 60 km. from the ground in the stratosphere. Approximately 95% of the global ozone is located in the stratosphere at the concentration of 1.5×10^4 ppb. This is higher, by a factor of 100 than ozone concentrations at ground level, even in the most polluted regions. However, there is a few content of ozone in the lower atmosphere called either tropospheric ozone or ground level/surface ozone (hereafter called O_3). O_3 in the troposphere are at much lower concentration and decreasing from the top of the troposphere to ground level. Since the living things inhabit at the troposphere, the occasional high concentration of tropospheric O_3 can be harmful to plants and animals, and eventually ecosystem. (Chan et al., 1998; Finlayson-Pitts & Pitts, 1993; Fishman, 1991; Guicherit & Roemer, 2000; Jenkin & Clemitshaw, 2000; Lam et al., 2001; Sillman, 2003; Toh et al., 2013; West et al., 2007)

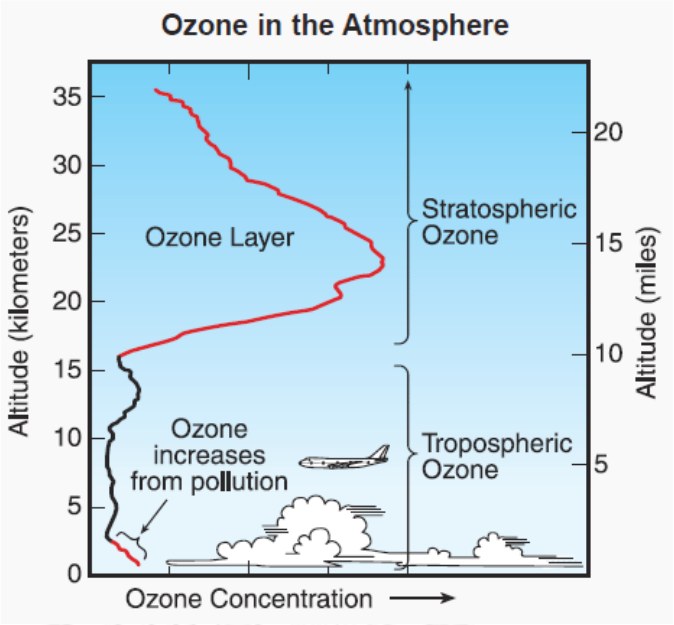

Figure 2.1 Ozone concentrations with height in mid latitude (Ajavon et al., 2007)

O_3 plays an important role in the troposphere, it controls the chemical composition. O_3 is the third most powerful greenhouse gas after carbon dioxide and methane (IPCC, 2007). Moreover, O_3 is a photochemical precursor of the hydroxyl radical which is related to oxidization and controls the tropospheric chemistry. Initiation of oxidation in the natural atmosphere depends on O_3, then, the tropospheric O_3 is important to the oxidizing capacity of the atmosphere. O_3 also plays a key role in biogeochemical cycles and global climate change. And O_3 in the stratospheric controls the temperature structure of stratosphere (Lam et al., 2001).

The increase of coal, fossil fuel and other biomass fuel consumption occurred in the Europe and the USA, led to directly pollutant emissions especially primary pollutants, including sulfur dioxide (SO_2), carbon monoxide (CO), and particulates. They were emitted during fall and winter when the sunlight is low. These events raised “smog” (smoke combines fog). In the 1950s, photochemical smog became an important problem. It consists of O_3 and related species of “secondary pollutants” which are formed by photochemical reaction of primary pollutants, a process is driven by presence of sunlight and warm temperature as a catalyst (Sillman, 2003).

The major sources of O_3 are intrusion from the stratosphere (stratosphere/troposphere exchange - STE) and in situ photochemical production in the troposphere (Tsutsumi & Matsueda, 2000). O_3 photochemical production occurs with presence of light and ozone precursors i.e. Volatile organic compounds (VOCs), Carbon monoxide (CO) and Nitrogen oxide species (NO_x). These gases emitted from fossil fuel combustion, biomass burning, industrial, agricultural waste burning, vegetation, microbial activities in soils. Among of these sources, the human activities, in particular fossil fuel combustion is a major source of ozone precursors (Lal et al., 2000; H. Liu et al., 2002; S. C. Liu & Trainer, 1988; Sillman, 2003).

However, O_3 can be destroyed by deposition on the Earth's surface or on the forest or destroyed by OH radical on the unpolluted area in which has very low concentration of NO_x such as remote oceanic area (S. C. Liu & Trainer, 1988; Mauzerall et al., 2000; Pochanart et al., 2001; Sillman, 2003). And also be destructed by ozone titration reaction in the extremely high NO_x concentration area i.e. center of pollution plume (Lal et al., 2000; Lam et al., 2001; Latif et al., 2012; S. J. Oltmans et al., 2013; Wang et al., 2001; Yonemura et al., 2002). O_3 removal in the troposphere happens on a timescale of three months approximately (Silman, 2003).

2.1.1 O_3 productions

As mentioned earlier, source of O_3 is the precursors that are emitted from anthropogenic and natural activities. Generally, O_3 is a secondary pollutant which cannot be produced independently. The O_3 formation requires the presence of light, NO_x and another precursor species. The reaction which energy from the sunlight is absorbed in order to conduct the process is called "Photochemical reaction". Such reaction involves directly in the production of O_3 which will be furthur explained in this topic.

In the urban areas, O_3 is produced from two major precursors, i.e. volatile organic compounds (VOCs) and NO_x namely Nitric oxide (NO) and Nitrogen dioxide (NO_2). While, in the remote area, the O_3 formation process is initiated primarily by the oxidation of CO and methane (CH_4) rather than volatile organics. However, the ozone formation is also closely associated with the OH radical.

The O_3 formation is explained by these following processes (Guicherit & Roemer, 2000; Mohnen et al., 1985; Sillman, 2003).

The existing O_3 in the troposphere absorbs the energy from the short wave ultraviolet (UV) to form O radical.

$$O_3 + h\nu\ (\lambda<320\ nm) \longrightarrow O(^1D) + O_2 \quad (1)$$

O radical reacts with water vapor and forms OH radical.

$$O(^1D) + H_2O \longrightarrow 2OH \quad (2)$$

$$HO + O_3 \longrightarrow HO_2 + O_2 \quad (3)$$

In the urban area HO_2 reacts with emitted NO to forms NO_2.

$$HO_2 + NO \longrightarrow OH + NO_2 \quad (4)$$

Photolysis of NO_2 results in the formation of atomic oxygen (O), which reacts with atmospheric O_2 to form ozone.

$$NO_2 + h\nu\ (\lambda\ 300\text{-}400\ nm) \longrightarrow NO + O(^3P) \quad (5)$$

And then O_3 is formed by the association reaction of ground state O atoms with O_2.

$$O(^3P) + O_2 + M \longrightarrow O_3 + M \quad (6)$$

M is the third body species i.e. N_2 or O_2.

In the case of remote area, the inconspicuous NO_x together with the dominant CO and CH_4 (RH), both CO and CH_4 react with exiting OH radical. RO_2 represents a variety of complex organic peroxy radicals.

$$CO + OH + O_2 \longrightarrow HO_2 + CO_2 \quad (7)$$

$$RH + OH + O_2 \longrightarrow RO_2 + H_2O \quad (8)$$

This is followed by reactions of RO_2 and HO_2 with NO.

$$HO_2 + NO \longrightarrow OH + NO_2 \quad (4)$$

$$RO_2 + NO + O_2 \longrightarrow R'CHO + HO_2 + NO_2 \quad (9)$$

NO_2 from reaction (4) and (9) then continue to reaction (5) and form O_3 by (6).

The NO-NO_2 conversion (reaction (5)) is the characteristic step which led to ozone formation, and the rate of conversion of NO to NO_2 is often calculated as the ozone formation rate.

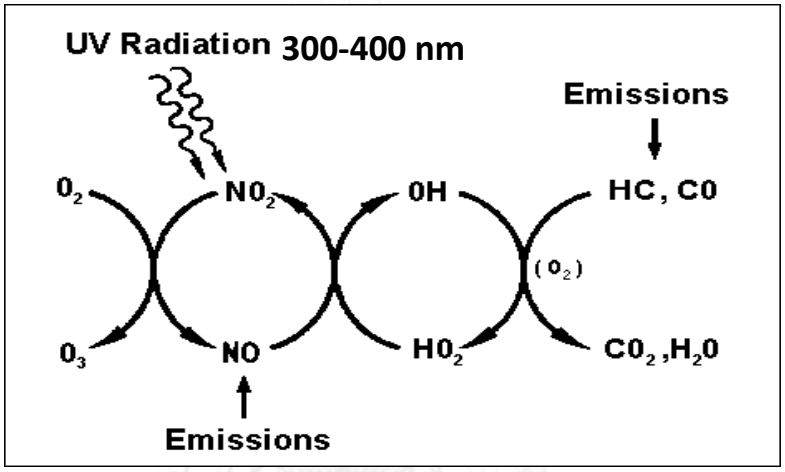

Figure 2.2 Schematic display of photochemical O_3 formation in the troposphere (Volz-Thomas & Mihelic, 1990).

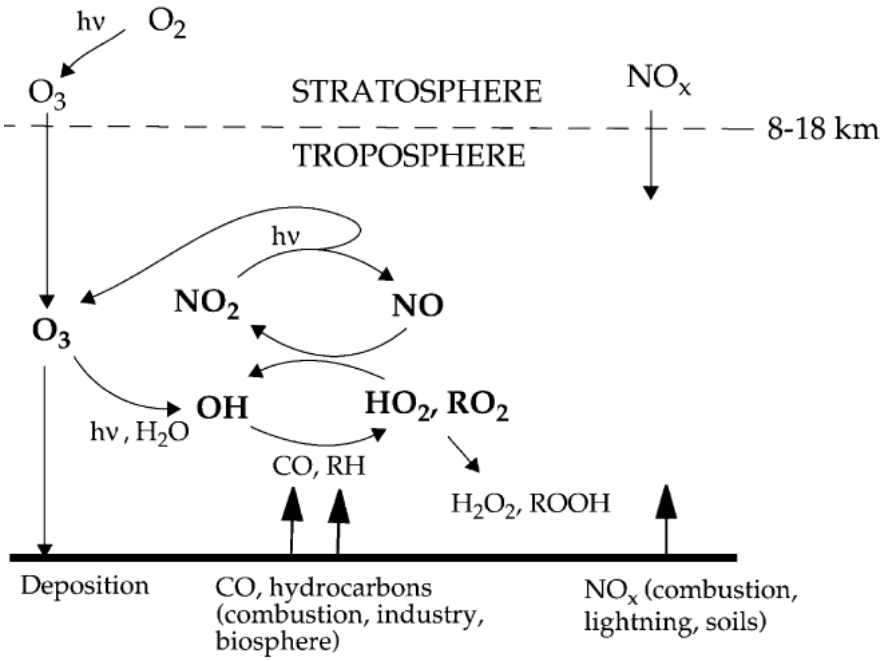

Figure 2.3 Schematic of tropospheric O_3 chemistry (Jacob, 2000)

Figure 2.2 and 2.3 shows the schematic display of photochemical O_3 formation. Production of O_3 in the troposphere can be described that this process acts as a HO_x catalyzed chain oxidation of CO and hydrocarbons in the presence of NO_x. The chain is propagated by the cycling conversion of HO_x between OH and peroxy (Jacob, 2000; Volz-Thomas & Mihelic, 1990).

Once the O_3 in urban plumes is formed, it has an effective lifetime about three days. For this reason, urban polluted plumes with the high ozone concentrations can travel over a long distances. These high ozone concentrations can be transported even longer in the middle and upper troposphere, in which the lifetime of ozone extends to three months (Sillman, 2003).

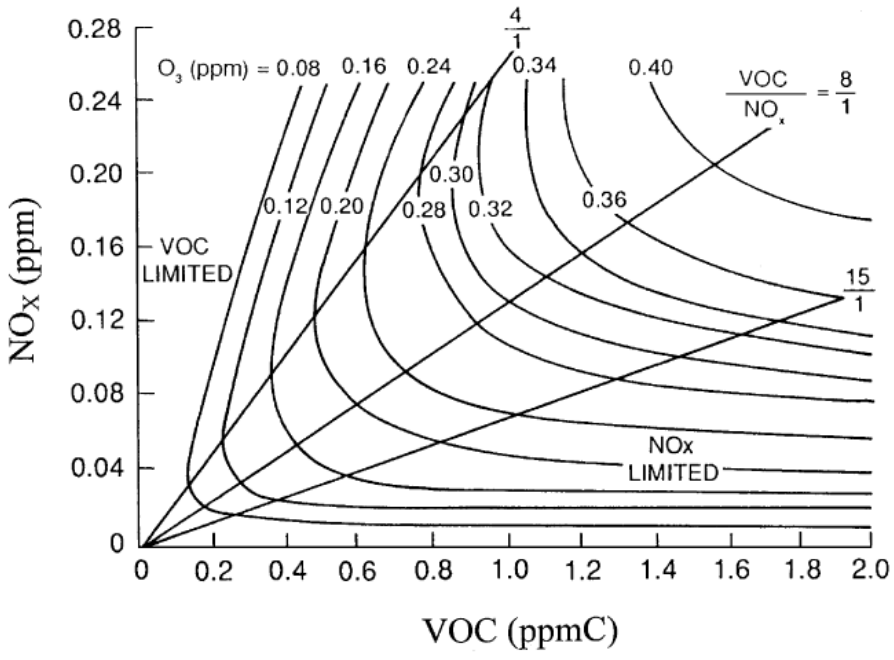

Figure 2.4 O_3 production isopleth diagrams vs. initial mixtures of VOC and NO_x in air (Finlayson-Pitts & Pitts, 1993)

The efficiency of O_3 production that related to the concentrations of NO_X and VOCs was first investigated in 1950s in the smog chamber studies of Haagen-Smit and coworkers (e.g., Haagen-Smit and Fox, 1954,1956). Examination of the peak 1-hour O_3 formed when mixtures of various initial concentrations of NO_x and VOCs are irradiated with ultraviolet radiation in the chamber. The results are frequently shown in the form of isopleths as in the figure 2.4 (Finlayson-Pitts & Pitts, 1993).

As show in Fig. 2.4 the production rate of O_3 is a non-linear function of NO_x and VOCs concentrations. When VOCs/NO_x ratios are high, the O_3 production rate increase with increasing of NO_x concentration until the rate reaches the maxima and subsequently decrease if NO_x concentrations are further increased. Such maximum rate (the ridge line pattern) prescribes NO_x-sensitive and NO_x-saturated regimes. At high VOCs/NO_x ratios the O_3 production rate increases with NO_x increasing and insensitive to VOCs concentrations. The case of low VOCs/NO_x ratios (area above the ridge line) the O_3 production rate increases with increasing of VOCs concentrations and decreases with increasing NO_x concentrations. The definition of NO_x-sensitive and NO_x-saturated regimes is useful for the design of O_3 control policies. O_3 in the NO_x-saturated can be reduced either by reducing NO_x or VOCs concentrations. Likewise, O_3 in the NO_x-sensitive area can be reduced by reducing NO_x concentration (Sillman, 2003).

However, this isopleth diagram is also sensitive to various assumptions (solar radiation, ozone and water vapor concentrations and composition of VOCs). The increasing of CO and VOCs always contribute to increasing O_3 in the remote areas, even under NO_x-sensitive conditions (Jaeglé et al., 2001). In contrast, the O_3 in polluted areas with NO_x-sensitive chemistry is mostly insensitive to CO and VOCs.

Although there are several of the photochemical O_3 formation processes, there is a non-chemical process that adds O_3 from the stratosphere to the troposphere called stratosphere-troposphere exchange (STE) of ozone. The STE mostly occurs at the junction between mid-latitude and tropic (Voulgarakis et al., 2011).

Recent studies of Kim et al. (2002) reported that the ozone enchantment in the top troposphere over Pohang, Korea in winter and spring corresponded to the central axis of jet stream near the tropopause. It was considered that ozone of the upper level over East Asia penetrated into the lower level because of the downstream due to tropopause folding (TF) near the jet stream and the sinking of surface high pressure.

2.1.2 O_3 destructions

The net O_3 amount in the troposphere is not only results from O_3 productions, but it is results from a combination of formation, transport, destruction and deposition. The processes that reduce O_3 concentrations in the troposphere also associated with OH radical similar to O_3 productions. The destruction of O_3 occurs either during the night time which is the absence of sunlight condition or in the clean remote troposphere with the extremely low NO_x concentration.

During daytime, the primary loss of O_3 is the photochemical reaction (1). The O_3 molecule disassociates by the absorption the sunlight.

$$O_3 + h\nu\ (\lambda<320\ \text{nm}) \longrightarrow O(^1D) + O_2 \qquad (1)$$

and the NO_2 is slowly converts to NO_3 by reaction with O_3.

$$NO_2 + O_3 \longrightarrow NO_3 + O_2 \qquad (10)$$

During the nighttime, with the absence of sunlight, the concentration of the OH radical is significantly lower, due to the suppression of photolysis of stable molecules. Thus, NO_2 cannot be photolysed to regenerate NO for re-cyclic the O_3 formation process (Jenkin & Clemitshaw, 2000).

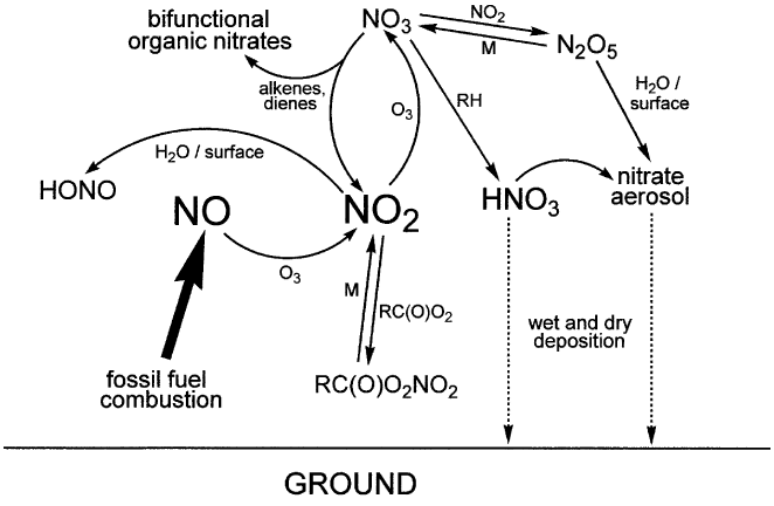

Figure 2.5 Nighttime interconversions of oxidised nitrogen compounds in the troposphere (Jenkin & Clemitshaw, 2000).

Even at the center of polluted troposphere (i.e. center of urban, nearby emission plume area) the O_3 destruction is occurred by the reaction called NO_x titration. Generally, the two components of NO_x (NO and NO_2) adjust to a near-steady state by reactions (4) and (9).

$$HO_2 + NO \longrightarrow OH + NO_2 \quad (4)$$

$$RO_2 + NO + O_2 \longrightarrow R'CHO + HO_2 + NO_2 \quad (9)$$

Over 90% of NO_x emissions consist of NO rather than NO_2, then the process of becoming to a steady state in reactions (5) and (11)

$$NO_2 + h\nu\ (\lambda\ 300\text{-}400\ nm) \longrightarrow NO + O(^3P) \quad (5)$$

$$NO + O_3 \longrightarrow NO_2 + O_2 \quad (11)$$

which usually the NO_2 equal to/greater than NO. The reactions (5) and (11) involve to the O_3 destruction. This NO_x titration process occurs mainly in the emission plumes from the large point sources and can led to a significant decreasing of O_3 concentrations in the neighborhood of large NO_x emissions.

However, in the condition of photochemical is dominant (daytime), the NO_x titration process has a few impact on the net O_3 concentration because the O_3 production rates surpass the O_3 destruction rate that related to NO_x titration. Nevertheless, during the nighttime, the NO_x titration process also leads to extremely low net O_3 concentration in the urban centers (Fig. 2.5). The ratio of NO_2/NO is controlled by the inter-conversion reactions ((5) and (11)) and O_3 production reactions. Since the O_3 production reactions affect the NO_2/NO ratio, for this reason, NO_2/NO ratio can be used to the identification of process of O_3 production especially in the rural troposphere (Sillman, 2003).

Recent study of Wang et al. (2001) indicated that O_3 concentrations obviously decreased during rush hours in the center of urban area in Hong Kong. Such evidences revealed the NO_x titration due to the high emission. Another study, Zhang and Kim Oanh (2002) analyzed the photochemical pollution of O_3 around the

Bangkok metropolitan region. The result showed the O_3 concentration was low in the polluted city center area and higher concentration at the downwind locations, reflects that the low O_3 was titrated by NO_x titration effect of NO emitted from the mobile sources.

In the remote troposphere or NO_x-poor environment (extremely low NO_x concentration) such as oceanic troposphere, the O_3 production is low and the photolysis of O_3 destruction (reaction (1)) is dominant

$$O_3 + h\nu\ (\lambda<320\ nm) \longrightarrow O(^1D) + O_2 \quad (1)$$

the O radical reacts with water vapor leads to OH radicals.

$$O(^1D) + H_2O \longrightarrow 2OH \quad (12)$$

The OH radicals can react directly with O_3 or with CO and methane in the low NO_x concentrations condition to form peroxy radicals which can further react with ozone, leading to further ozone destruction (Samuel J. Oltmans & Levy Ii, 1994).

$$OH + O_3 \longrightarrow HO_2 + O_2 \quad (3)$$

$$HO_2 + O_3 \longrightarrow OH + 2O_2 \quad (13)$$

The evidences of the O_3 destruction associated to OH reactions were revealed in various researches. Pochanart et al. (1999) published the results of surface O_3 and CO in the remote area of Oki, Japan, in order to investigate the influence of the long-range transport effect and photochemical activity, found that the low O_3 and CO concentrations in summer involved to the long-range transport of the maritime originated air masses from Pacific which is a cleaner air. Lam et al. (2001) reported that the O_3 minimum (16 ppbv) in Hong Kong was found in the summer associated with the marine air mass. And Pochanart et al. (2001) found that the O_3 concentrations at remote area of Thailand (Inthanon and Srinakarin) were low during the wet season in both areas which south west monsoon is dominant; such low O_3 concentrations were controlled by the long-range transport of marine air mass originated from Indian Ocean.

2.1.3 Diurnal and Seasonal variations of O_3

As explained above in the previous topic that the net O_3 concentration is the result between ozone productions and destructions. The O_3 amounts depend on the variables. The variations of O_3 are complex under the spatially and temporal condition characteristics of in situ area. Most of previous studies have done in the mid-latitude of northern hemisphere; those studies showed agreeable results.

The variations of O_3 in the remote clean troposphere normally vary in narrow fluctuations, while, in the urban/sub-urban area and the rural area in which affected by downwind from urban are vary in different fluctuation patterns which associated with O_3 precursors and weather conditions. Nevertheless, the diurnal variations of O_3 in several areas show significantly similarity fluctuations, the increasing of O_3 occurs during the daytime due to the presence of sunlight and the decreasing of O_3 occurs during the nighttime.

The example of diurnal variations is shown below in the Fig. 2.6. The variation of O_3 in daily period varies with its precursors i.e. CO, NO and NO_2. These diurnal variations are studied in a polluted troposphere. It begins with the emission of precursors in early morning when the NO is converted to NO_2 and O_3 begins accumulation when the sunlight presents and most of NO has been oxidized. O_3 concentration accumulates until it reaches the maximum concentration at noon during where the light intensity is highest and then declines in the afternoon. During the increasing of O_3, other precursors are declining simultaneously due to contribution the photochemical production of O_3. In the afternoon, once the O_3 destruction exceeds O_3 production, the declining trend of O_3 appears obviously along this period until dusk with the gradually declination and remain steady at night.

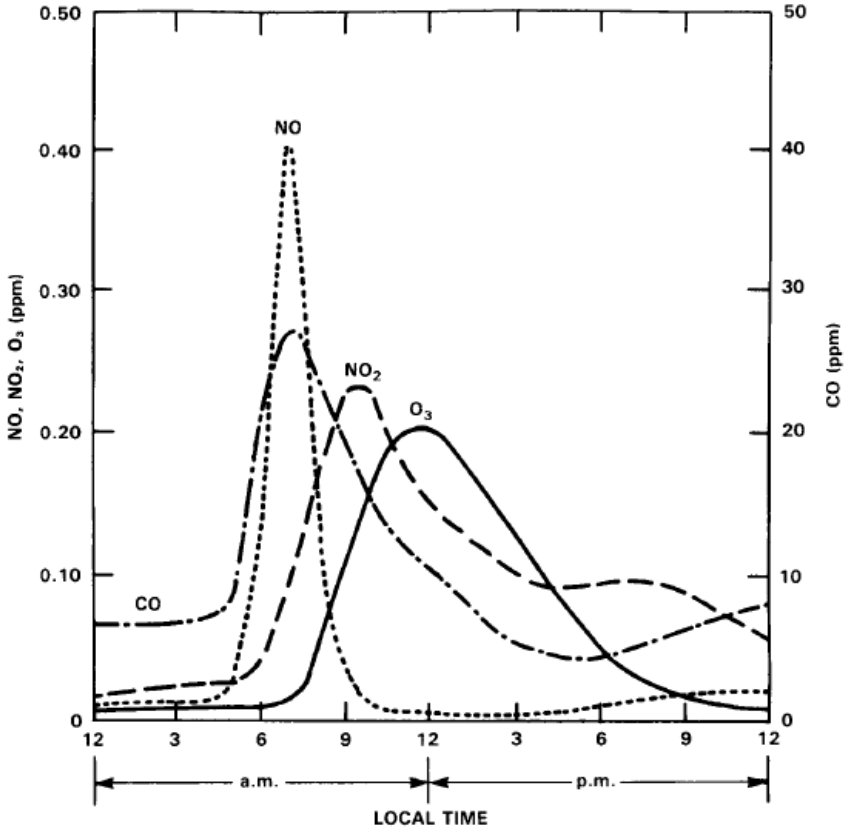

Figure 2.6 Average daily 1-hour concentrations of selected pollutants in Los Angeles, California, July 19, 1965. From U.S. Department of Health, Education and Welfare (Mohnen et al., 1985).

Although, the diurnal variation of O_3 shows a significant fluctuation pattern, the seasonal variations also influences diurnal variations. Diurnal variations during different season have different characteristic. Fig. 2.7 illustrates the results of diurnal variations of O_3 from study of Lam et al. (2001) in Hong Kong. It can be seen that the diurnal variations of O_3 are distinct in each month. Such distinction associated to wind directions which are the results from Asian monsoon system. It forces the long-range transport of air masses that reaching to observed locations. The higher diurnal variation occurred in fall (October) when the wind blown across the North-China continent with high CO concentrations. In contrary, the lower diurnal variations are in summer (July) with the wind blown from South China Sea with low CO concentration.

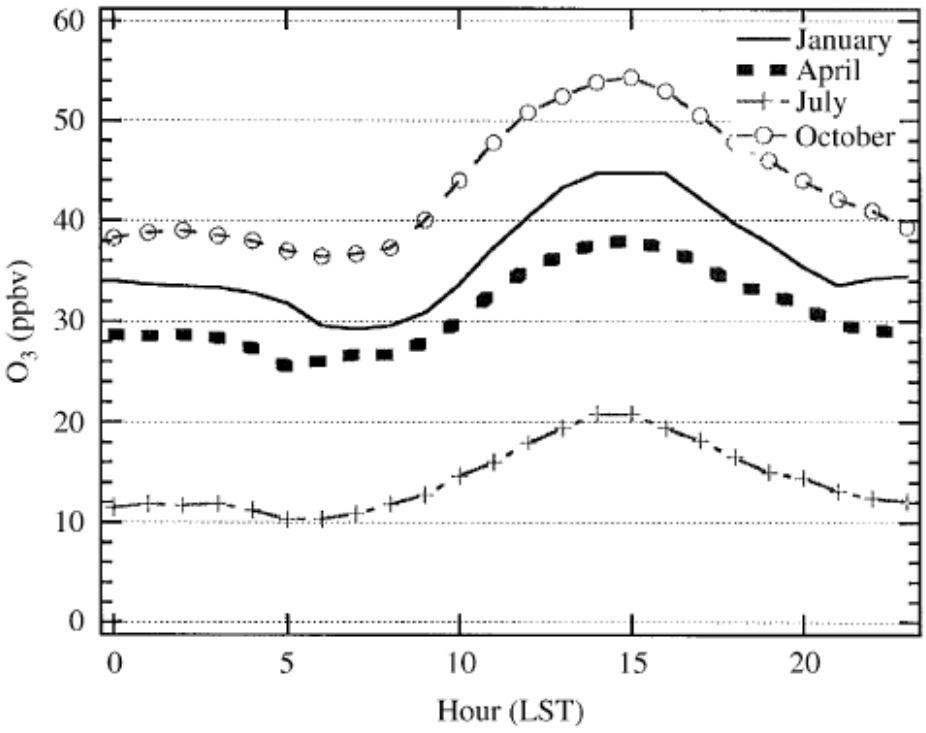

Figure 2.7 Diurnal variations of surface O_3 (Lam et al., 2001).

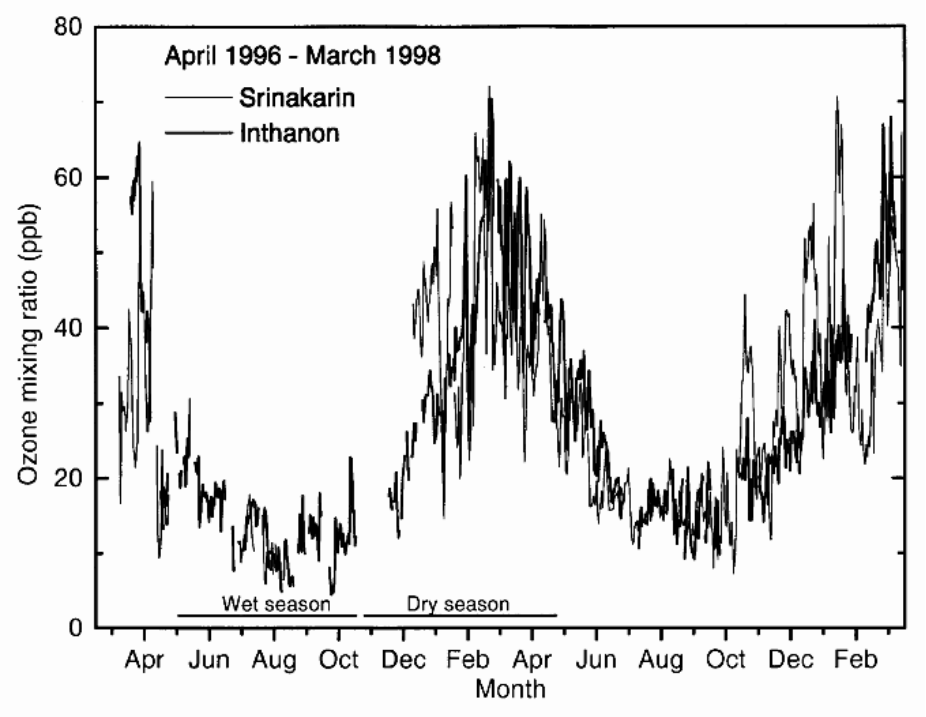

Figure 2.8 Seasonal variations of O_3 at Inthanon and Srinakarin during April 1966 – March 1998. O_3 presented as daily averages (Pochanart et al., 2001).

The results of seasonal variations of O_3 in Thailand were discussed in the study of Pochanart et al. (2001). Fig. 2.8 illustrates the interannual fluctuations of O_3 at two sites over period of two years, the results shows a broad view that O_3 mixing ratios were low in wet season and high in dry season and also shows the corresponding results in both sites. The low O_3 in wet season occurred with the dominant wind direction form south west which originated form Indian Ocean while the high O_3 in dry season occurred with the circulated wind within South-East Asia continent and wind from west/northwest which originated from India. It is note that these seasonal variation characteristics of O_3 are under influence of monsoon winds which carry air masses form different sources to the sites.

However, these variation characteristics of O_3 are not representative for all areas. It is depend on other variables such as solar intensity, O_3 precursor concentration, temperature, wind speed/direction, humidity; etc. Therefore, O_3 would probably show either analogous or distinct variation patterns which are the unique for those areas. Nevertheless, the results from various researches showed corresponding behaviors that high O_3 concentration take place with a polluted air mass from continent and low O_3 concentration take place with a clean air mass from the ocean (Chan et al., 1998; Huang et al., 2013; Lam et al., 2001; H. Liu et al., 2002; Mauzerall et al., 2000; Pochanart et al., 2001; Sikder et al., 2011; Tsutsumi & Matsueda, 2000; Zhou et al., 2013).

From those studies, it can be marked that the monsoon system influences the long-range transport of air masses, especially in Asia. As mentioned in Chapter I, Thailand is located at the affected area by monsoon, therefore, the O_3 variations in Thailand probably show the same pattern with other study areas in Asia, which the results will be discussed in Chapter IV and V.

2.1.4 O_3 associated with the long-range transport of air masses

As in topic 2.1.3, the variations of O_3 concentration involves photochemical reactions and others factors, particularly sources of an ozone precursors. Ozone precursors are emitted by anthropogenic activities which are the major sources, especially biomass burning. Those emissions are usually happen in the continental

urban areas. The plume of emissions emitted to the troposphere and then transported by winds. The long transportation of fresh emissions in an air mass accumulates primary pollutants and formed secondary pollutants (i.e. O_3) subsequently. Therefore, the areas that located along the pathway (downwind) of such air mass are founded to have high O_3 concentration with high concentration of others primary pollutants.

On the other hand, if the pathway of the air mass either transported or originated over the clean troposphere especially maritime region, the accumulated pollutants will be diluted or destroyed, formation of O_3 is then inhibited and replaced by destruction process. With this reason, low O_3 concentration is detected at the downwind area of such clean aged air mass.

Two studies of (Pochanart et al., 2003; Pochanart et al., 2001), first investigates of O_3 and CO concentrations in Thailand, reported that high mixing ratios of O_3 and CO were found in the local dry season associated to the wind from continent. Biomass burning activities in continental Southeast Asia are found to be the main factors controlling O_3 and CO variations. While in the wet season, the observed sites received clean oceanic air from the Indian Ocean and low mixing ratios of O_3 and CO were found. Both cases are associated to the long-range transport of air masses that driven by the Asian monsoon.

All of mentioned above, it can possibly classified two major group of air masses i.e. the continental air mass and maritime air mass. The characteristics of each air mass are described following below.

Continental air mass: The air mass that originated on the continent and accumulates pollutants from the land emissions during transportation. This air mass is polluted and dry which often occurs during winter Asian monsoon. The back trajectory analysis shows in Fig. 2.9.

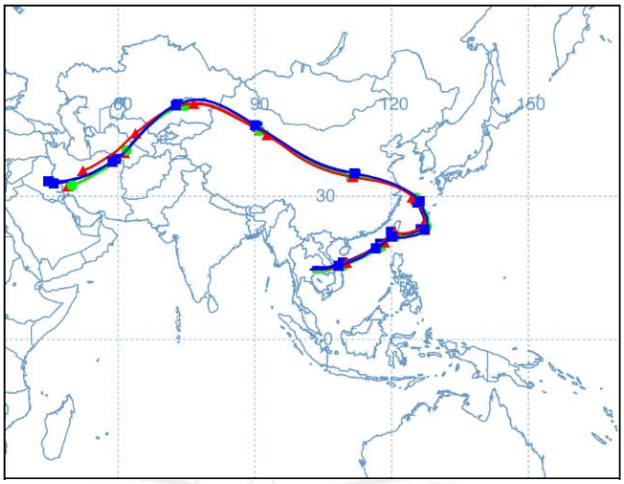

Figure 2.9 Air mass from continent by backward trajectory

Maritime air mass: The air mass that originated on the oceanic regions. Since these areas have sparse anthropogenic activities, it is thought to be a cleaner air mass than the air from continents. This air mass is unpolluted and moist, usually occurs during summer Asian monsoon. Back trajectory analysis shows the trajectory of the air as in Fig. 2.10.

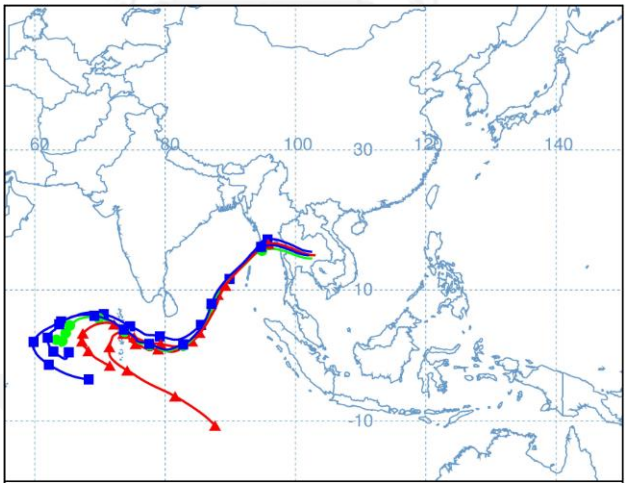

Figure 2.10 Air mass from oceanic by backward trajectory

The aged continental air mass that contained ozone precursors from emissions might be transported for a long distance and take a long time. Species of precursors have a different lifetime. Table 2.1 illustrates the lifetime of such trace gas in the boundary layer and the free troposphere.

Table 2.1 Approximate lifetime of trace gases in the atmospheric boundary layer and the free troposphere (Dentener et al., 2010).

Trace gas	Approximate lifetime in the atmospheric boundary layer	Approximate lifetime in the free troposphere
NO_2	hours	days
CO	weeks to months	weeks to months
VOCs	hours to months	hours to months
CH_4	8-9 years	8-9 years
NH_3	hours to days	hays to weeks
O_3	hours to days	weeks to months

As presented in table 2.1, the lifetimes of primary pollutants such as CO and VOCs are long when compared to others species. CO is an important precursor of O_3 which came from biomass burning, fossil fuel combustion and oxidation of methane (CH_4) and non-methane hydrocarbons (NMHCs). Since CO has long lifetime (1-2 months), therefore, it can be a good tracer gas of long-range transportation of anthropogenic emissions (Pochanart et al., 1999).

In this study, CO and O_3 and the backward trajectory analysis are used to reveal the long-range transport of emissions. Study of Suthawaree et al. (2008) is an example for investigation of long-range transport of CO and O_3 by using backward trajectory analysis. Fig. 2.11 shows four types of air masses that were classified by backward trajectory analysis. The results revealed similar for the O_3 and CO concentrations in the C (for China) and K (for Korea) air masses groups with the highest monthly averaged concentrations. High O_3 and CO concentrations appeared within the air mass group J and the lowest concentrations were found in the O group. However, the trajectory analysis will be thoroughly reviewed again in topic 2.3.

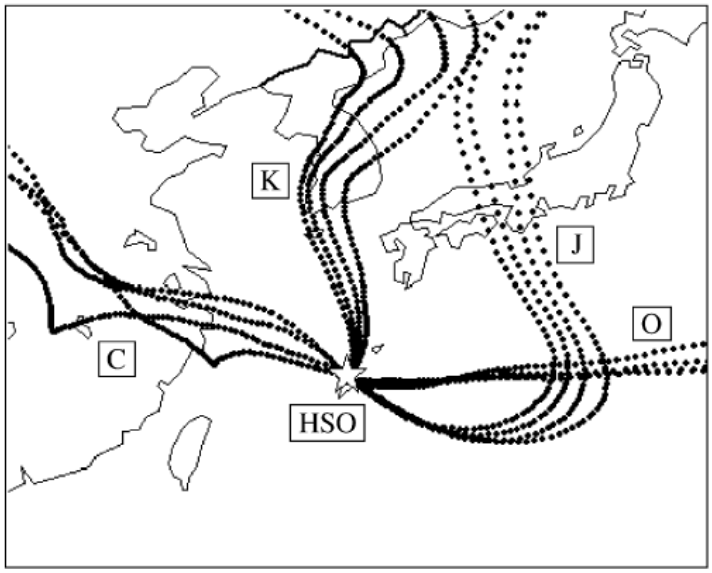

Figure 2.11 Four typical air masses patterns were classified by backward trajectory analysis at Hedo Station Observatory (HSO), Okinawa main island, Japan. ''C'' for China, ''K'' for Korea, ''J'' for Japan, and ''O'' for the Pacific Ocean (Suthawaree et al., 2008).

2.1.5 Effects of O_3 on living organisms and climate

O_3 is a strongly oxidant substance which can harm the surface of living things its contact with. Many evidences of the O_3 harmful effect have been published with the agriculture and human health are the most considered. In addition, since O_3 can absorbs the shortwave from the sunlight radiation lead to warming of the troposphere, hence, its effects to the energy balance in the atmosphere which subsequently affects the climate.

- Effects on living organisms

As reviewed in the earlier topic, O_3 is a secondary pollutant which is a cause of photochemical smog in the polluted urban area, such smog is causes of health effects.

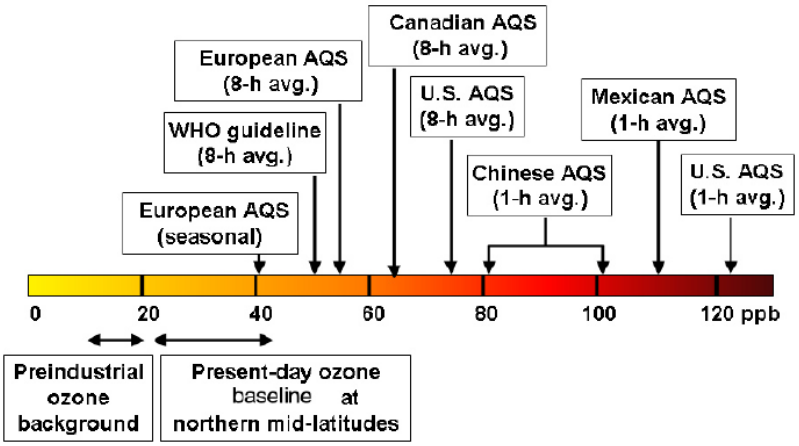

Figure 2.12 Ozone air quality standards in different countries, and the preindustrial background (no anthropogenic emissions) and present-day baseline (not affected by local pollution).

Fig. 2.12 shows the selected Air Quality Standards (AQS) and guidelines for O_3 from around the world. In Thailand, the pollution control department has determined the ozone air quality standard at below 100 ppb for 1 hour average, and 70 ppb for 8 hours average.

O_3 directly effects to the respiratory system. Its effects include decrements in lung function, inflammation of airways, and induction of respiratory symptoms. Fig. 2.13 shows the pyramid of effects caused by ozone.

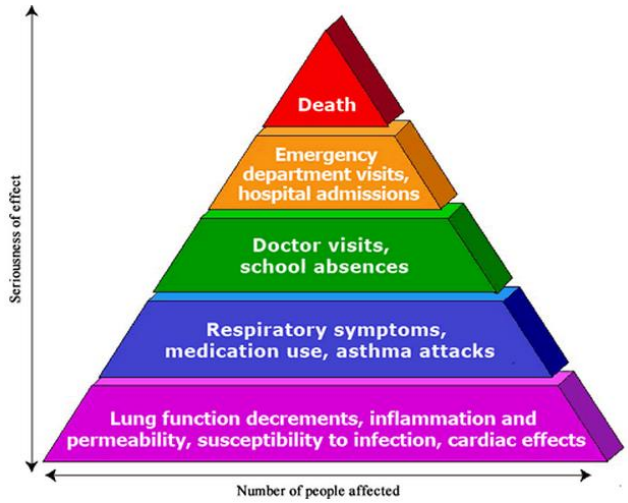

Figure 2.13 Pyramid of effects caused by ozone (U.S.-Environmental-Protection-Agency).

From Fig. 2.13 the strongest effects are in the lowest part of pyramid which is the effect to the respiratory system. How can we expose to O_3? Once we breathe ambient air that containing O_3. The rate of exposure is related to concentration of O_3 and breathing rate per minute. The rate and duration of exposure are the factors strengthen the level of cumulative exposure.

Peoples who have heavily outdoor activities especially long period exercising in the time where O_3 concentrations are high, have greater cumulative exposure to O_3 than peoples who have indoor activities because the O_3 concentration indoor varies between 20 to 80% of outdoor levels. During exercise people breathe deeply and O_3 is then inhaled may shift from the upper airways to deeper of respiratory tract. From this reason it might increases the possibility of health effects (U.S.-Environmental-Protection-Agency).

WHO (World Health Organization) published in 2005 (WHO, 2006) the air quality guideline and interim target information about the health effects of ozone which has been obtained from either chamber studies or field studies. The new publication in 2005 reduced the guideline level from 120 μg/m^3 to 100 μg/m^3 (daily maximum 8-hour mean). This new guideline is in Table 2.2.

Table 2.2 WHO air quality guideline and interim target for ozone 8-hour concentrations.

	Daily maximum 8-hour mean (μg/m^3)	Basis for selected level
High levels	240	Significant health effects; substantial proportion of vulnerable populations affected.
Interim target-1 (IT-1)	160	Important health effects; does not provide adequate protection of public health. Exposure to this level of ozone is associated with: • physiological and inflammatory lung effects in healthy exercising young adults exposed for periods of 6.6 hours; • health effects in children (based on various summer camp studies in which children were exposed to ambient ozone levels). • an estimated 3–5% increase in daily mortalitya (based on findings of daily time-series studies).
Air quality guideline (AQG)	100	Provides adequate protection of public health, though some health effects may occur below this level. Exposure to this level of ozone is associated with: • an estimated 1–2% increase in daily mortalitya (based on findings of daily time-series studies). • Extrapolation from chamber and field studies based on the likelihood that real-life exposure tends to be repetitive and chamber studies exclude highly sensitive or clinically compromised subjects, or children. • Likelihood that ambient ozone is a marker for related oxidants.

The recent study of West el al. (2007) investigated effects of changes of global O_3 concentrations in the future on premature human mortality by three scenarios for the year 2030. The study showed that O_3 changes are causes of highly changes premature human mortality. The CLE (current legislation) scenario revealed the reduction of 190,000 in annual mortalities due to the emission reductions. The MFR (maximum feasible reduction) scenario showed reductions about 460,000 mortalities and 270,000 relative to CLE.

In addition to effects to human health, O_3 can effects plants on crop production and forest productivity. Effects of O_3 on vegetation have been observed in several areas. Especially In the areas that are located in downwind from the polluted urban, frequently found high O_3 concentrations even in rural areas or agricultural sites.

O_3 forces a phototoxic effect when the sufficient O_3 amount reaches to sensitive cellular in the leaf. O_3 diffuses from the air into the leaf through its gas exchange pores in the stomata. O_3 is dissolved in the water inside the plants and reacts with other chemicals, causing of several problems. Ability of O_3 that interacts with lipid components or membrane proteins, causes cell membranes to becomes leaky. Figure 2.14 shows example of O_3 phototoxic effect on leaf.

Figure 2.14 O_3 induced symptoms including bifacial necrosis (Karnosky et al., 2007).

O_3 impacts forest trees in many ways including inducing visible foliar symptoms, decreasing foliar chlorophyll content, accelerating leaf senescence, decreasing photosynthesis, increasing respiration, altering carbon allocation, water balance, and epicuticular wax composition and structure, affecting canopy architecture, predisposing trees to attack by pests, and decreasing growth and productivity and fitness (Karnosky et al., 2007).

Prevention of photosynthesis led to slower plant growth. O_3 oxidation forms the compounds which intervene the cell's energy production, resulting in decreasing of fruits. When plants became weakened they may be susceptible to diseases and pests. These bring about to the reductions of agricultural products and economic value.

Study of effects of O_3 on future crop yield productivity was published by Avnery et al. (2011). They examined the risks of increasing O_3 to three crops (soybean, maize, and wheat) in the future (year 2030) under two scenarios of projected O_3 precursor emissions. IPCC SRES A2 represent the upper boundary projections of most O_3 precursor emissions in the year 2030 and IPCC SRES B1 represent the lower-boundary projections of most O_3 precursor emissions in the year 2030. The results then compared to their previous study (impacts of O_3 on global agriculture in year 2000). The results revealed:

i). in the A2 scenarios global yield loss of wheat in year 2030 from 5.4-26% (with +1.5-10% reduction from year 2000), 5-19% for soybean (reduction of +0.9-11%), and 4.4-8.7% for maize (reduction of +2.1-3.2%).

ii). in B1 scenario revealed less severe but still plenty reductions, 4.0-17% for wheat (reduction +0.1-1.8% from 2000), 9.5-15% for soybean (decrease of +0.7-1.0%), and 2.5-6.0% for maize (decrease of +0.3-0.5%).

- Effects on climate

From the IPCC 4th assessment report (2007), O_3 is the third important greenhouse gas after carbon dioxide and methane, this mean that O_3 plays an important role on the radiative forcing in the atmosphere because of O_3 can absorbs the short wave radiation. Although the troposphere contains O_3 only about 10% of total O_3, the longwave opacity of existing tropospheric O_3 amounts is closely the same as stratospheric O_3 amounts. Solar radiation effects to tropospheric O_3 change influence the surface temperature in the troposphere in the same direction. The surface temperature is more sensitive to changes of tropospheric O_3 than changes of stratospheric O_3.

Chemical pollutants in the atmosphere can influence the climate through one or more of the following processes:

i) Radiatively active gases: If the pollutants are radiatively active, they will enhance the atmospheric greenhouse effect.
ii) Chemically active gases: such as CO and NO, that have negligible radiative effects, can produces radiatively active gases such as CH_4 and O_3 by chemical interactions.
iii) Radiatively and chemically active gases, such as CH_4, can oxidize in the troposphere and lead to increasing of tropospheric O_3, both are influence on the greenhouse effect.
iv) Ozone changes and stratosphere-troposphere radiative interactions: O_3 absorbs solar radiation; hence, stratospheric O_3 modulates the shortwave solar and longwave reaching the troposphere. Stratospheric O_3 influences tropospheric climate through stratospheric-tropospheric radiative interactions in both the shortwave and longwave radiation. The greenhouse effect of tropospheric O_3 also plays a important role in climate to O_3.
v) Radiative-chemical interactions: These effects arise because of the strong temperature dependence of the reaction rates of the various chain reactions in the stratosphere such as stratospheric O_3 concentration. The temperature increase (decrease) in the upper stratosphere leads to

stratospheric O_3 decrease (increase). Furthermore, decreasing of stratospheric O_3 allows deeper penetration of sunlight to lower layer and permits enhanced tropospheric O_3 production.

vi) Climate-chemistry interactions: The greenhouse effect causes an increasing in the evaporation from the land and oceans led to an increase in the tropospheric water vapor (H_2O). By Photolysis, H_2O perturbs OH in the troposphere which OH plays a dominant role as a cleansing and oxidizing agent for tropospheric pollutants and radiatively active species such as CH_4 and O_3 (and possibly others).

Changes in well-mixed greenhouse gases and O_3 effect directly on radiative transfer, these influence on temperature and air circulation. In term of radiative transfer, the enchantment of greenhouse gases and O_3 are assumed to lead to the tropospheric warming.

Previous studies have revealed the evidences of O_3 changes in the troposphere and the stratosphere which effect on the radiative forcing. Gauss et al. (2006) reported the results from study of radiative forcing since preindustrial times (1850-2000) due to O_3 change in the troposphere and the lower stratosphere, they employed the several models to simulate global changing of O_3 and radiative forcing. The results showed that tropospheric O_3 column change has led to a radiative forcing of 0.32 Wm^{-2} from overall averaged of the models.

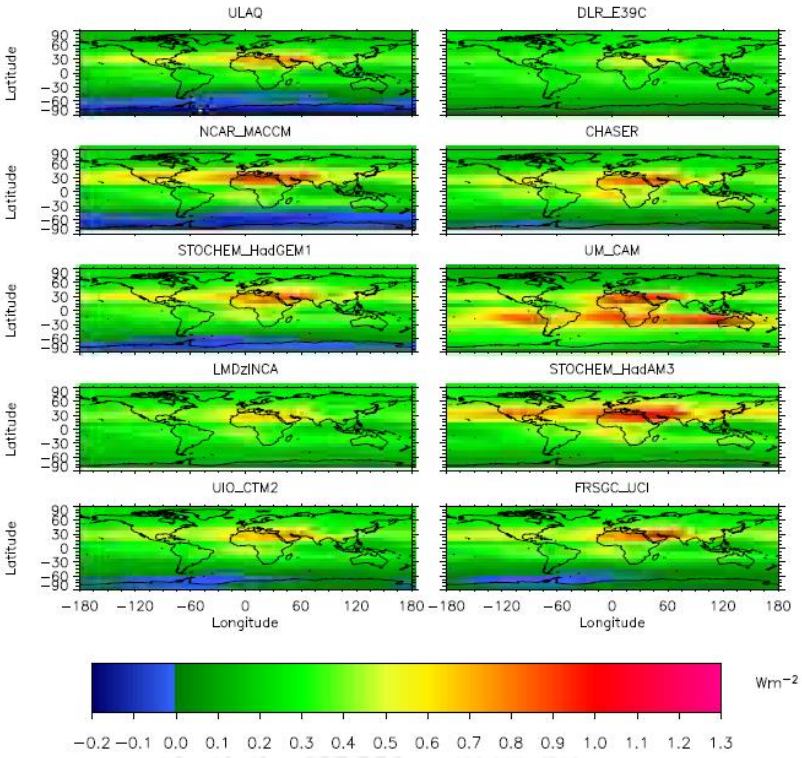

Figure 2.15 Adjusted radiative forcing (Wm^{-2}) between 1850 and 2000 due to tropospheric ozone change (Gauss et al., 2006).

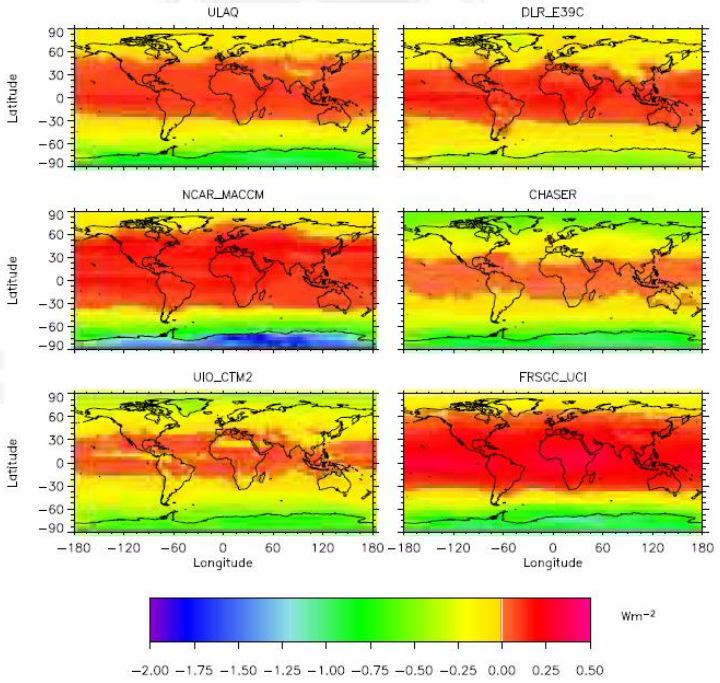

Figure 2. 16 Adjusted radiative forcing (Wm^{-2}) between 1850 and 2000 due to stratospheric ozone change (between the tropopause and 30 km altitude) (Gauss et al., 2006).

Fig. 2.15 shows the calculated results of annual-mean radiative forcing due to changes in tropospheric O_3 between 1850 and 2000. It can be seen that radiative forcing have changed more positive in the northern hemisphere than the southern hemisphere especially in low latitudes as the results of tropospheric O_3 enhancement. While, negative radiative forcing are seen in high southern latitudes in some of the models which is due to slight decreases in tropospheric O_3 connected with the stratospheric O_3 depletion of the last few decades.

Figure 2.16 shows results of annual-mean radiative forcing due to changes in stratospheric O_3 between 1850 and 2000, the negative radiative forcing appears at the middle to high latitudes in both the northern and southern hemisphere particularly in southern high latitude near the Antarctica which is results from stratospheric O_3 depletion while the slightly positive forcing can be seen in low latitudes.

2.2 Monsoon and seasons in Thailand

Thailand is located on Indo-china peninsular in which is under the influence of Asian monsoon circulation. The schematic picture of surface-level flow is illustrated in Fig. 2.17. The monsoon meteorology can be divided into three basic periods: the summer or southwest (SW) monsoon (June–September), the winter or northeast (NE) monsoon (November–March), and the monsoon transition periods (MTP) which vary year to year, but mostly occur during April and May for the winter to summer transition, and in late September to October for the summer-to-winter transition (Lawrence & Lelieveld, 2010).

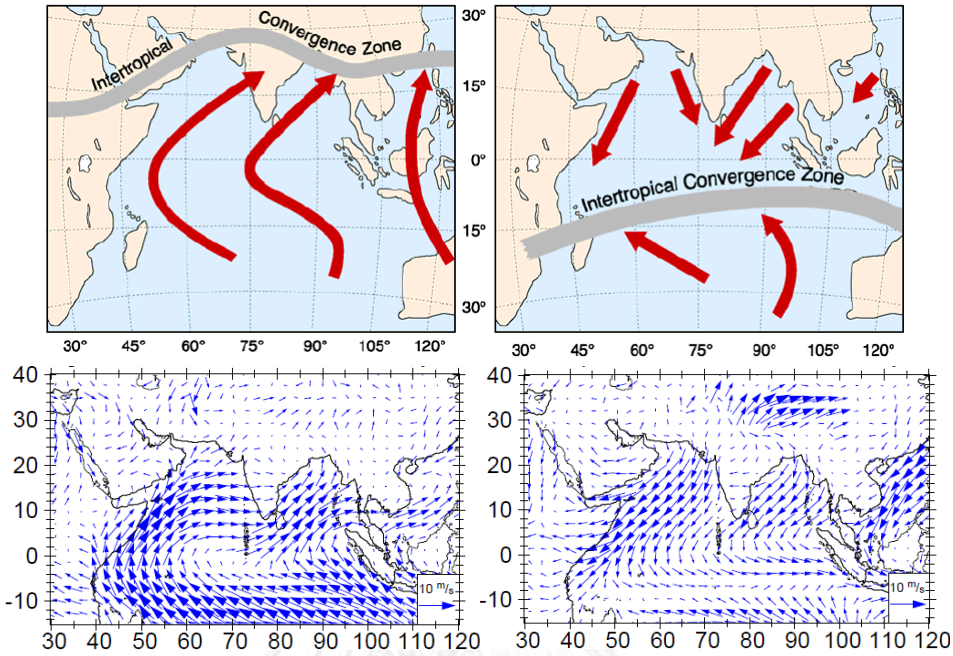

Figure 2.17 Transport pathways (upper pic.) and surface wind fields (lower pic.) of Asian monsoon over the Indian Ocean during the (left) summer and (right) winter monsoon periods (Lawrence & Lelieveld, 2010).

Each monsoon period carries the different chemistry and physical compositions of air masses that reach Thailand. SW monsoon carries the air mass from the Indian Ocean, while NE monsoon carries the air mass from the Asian continent; these are causes of the different seasons.

Seasons in Thailand are classified to two major seasons. The wet season (rainy season) usually occurs in early May and lasts to late October. During rainy season, the southwest wind (southwest/summer monsoon) prevails over Thailand. These conditions lead to precipitation, heavy rainfall, and high humidity air. The dry season usually starts in November with the north east wind (northeast/winter monsoon). This wind brings the cold and dry air mass from the northern or northeastern part of the Asian continental. The winter monsoon generally finishes in late February, but dry season continues until early May. However, the dry season in Thailand can be classified into 2 local season periods: during December to February is referred as the winter season, March to April are referred as the local summer which is extremely hot and harsh because of the strong solar intensity and low pressure in Thailand (Pochanart et al., 2001).

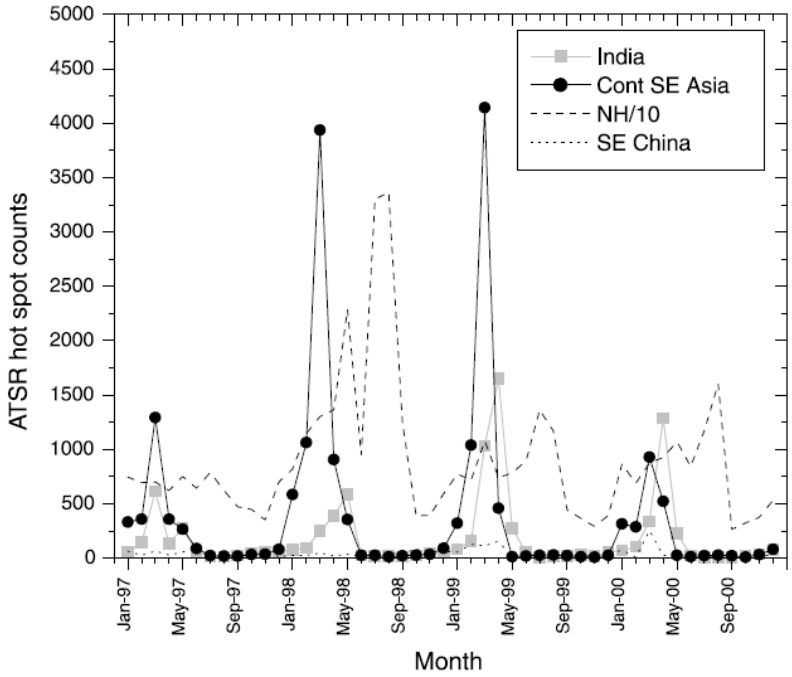

Figure 2.18 The seasonal cycles of ATSR hot spots over continental Southeast Asia, India and southeast China in comparison with those over the entire Northern Hemisphere during January 1997-December 2000 (Pochanart et al., 2003).

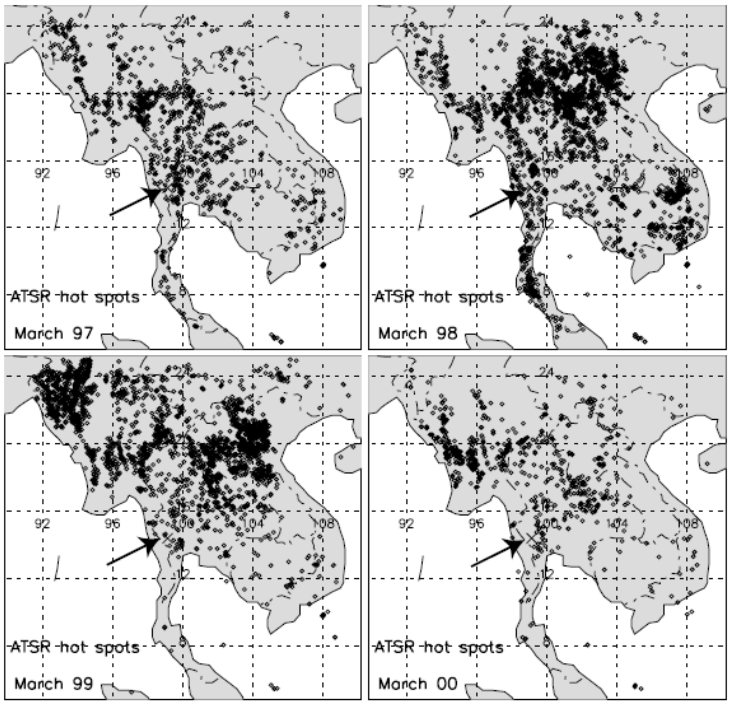

Figure 2.19 ATSR hot spots detected over continental Southeast Asia for the month of March 1997–2000 (Pochanart et al., 2003).

During the local summer season in Thailand, the biomass burning occurs in a broad area with high frequency. Pochanart et al. (2003) have reported that the hotspots in continental Southeast Asia and Thailand were observed by the Along Track Scanning Radiometer (ATSR). They found that the biomass burning are significantly high during January to April and maximum in March (Fig. 2.18 for number of hotspot, and 2.19 for hotspot area in March) which related to high CO and O_3 concentrations in the same period. For these reasons, the local summer in Thailand is considered to the burning season which that extremely emissions occur.

2.3 Trajectory analysis by HYSPLIT model

The purpose of this study is investigation the variations of O_3. The mainly cause of this variations is the long-range transport of air masses which is like a conveyance that carries the pollutants. The route of pollutant transportations are the key of such purpose that could reveal the schematic variations of O_3. To reach this purpose, the trajectory analysis is conducted under the HYSPLIT model version 4 (Fig. 2.20).

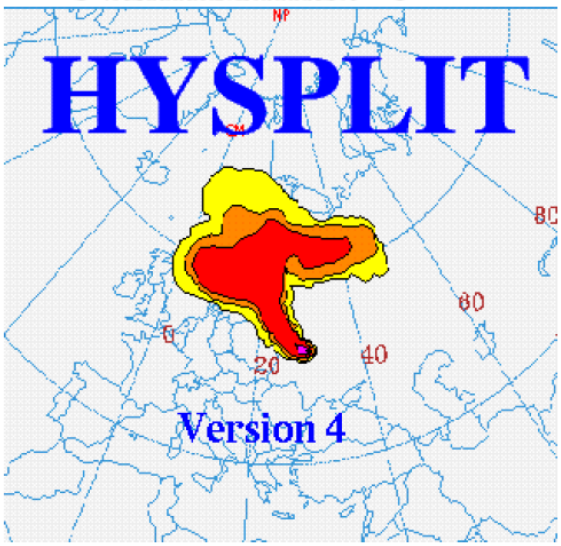

Figure 2.20 HYSPLIT model version 4

The HYSPLIT (HYbrid Single-Particle Lagrangian Integrated Trajectory) model is a complete system for computing simple air parcel trajectories. It helps to illustrated how, when, and where chemicals and materials are transported, dispersed, and deposited simulations (Fig. 2.21). Moreover, it is designed for immediate response to

atmospheric pollution problems, research case studies, or climatological analysis using previously gridded meteorological data (Draxler and Hess, 1998). The HYSPLIT was a result of a joint effort between NOAA (National Oceanic and Atmospheric Administration) and Australia's Bureau of Meteorology. (See also: http://www.arl.noaa.gov/HYSPLIT_info.php.)

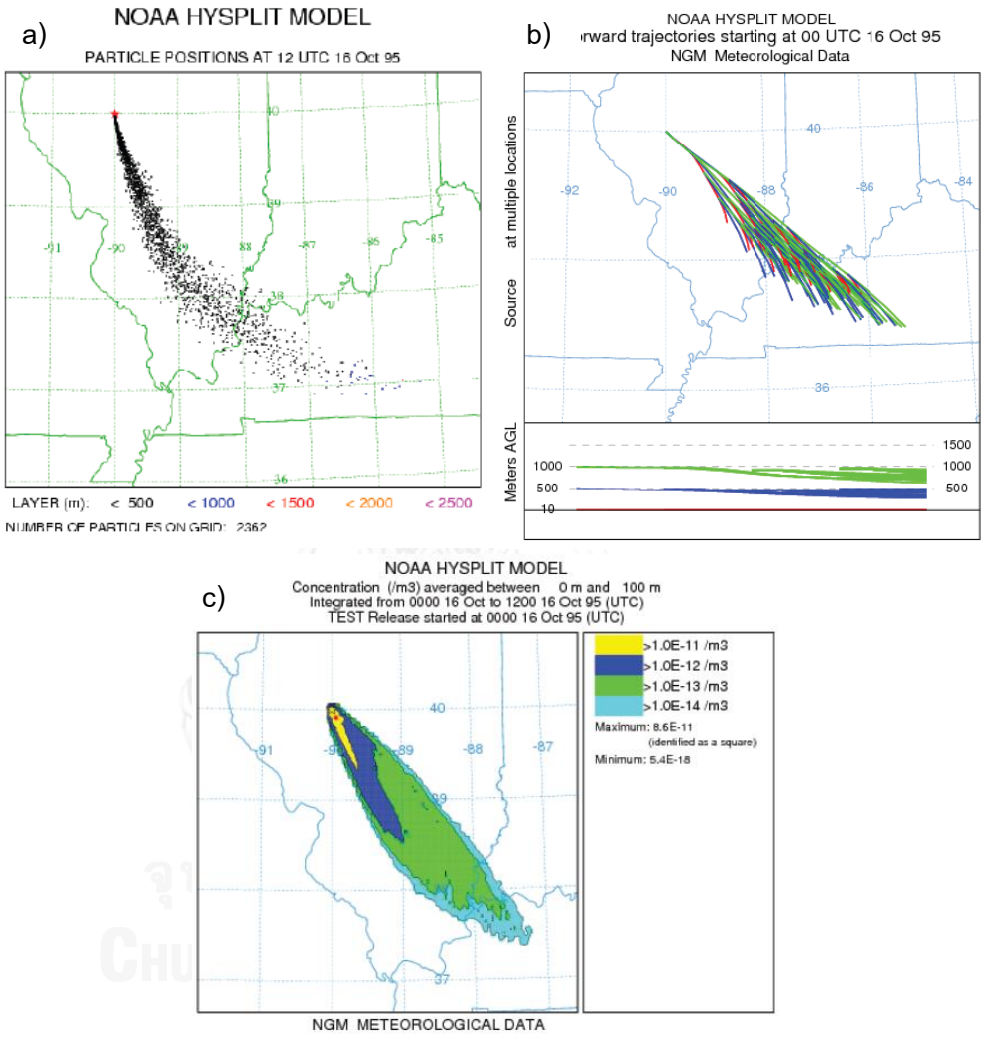

Figure 2.21 Functionality of HYSPLIT model a).Particle display, b).Trajectory display, and c).Concentration display (NOAA-Air-Resources-Laboratory, 2012).

The calculation method of HYSPLIT model is a hybrid between the Lagrangian approach (which uses a moving frame of reference for the advection and diffusion calculations as the air parcels move from their initial location) and the Eulerian approach (which uses a fixed three-dimensional grid as a frame of reference to

compute the pollutant air concentrations). HYSPLIT uses existing meteorological forecast fields from regional or global models for calculation the advection, stability, and dispersion (NOAA-Air-Resources-Laboratory, 2012).

The trajectory analysis was installed already within HYSPLIT model and it is conveniently employed and favorable to the public or who those interests because HYSPLIT is the free software which can be either run directly in ARL's READY (Real-time Environmental Applications and Display sYstem) online website or can be installed and run individually on PC.

There are several previous researches which have used the trajectory analysis for research investigations (Kondo et al., 2004; Lam et al., 2001; Latif et al., 2012; Pochanart et al., 2001; Suthawaree et al., 2008; Toh et al., 2013; Tsutsumi & Matsueda, 2000; Yonemura et al., 2002). Such researches demonstrated the highly usefulness of the trajectory analysis for trace either the source of pollutant or the pollutant dispersal direction.

For this study, the backward trajectory analysis in HYSPLIT model is also employed for investigation of the variations of O_3. The more details of such backward trajectory analysis and HYSPLIT will be explained in topic 3.5 (Chapter III).

2.4 Literatures review

After the beginning of industrial evolution, the atmospheric pollution has been considered to be the major problem. The anthropogenic emissions are the important sources of such problem. There are many of studies that revealed the necessary informations for any further research or governmental policy to resolves an emissions problem.

Several earlier studies of O_3 were published; in this topic such studies especially in Thailand are summarized.

The tropospheric O_3 in two rural/remote sites (Inthanon and Srinakarin) in Thailand were continuously measured for the first time during April 1996 to March 1998 by Pochanart et al. (2001). Their revealed the characteristics of surface O_3 in

Thailand. The seasonal variation of ozone at the both site showed maximum in dry season and minimum in wet season due to the long-range transport under influence of the Asian monsoon. From Fig. 2.22, the backward trajectory analysis showed that at Inthanon site the minimum O_3 was as low as 13 ppb on average which associated with the clean marine air mass from the Indian Ocean during the summer monsoon or wet season. During dry season O_3 that associated with long-range transportation of continental air mass from the Asian continent showed higher concentrations, 26 and 42 ppb in averages. The maximum O_3 mixing ratios of 46 ppb average were measured which associated with short-range transport within Southeast Asia continent during the local summer in dry season. These indicated the enhancement of photochemical O_3 production when air masses recirculate within Southeast Asia continent and accumulate pollutants. The extremely high O_3 that was observed during the local summer implied the significantly enhancement of local/sub-regional scale of biomass burning in Southeast Asia.

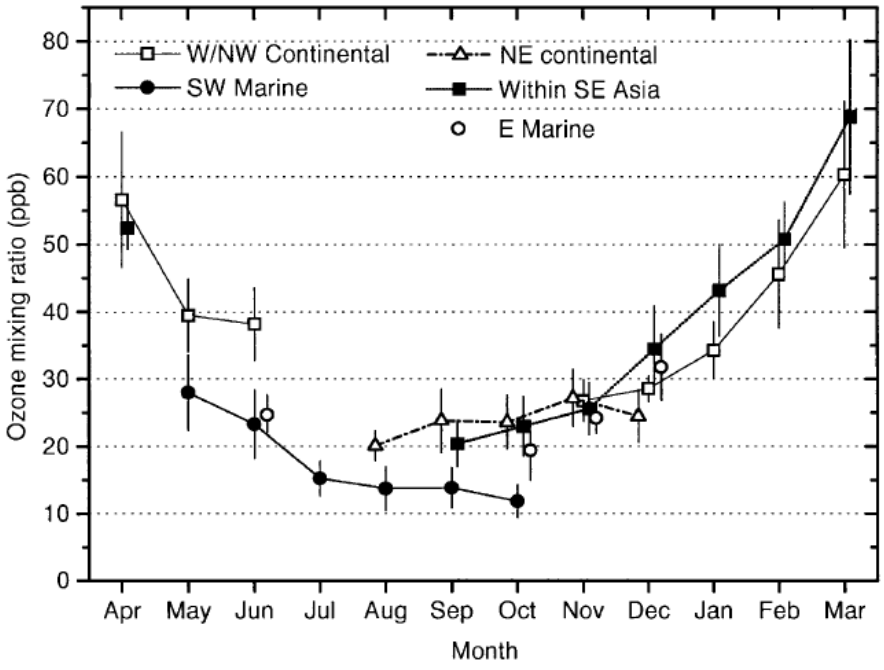

Figure 2.22 Two-year monthly averaged O_3 mixing ratios at Inthanon classified by the associated trajectory categories during April 1996 - March 1998 (Pochanart et al., 2001).

The study in urban area also has been reported particularly in the mega city. Bangkok metropolis is the capital area in Thailand which is polluted by emissions from various sources. Zhang and Kim Oanh (2002) have analyzed the photochemical pollution by using the available 5 years monitoring data (1996–2000) from 11 monitoring stations in Bangkok and 5 stations surrounding provinces. O_3 variations were analyzed with local meteorological conditions and the regional transport of pollutants that associated with the monsoon. The results showed that O_3 was found in the polluted urban areas with a lower concentration in the city center particularly in the curbside stations which reflects the titration effect of NO emitted from mobile sources, and higher concentration of O_3 at the downwind locations. This titration effect leads to the lower monthly average of hourly O_3 in Bangkok than other remote sites. Seasonal variations of O_3 were found to be related to the regional transport associated with the Asian monsoon. Highest O_3 was found during the winter and local summer (January to April) and lowest during mid-rainy season in August. The optimum NO_x/NMHC ratio for O_3 production in Bangkok metropolis is about 0.07 which was observed in summer consistent with seasonal variations of O_3, indicated more effective O_3 production in summer (0.07), followed by winter (0.05), and the lowest in rainy season (0.03). Highest O_3 concentration was found in 1997 together with the maximum hourly average of 370 ppbv and the total hours exceeding is 314 hours than the national hourly O_3 standard (100 ppbv) which is related to the strong El Ni-no and the forest fire in Southeast Asia in such year and O_3 slightly increased from 1998 to 2000.

In addition, Suthawaree et al. (2012) investigated the potential of volatile organic compounds (VOCs) to formation of O_3 in suburban Bangkok. The results showed the high mixing ratios of VOCs were found during the morning and evening time due to vehicular emissions and averaged VOCs were distinct between weekdays and weekend. Elucidating by O_3 formation potential, toluene was found to contribute the most to O_3 production followed by ethylene, m-, p-xylene, and propylene. Moreover, the study by the model of Milt et al. (2009), they simulated the effects on ground level O_3 of 10% of biofuel substitution into conventional fuels

in Bangkok. The model showed that 10% of biofuel substitution could lead the increasing of O_3 by as much as 16 ppb.

Another studies from several locations also were reported, studies in East Asia or west Pacific such as China, Japan, and Hong Kong (Chan et al., 1998; Deng et al., 2008; Huang et al., 2013; Lam et al., 2001; H. Liu et al., 2002; Sikder et al., 2011; Suthawaree et al., 2008; Tsutsumi & Matsueda, 2000; Wang et al., 2001; Zhou et al., 2013), in Southeast Asia such as Indonesia, Malaysia, and Singapore (Fujiwara et al., 2003; Komala et al., 1996; Latif et al., 2012; Toh et al., 2013; Yonemura et al., 2002), in South Asia such as India (Badarinath et al., 2007; Lal et al., 2000; Latha & Badarinath, 2004). Those studies of O_3 in Asia were showed the agreeable results that the anthropogenic emissions influences on the tropospheric O_3 combine with the Asian monsoon on the transportation of pollutants.

CHAPTER III

MEDTHODOLOGY

In this Chapter, the details of all instruments will be illustrated together with data measuring, data collecting, data preparation processes, setting of backward trajectory analysis and data analysis.

3.1 O_3 measuring and collecting

The Fig. 3.1 shows the O_3 measuring instrument. It was installed inside the observatory and connected with a long rubber tube in order to sampling the outside air. The tube's inlet was installed outdoor at 10 meters high above the ground. Then, this sample air will be measured in the special cell by UV-photometric system. The measurement processes details are described in the next subtopic.

Figure 3.1 O_3 measuring instrument (model 1006-AHJ)

3.1.1 Model 1006-AHJ measurement system

The Fig. 3.2 below illustrates the flow schematic of UV-photometric continuous ozone monitor (Dasibi model 1006-AHJ). The black line is the flowing way of sample air.

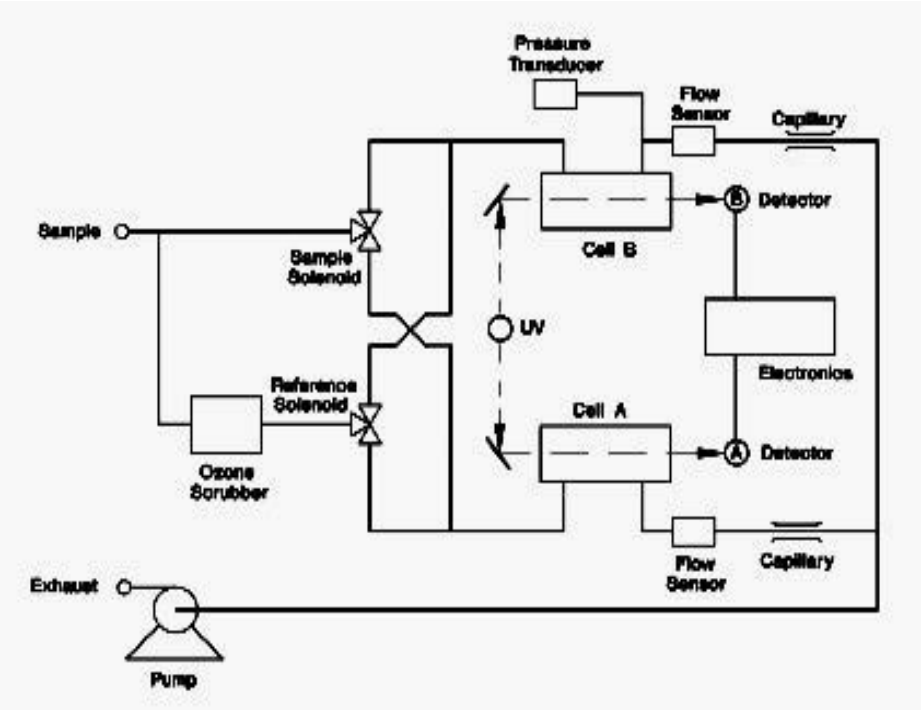

Figure 3.2 Model 1006-AHJ flow diagram

The step of processes are as follows,

1. The sample air is flowed through the outdoor tube by pumping and its flow rate is controlled by flow sensor. Flow rate should be more than 2 L/min, if the flow rate is too low, adjust the valve (Fig 3.3). Sample air flows into the particle filter (Fig 3.4) and then it passes into two lines.
   - First line sample air flows normally to cell B.
   - Second line sample air flows toward the ozone scrubber in order to eliminate O_3 in sample air entirely. This line produces the free O_3 air called reference air. Then, it flows into cell A.

Figure 3.3 Model 1006-AHJ flow sensor

Figure 3. 4 Particle filter connected with outdoor installed tube line.

2. Sample air flows continuously into the UV absorption cell A and B.
   - Sample air from the first line is measured in cell B. Simultaneously; sample O_3 free air from the second line is measured in cell A.
   - Both UV absorption cell A and B measure sample air by detection of the non-absorbed UV by the Beer Lambert's law.

$$\frac{I}{I_0} = exp^{(-KLC)}$$

I is the light intensity measured with O_3 in the gas sample.

I_0 is the light intensity measured without O_3 in the gas sample. (Reference air)

K is the O_3 absorption coefficient at 254 nm.

L is length of cell.

C is O_3 concentration.

UV lamp lays the UV light pass through cell A and B. O_3 in sample air absorbs UV light at a wavelength 254 nm. The degree of which O_3 absorb UV light is directly related to the O_3 concentration. Non-absorbed UV light is detected by detector in each cell and converted to O_3 concentration (C value in Beer Lambert's law) in ppb unit (part per billion).

Model 1006-AHJ's Specifications

- 0.1 ppb resolution
- 12 seconds measuring time interval
- +/- 5% absolute accuracy
- +/- 1 ppbv relative precision

3.1.2 Data from model 1006-AHJ and first preparation

Aforementioned, in 3.1.1, model 1006-AHJ measures every 12 second and stores raw data in .OZN type a file per day. Raw data is stored in main instrument's PC hard disk and it can be transferred to external hard disk directly. OZN raw data file can be run on documentary program such as Microsoft Excel Microsoft Word Notepad and Text document. For this study, Microsoft Excel is the main program that is used for OZN raw data and data preparation processes. The following lists are the details comprised in a raw file data and illustrated in Fig. 3.6.

A and B: Measuring second (+12 every each measuring)

C: Year	D: Month
E: Day	F: Hour
G: Minute	H: Second

I: O_3 concentration (ppb)

Normally, raw data has been filled in one column (Fig. 3.5). Fig. 3.6 shows the raw data that has been reformed. This is an important step because the data compositions require being separated into each column for assisting of analysis of raw data to become easier and convenience. After that, the reformed OZN data is saved in Excel file type.

A	B	C	D
7 20 2008 01 03 00 00 07 % 0.030			
19 32 2008 01 03 00 00 19 % 0.031			
31 44 2008 01 03 00 00 31 % 0.032			
43 56 2008 01 03 00 00 43 % 0.034			
55 68 2008 01 03 00 00 55 % 0.033			
67 80 2008 01 03 00 01 07 % 0.036			
79 92 2008 01 03 00 01 19 % 0.037			
91 104 2008 01 03 00 01 31 % 0.034			
103 116 2008 01 03 00 01 43 % 0.033			
115 128 2008 01 03 00 01 55 % 0.033			
127 140 2008 01 03 00 02 07 % 0.032			

Figure 3.5 OZN raw data

A	B	C	D	E	F	G	H	I
403	416	2008	1	3	0	6	43	0.033
415	428	2008	1	3	0	6	55	0.032
427	440	2008	1	3	0	7	7	0.033
439	452	2008	1	3	0	7	19	0.032
451	464	2008	1	3	0	7	31	0.032
463	476	2008	1	3	0	7	43	0.031
475	488	2008	1	3	0	7	55	0.032
487	500	2008	1	3	0	8	7	0.031
499	512	2008	1	3	0	8	19	0.031
511	524	2008	1	3	0	8	31	0.031
523	536	2008	1	3	0	8	43	0.03
535	548	2008	1	3	0	8	55	0.029
547	560	2008	1	3	0	9	7	0.032
559	572	2008	1	3	0	9	19	0.031
571	584	2008	1	3	0	9	31	0.031
583	596	2008	1	3	0	9	43	0.034
595	608	2008	1	3	0	9	55	0.032

Figure 3.6 OZN file data details

Apart from O_3, other data (i.e. CO, radiation, relative humidity and wind direction) were collected at the same time and shown in the next section.

3.2 CO measurement and collection

In order to measure the CO content, the model 48C CO analyzer had been installed. The same as with O_3 measuring instrument, CO analyzer is inside the observatory and connected with long rubber tube for the outside air sampling. The figure below shows the model 48C CO analyzer (Fig. 3.7). The Model 48C Trace Level is based on the principle that carbon monoxide (CO) absorbs infrared radiation at a wavelength of 4.6 microns.

Figure 3.7 model 48C CO analyzer

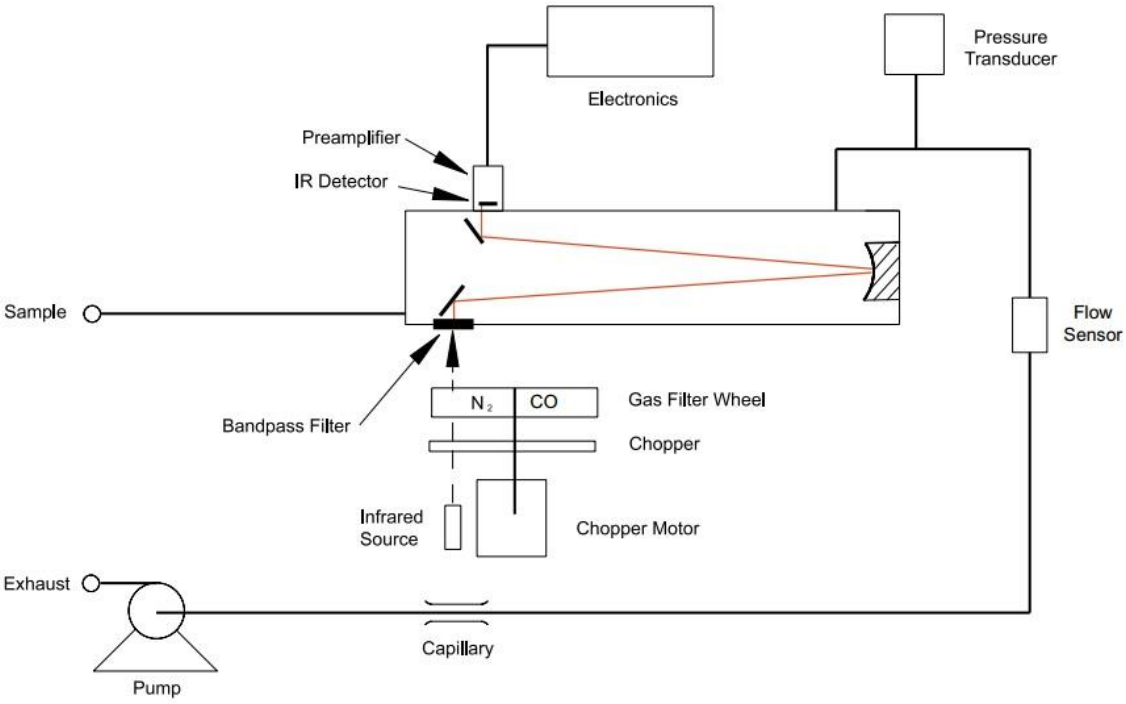

Figure 3.8 Model 48C CO analyzer flow diagrams

3.2.1 Model 48C CO analyzer measurement system

Figure 3.8 illustrates the flow diagram of the Thermo model 48C. The Model 48C uses an exact calibration curve to accurately linearize the instrument output over any range up to 10,000 ppm of concentration.

The sample flows through the optical bench. Radiation from the infrared source is chopped and then passed through a gas filter alternating between CO and N_2. The radiation then passes through a narrow band pass filter and enters the optical bench where absorption by the sample gas occurs. The infrared radiation then exits the optical bench and falls on the infrared detector.

The CO gas filter acts to produce a reference beam which cannot be further attenuated by CO in the sample cell. The N2 side of the filter wheel is transparent to the infrared radiation and therefore produces a measure beam, which can be absorbed by CO in the cell. The chopped detector signal is modulated by the alternation between the two gas filters with amplitude related to the concentration of CO in the sample cell. Other gases do not cause modulation of the detector signal since they absorb the reference and measure beams equally.

Specifications of model 48C CO analyzer

- 0-1 to 10000 ppm custom range
- 0.04 ppm lower detectable limit
- 30 seconds measuring time interval

3.2.2 Data from model 48C CO analyzer and first preparation

Like the model 1006-AHJ O_3 analyzer, model 48C CO analyzer stores the raw data in DAT file type (one file/day) on instrument PC's hard disk. Then DAT raw data can be transferred to external memory directly. DAT file can be run on Microsoft Excel in order to prepare raw data for the next analysis process.

The following figure and lists below show the details comprised in a raw file.

A	B	C	D
0	0	0	7464
0	0	30	7458
0	1	0	7154
0	1	30	6967
0	2	0	6963
0	2	30	6943
0	3	0	6946
0	3	30	6938
0	4	0	6942
0	4	30	6948

Figure 3.9 DAT data details from model 48C CO analyzer

A : Hour B : Minute

C : Second D: CO concentration (ppm)

However, Fig. 3.9 shows over high CO concentrations which were not the actual content. The measuring system in model 48C is divided into two phases, namely; 1) Air without CO and 2) Air with CO. Fig. 3.10 illustrates how model 48C has temporal measuring in 1 hour.

Generally, sample air is consisted of many gases; water vapor is an important gas with high efficiency of infrared radiation absorption. Therefore, the absorbed infrared by CO and the absorbed infrared by water vapor are mixed within sample air. For this reason, CO is required to be disposed from sample of air by heating under high temperature. By this method, CO is oxidized and reformed to CO_2 which does not absorb infrared radiation.

Therefore, [actual CO content = Sample air with CO – Sample air without CO].

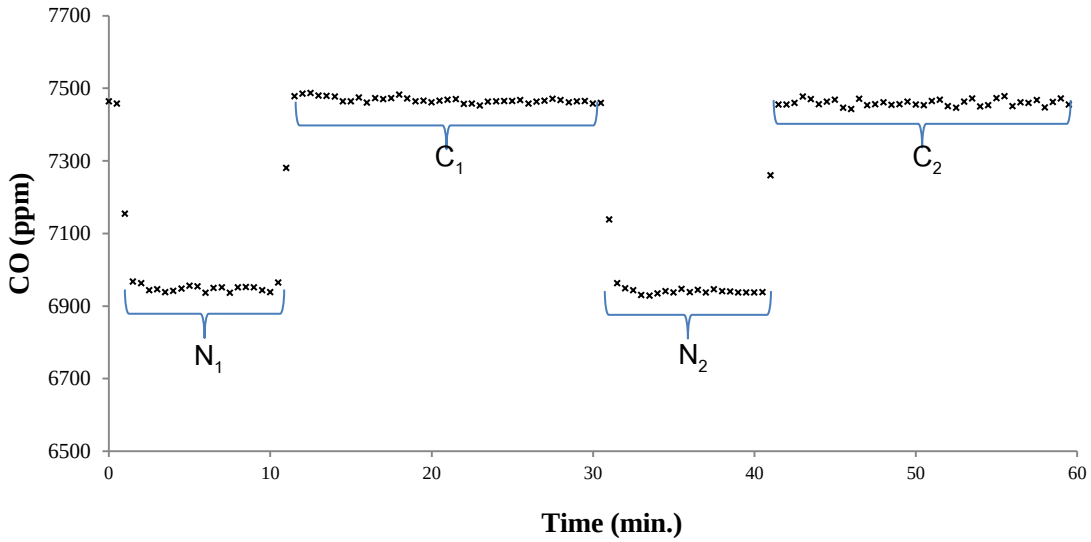

Figure 3.10 Model 48C CO analyzer raw data in one hour

As illustrated in Fig 3.10, **N** is sample air without CO, while **C** is sample air with CO, respectively. Both phases are set for alternating by 10 minutes in **N** and 20 minutes in **C** phase, 30 minutes/cycle.

Actual CO concentration can be calculated by

$$CO = C_x - \frac{N_x + N_{x+1}}{2}$$

Where CO is CO concentration

C_x is average concentration in **C** phase, order **x**

N_x is average concentration in **N** phase, order **x**

N_{x+1} is average concentration in **N** phase, order **x+1**

In order to minimize the errors due to unstable data during alternation between phases, first 6 minutes of each phase is not utilized for calculation. Whereby, CO concentration in this step is representative of 30 minutes measurement.

All CO raw data in this study were calculated by above method, then, saved as Excel file type. Figure 3.11 shows the example of raw data which was calculated. The actual CO concentration is shown in column M in the unit of ppm (Fig. 3.11).

G	H	I	J	K	L	M
N01	6948	**C01**	7465		0.00-0.29	521
N02	6939	**C02**	7459		0.30-0.59	521
N11	6937	**C11**	7445		1.00-1.29	510
N12	6932	**C12**	7452		1.30-1.59	522
N21	6928	**C21**	7444		2.00-2.29	517
N22	6924	**C22**	7441		2.30-2.59	522
N31	6916	**C31**	7431		3.00-3.29	522
N32	6904	**C32**	7434		3.30-3.59	530
N41	6904	**C41**	7451		4.00-4.29	551
N42	6895	**C42**	7512		4.30-4.59	620
N51	6889	**C51**	7445		5.00-5.29	555
N52	6890	**C52**	7373		5.30-5.59	488
N61	6879	**C61**	7372		6.00-6.29	494

Figure 3.11 Real CO concentration data

G : N phase H : concentration in N phase (ppm)

I : C phase J : concentration in C phase (ppm)

L : Time M : actual CO concentration (ppm)

3.3 Meteorological and Radiation data measurement and collection

The meteorological and direct radiation were measured to study relations between O_3 and its factors, excluding CO. Meteorological data in this study includes wind direction and relative humidity which have been measured by different instrument. However, they were recorded in the same file. Also, direct radiation has been measured and recorded.

3.3.1 Meteorological measurement instruments and raw data

Wind direction and relative humidity have been measured by two instruments illustrated in Fig. 3.12 Ultrasonic Anemometer for wind direction and 3.13 Relative humidity sensor for relative humidity.

Figure 3.12 Ultrasonic Anemometer at Phimai station.

Figure 3.13 Relative humidity sensor at Phimai station.

Ultrasonic Anemometer was installed on the roof of the observatory and Relative humidity sensor was installed inside the shell two meters high from the ground in the observatory's backyard. These meteorological instruments operate simultaneously and store by one raw data file/day as illustrated in Fig. 3.14 below.

B	C	D	E	F	G	H	I	J	K	L
Date	Time	UTC	Julian_day	Temperature	Wind_speed	Wind_directio	Pressure	Temperature_room	Relative_humidity	Pmsl
yyyymmdd	Local									
Date	hh:mm:ss	hh:mm:ss		C	m/s	degree	hPa	C	%	
20070108	8:54:32	1:54:32	8.371204	19.578	0.03975474	0.24816715	994.605	23.579	59.321155	1017.786
20070108	8:54:36	1:54:36	8.37125	19.533	0.088243368	0.23623877	994.598	23.546	59.432039	1017.785
20070108	8:54:46	1:54:46	8.371366	19.478	0.07915806	0.44984038	994.671	23.626	59.693172	1017.869
20070108	8:54:56	1:54:56	8.371481	19.453	0.052170984	0.24284023	994.61	23.759	60.109044	1017.809
20070108	8:55:06	1:55:06	8.371597	19.424	0.078192876	0.28749298	994.647	23.573	60.302816	1017.852
20070108	8:55:16	1:55:16	8.371713	19.399	0.103665312	0.46907856	994.641	23.782	60.533878	1017.85
20070108	8:55:26	1:55:26	8.371829	19.396	0.068103036	0.46276034	994.626	23.783	60.567777	1017.835
20070108	8:55:36	1:55:36	8.371944	19.402	0.08856072	0.4311059	994.621	23.63	60.401234	1017.828
20070108	8:55:46	1:55:46	8.37206	19.401	0.063361056	0.34512084	994.629	23.818	60.63656	1017.837
20070108	8:55:56	1:55:56	8.372176	19.391	0.091997868	0.3385193	994.601	23.624	60.647386	1017.81
20070108	8:56:06	1:56:06	8.372292	19.397	0.071293644	0.23017226	994.623	23.639	60.707639	1017.831
20070108	8:56:16	1:56:16	8.372407	19.396	0.066556908	0.24315502	994.584	23.656	60.627921	1017.792
20070108	8:56:26	1:56:26	8.372523	19.383	0.07131594	0.43427686	994.638	23.814	60.670022	1017.849
20070108	8:56:36	1:56:36	8.372639	19.385	0.09418788	0.36118793	994.599	23.643	60.564387	1017.809

Figure 3.14 Meteorological raw data

Raw data has 10 seconds measuring time interval and many meteorological contents. Therefore, these raw data files were reformed to the file that consists of required contents i.e.: Time (Local), Wind direction and Relative humidity (Fig. 3.15)

A	B	C	D	E
Time			Wind_direction	Relative_humidity
Local				
hh	mm	ss	degree	%
0	2	28	168.2348976	90.884803
0	2	32	184.2770592	90.909298
0	2	42	172.156968	90.914438
0	2	52	183.2730912	90.924389
0	3	2	195.2820432	90.90733
0	3	12	190.2921768	90.933137
0	3	22	172.1695752	90.951399
0	3	32	173.1727512	90.941666
0	3	42	165.2253552	90.955664
0	3	52	197.3199384	90.977862

Figure 3.15 Reformed meteorological data

The data as shown in Fig. 3.15, finally, will be taken to next process.

3.3.2 Direct radiation measurement instrument and raw data

The solar radiation is the energy released from the sun to the earth's surface which includes direct and diffuse radiation. In this study, we focus on direct radiation which could affect the amount of O_3. The instrument utilized for measurement of energy emitted from the sun is called Pyrheliometer which is illustrated in Fig. 3.16 and was installed on the roof of the observatory.

Figure 3.16 Pyrheliometer at Phimai station.

A pyrheliometer is an instrument for measurement of direct beam solar irradiance. After sunlight enters the pyrheliometer, it is converted to an electrical voltage by a thermopile. This voltage can then be calibrated to give units of watts per square meter (Watt/m^3), the standard units of solar irradiance.

Pyrheliometer measures both of direct and diffuse solar radiation every 10 seconds in Watt/m^2 unit. The raw data from Pyrheliometer is stored together with another radiation data from different instrument. Radiation raw data is shown in Fig. 3.17 below.

B	C	D	E	F	G	H	I	J
Date	Time		Julian day	Swflux up	Diffuse solar	Direct solar	Lwflux down	Lwflux down
yyyymmdd	Local	UTC		VIS reflect	VIS diffuse	VIS direct	PIR down therm	PIR down case
Date	hh:mm:ss	hh:mm:ss		Wm^-2	Wm^-2	Wm^-2	V	K
20070108	8:54:32	1:54:32	8.371204	323.2544939	41.81467125	402.081927	-77.05938303	294.7119805
20070108	8:54:36	1:54:36	8.37125	322.7766802	41.87904809	404.36776	-76.58200514	294.7121899
20070108	8:54:46	1:54:46	8.371366	322.1927126	41.63238469	394.361203	-76.91902314	294.7207641
20070108	8:54:56	1:54:56	8.371481	321.4936032	38.27026497	332.77409	-76.8066838	294.7283657
20070108	8:55:06	1:55:06	8.371597	320.8123077	33.17615309	258.46307	-75.54241645	294.7354363
20070108	8:55:16	1:55:16	8.371713	321.2812955	36.97257115	337.269258	-74.58714653	294.743274
20070108	8:55:26	1:55:26	8.371829	322.5820243	44.67276742	452.037328	-71.44087404	294.7523735
20070108	8:55:36	1:55:36	8.371944	323.5111741	43.23032385	413.38331	-69.16529563	294.7638287
20070108	8:55:46	1:55:46	8.37206	324.6614575	41.69136408	396.316567	-71.8622108	294.7780168
20070108	8:55:56	1:55:56	8.372176	326.617085	46.0186948	464.202187	-70.79460154	294.7916324
20070108	8:56:06	1:56:06	8.372292	328.5814575	48.47458292	495.288122	-74.1940874	294.8038076
20070108	8:56:16	1:56:16	8.372407	330.8998381	51.87423945	546.157918	-73.23881748	294.8143804
20070108	8:56:26	1:56:26	8.372523	333.182834	55.28459274	596.976809	-73.68817481	294.8250031
20070108	8:56:36	1:56:36	8.372639	335.1472874	56.06211973	599.871934	-72.19922879	294.8364291
20070108	8:56:46	1:56:46	8.372755	336.4834008	55.77257115	593.90348	-72.36786632	294.8483252
20070108	8:56:56	1:56:56	8.37287	337.7930364	56.42679097	603.706573	-72.78920308	294.8603942
20070108	8:57:06	1:57:06	8.372986	339.0495547	56.57154073	605.585895	-76.02005141	294.8728919

Figure 3.17 Radiation raw data

This raw data consists of various data contents from different instruments, but only direct solar radiation is required, then, all radiation raw data are reformed.

3.4 Data validation and preparation

3.4.1 Data validation

When observatory instruments are measuring, perhaps, the incorrect results may occur from unknown error operations. These errors occur mostly in a short period (a few minutes). However, those errors still were recorded in raw data. But it can be checked directly from such raw data. Therefore, the data validation is necessary in order to eliminate any error in raw data which is the essential step for obtainment of precise results.

For this study, raw data were validated by checking unusual values. All daily raw data were plotted, then, the unusual values will appear obviously as too high or too low narrow peak (comparing to surrounding normal value) in a short time (few minutes) example is shown in Fig. 3.18. After that, such unusual values will be deleted.

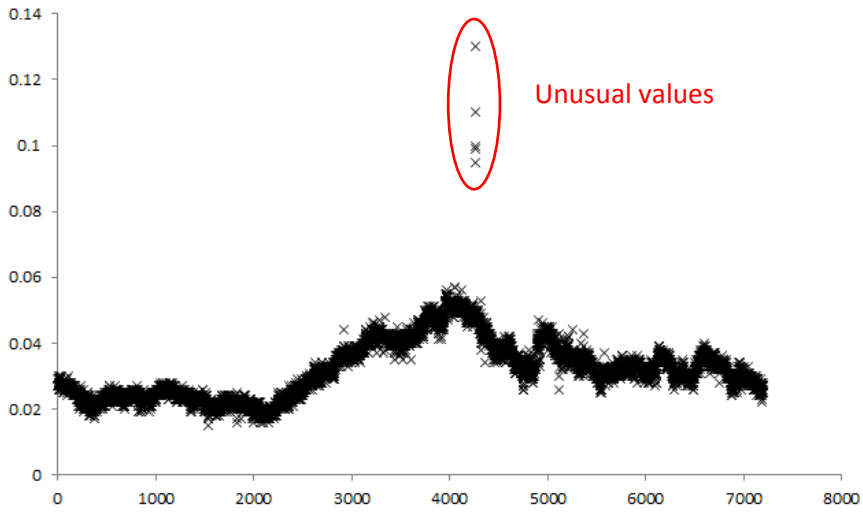

Figure 3.18 Unusual values in ozone raw data.

However, sometimes, instruments may fail for many days. It could not operate normally but raw data were still be recorded. In this case, raw data in those days of instrument failure were also deleted.

3.4.2 Data preparation

After all raw data had completely been validated; these data will be prepared for the next step. The averaged 30 minutes data is necessary for analysis in this study. So, such validated data will be reformed to the half hourly average data before they will used as the data base in the analysis procedures.

3.5 Air mass classification by trajectory analysis (HYSPLIT model)

In order to classify the type of air mass, trajectory analysis is necessary. It is helpful to calculate air mass movements, where an air mass began and their routes. Every air mass type that was classified could explain the O_3 seasonal variations together with its factor variations.

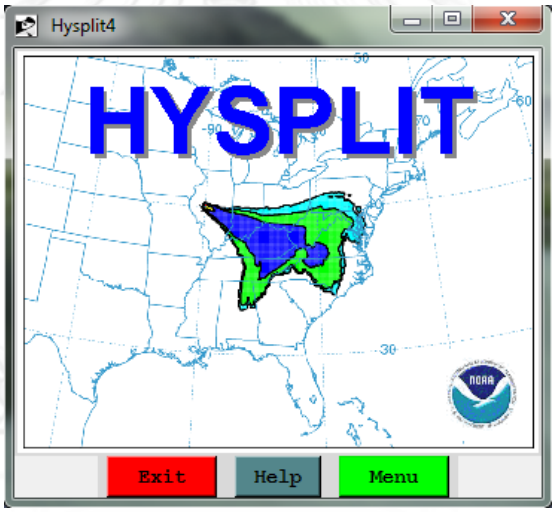

Figure 3.19 HYAPLIT model versions 4

To categorize an air mass sources, it needs the backward trajectory analysis to reveal the result. The Hybrid Single-Particle Lagrangian Integrated Trajectory (HYSPLIT) model (Fig. 3.19) is an answer, the backward trajectory analysis is provided inside. HYSPLIT model is a complete system for computing simple air parcel trajectories to complex dispersion and deposition simulations. This was a result of a joint effort between National Oceanic and Atmospheric Administration (NOAA) and Australia's Bureau of Meteorology. See also: http://www.arl.noaa.gov/HYSPLIT_info.php. Therefore, HYSPLIT model is chosen in this study because it is high reliable, free download, and mostly used in previous studies.

HYSPLT model can be run interactively on the website but with some limitations to avoid computational saturation of web server. The PC version (used in this study) can be downloaded directly from the foregoing website and is complete without computational restrictions, except that user must obtain their own meteorological data files in PC. In this study, National Centers for Environmental Prediction (NCEP) and the National Center for Atmospheric Research (NCAR) or NCEP/NCAR reanalysis meteorological data (1948 – present) were used for computation.

3.5.1 Primary setting for backward trajectory analysis on HYSPLIT model.

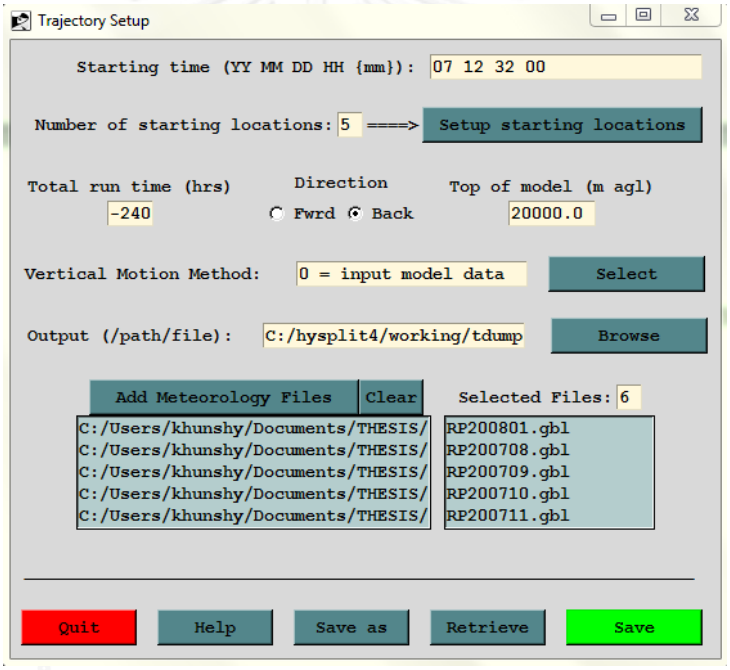

Figure 3.20 Backward trajectory analyses setting on HYSPLIT model

The backward trajectory analysis is runs out a single file per day. Fig. 3.20 shows how to set the parameters before analysis.

Which the details are as follows:

1. *Starting date* - The end time that backward trajectory reached to. (Set at 00 UTC for 07.00 AM local time)
2. *Number of starting locations* – The location point that backward trajectory reached to. For this study, shows in Fig. 3.21, Phimai observatory's

location (15.184N 102.565E, Location 1) is the observed point. In this study, the location is at 212 meters above mean sea level, but needs to set up at 1000 meters in order to dispose an error of surface frictions. Moreover, more 4 locations (+0.5N, -0.5N, +0.5E & - 0.5E) are required in order to investigate a homogeneous trajectory.

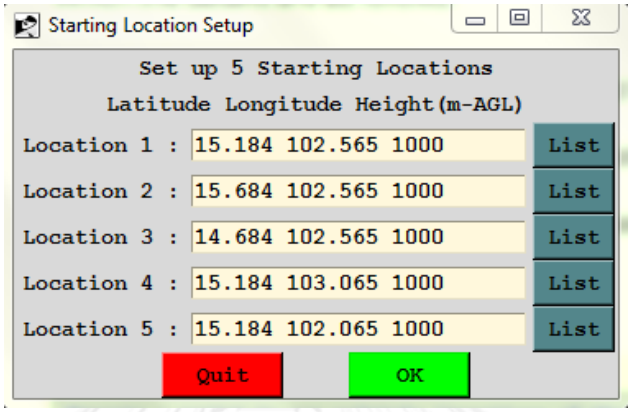

Figure 3.21 Starting location setup for trajectory analysis

3. *Total run time* – The time that is used for illustrates the backward trajectory. For this study is set up back 10 days (-240 hours) illustration.
4. *Direction* – Choose "back" for backward trajectory.
5. *Top of model* – The highest height that need to be the computing border. This set up at 20 km. (20000 m.) above mean sea level.
6. *Vertical motion method* – Choose "0 = input model data"
7. *Meteorology files* - NCEP/NCAR reanalysis meteorological data are added.

After set up step, the model is ready to run a simulation. This simulation can provide out only a single result file in a run, then, it takes a long time for run out all simulations. However, HYSPLIT model provides a special feature, "Automated multiple trajectories" (Fig. 3.22) which can run many daily simulations in a month by takes only a few minutes.

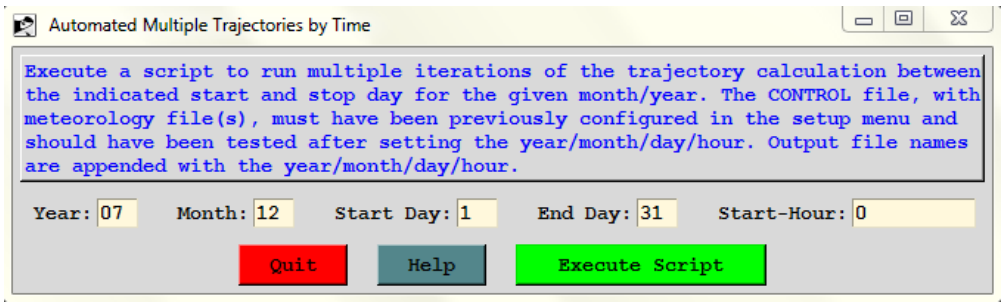

Figure 3.22 Automated multiple trajectories in HYSPLT model

In order to simulate daily backward trajectories during 1 to 31 Dec, 2007 and starting trajectory time at 0000UTC (07.00 AM at local time), we set the date and time as shown in Fig. 3.22 and execute script to run simulations. However, before do this special feature, we have to make sure that had set up all steps as shown in Fig. 3.20.

3.5.2 Results from backward trajectory analysis.

After simulation, the model gives 2 files: 1.Picture of trajectory illustration and 2.Trajectory informations. The result is shown in the Fig. 3.23 below.

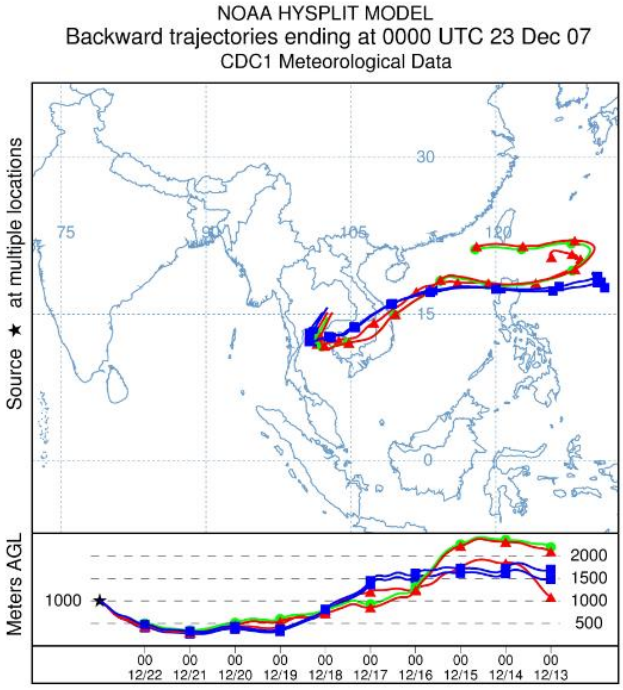

Figure 3.23 Result picture of backward trajectory

Figure 3.23 shows a sample result of backward trajectories (trajectory illustration picture) that started at 0000 UTC (0700 AM local time) 23 Dec, 2007 and finished at 0000 UTC 13 Dec, 2007 (10 days long). The picture also shows the same pattern of all trajectories (5 trajectories) which reveals a homogenous air mass.

Another result is the trajectory information which contains details of trajectory i.e. starting position, trajectory position, date, time, pressure and height.

After simulated all trajectories, these results will be used as a data base for classification of air mass types which is reported in Chapter IV

3.6 Data analysis procedures

This is an important step after all data were prepared and analyzed. This step is the key to answer the study's objectives. This study carries on for investigation the tropospheric O_3 seasonal variations and relations between its factors which depend on air mass types. To clearly understand, the chart below shows the flow step of data analysis.

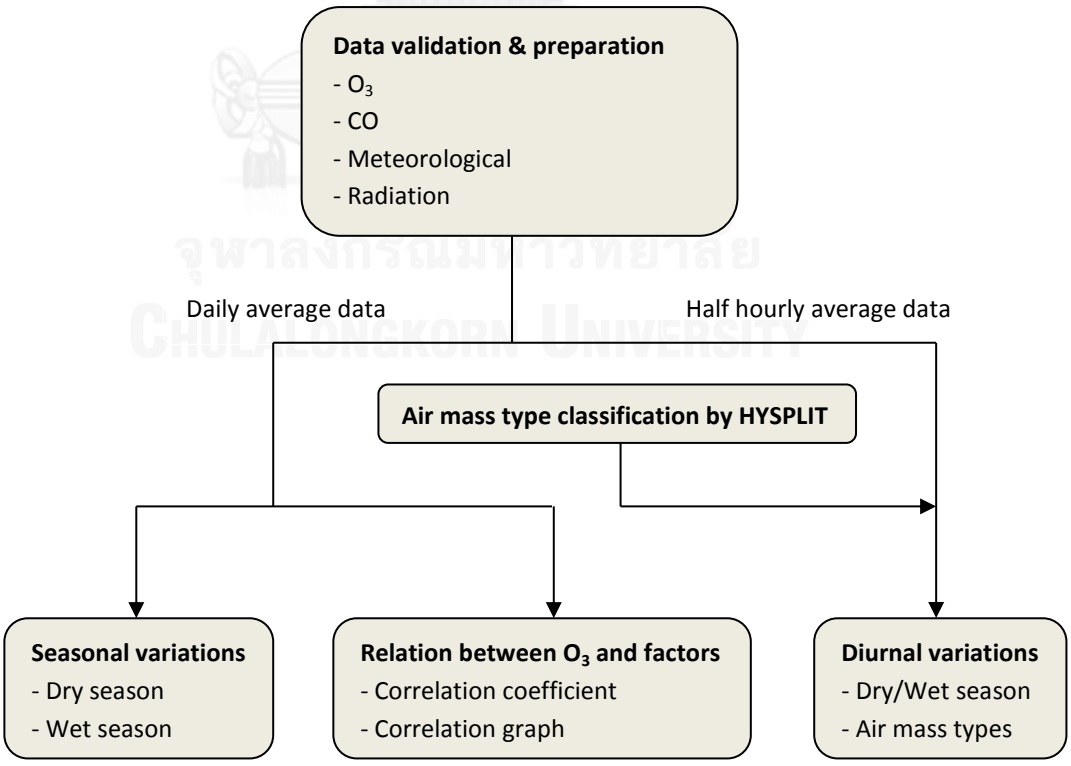

Figure 3.24 Data analysis flow chart

The analysis is divided into 3 main categories which are O_3 seasonal variations, O_3 diurnal variations and relation between O_3 and its factors. This flow chart started at step which all data were prepared, these data were separately calculated into daily average and half hourly average data. Daily average data were used for analysis of seasonal variations and O_3- factors relations. Half hourly average data were used together with results from air mass classification for analysis of diurnal variations.

The detail of each analysis category is briefly described below.

1) O_3 seasonal variations analysis

To reveals the O_3 change pattern due to seasonal alternation, the daily average O_3 data were used. The used data are collected from September, 2007 to August, 2009. The results of this analysis could show a broad view of how O_3 changes and trends in 2 years. In addition, another daily data, such as CO, were also used to estimate the relations between them and O_3.

2) O_3 diurnal variations analysis

O_3 changes in one day (24 hrs.) are the results from this analysis. To shows how O_3 vary in a whole day, the half hourly average O_3 data were employed. These results could reveal a general pattern of daily O_3 variation. Moreover, in order to understand i) the O_3 and factors interactions, another half hourly average data were co-analyzed, and ii) how does the season influences on O_3 behavior, the results from air mass classification are used to describe results from this analysis such type of air mass.

3) Relations between O_3 and tis factors

The statistical method is a useful tool to demonstrate any hypothesis. This study employs the correlation analysis. Which is a tool to determine the direction and strength of relationship between two variables in linear form. From calculation of the correlation coefficient (***R***), it can imply how strong and which direction the relation is. Also, relationships between O_3 and each factor are investigated with correlation analysis by using SPSS program and daily average data bases.

CHAPTER IV

RESULTS

In this Chapter the results of O_3 and other parameters observed at Phimai site during September 2007 to August 2009 from overall analysis will be presented in seasonal variation, diurnal variation, variations based on type of air masses, and relation between O_3 and factors by correlation coefficient.

4.1 Seasonal Variations of O_3

The long term plots (2 years) of the daily average of O_3 and CO are illustrated in Figure 4.1. It can be seen that the seasonal variations of O_3 and CO were high in dry season during December to April and low in wet season during June to October. Moreover, it also shows the fluctuations of O_3 and CO that were high during December to April and low during June to October. The figure also shows the coincident seasonal variations between O_3 and CO, though there were incomplete data in CO, but it could imply their relations. As reviewed in Chapter 2, CO is a precursor of O_3 that supports to O_3 production.

The highest daily O_3 and CO concentrations were 63.8 and 909.4 ppb on 5 March 2008 and 25 January 2008 (dry season) respectively. The lowest daily O_3 and CO concentrations were 9.0 and 105.3 ppb in 19 June 2009 and 18 July 2008 (wet season) respectively.

In order to substantiate the resemblance of 2 years seasonal variations of O_3, the Fig. 4.2 is illustrated with division into two periods; Sep 07 – Aug 08 and Sep 08 – Aug 09. Overview, the variations in both periods were agreeable, the variations were high during December to April especially in the local summer and low during June to late September.

Seasonal variations of O_3 will be discussed again in Chapter V with the results from previous studies.

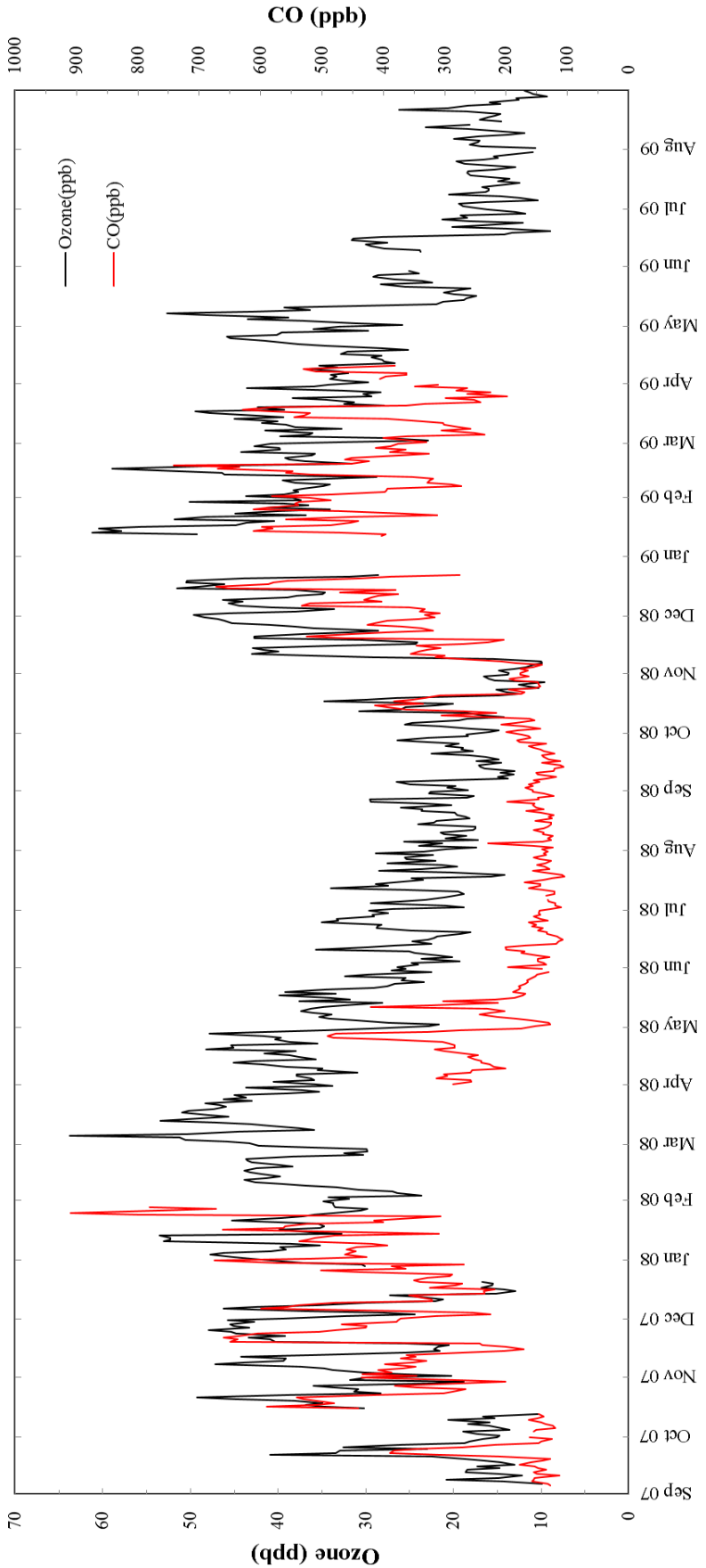

Figure 4.1 Seasonal variations of O_3 and CO during September, 2007 - August, 2009.
O_3 and CO showed as daily average.

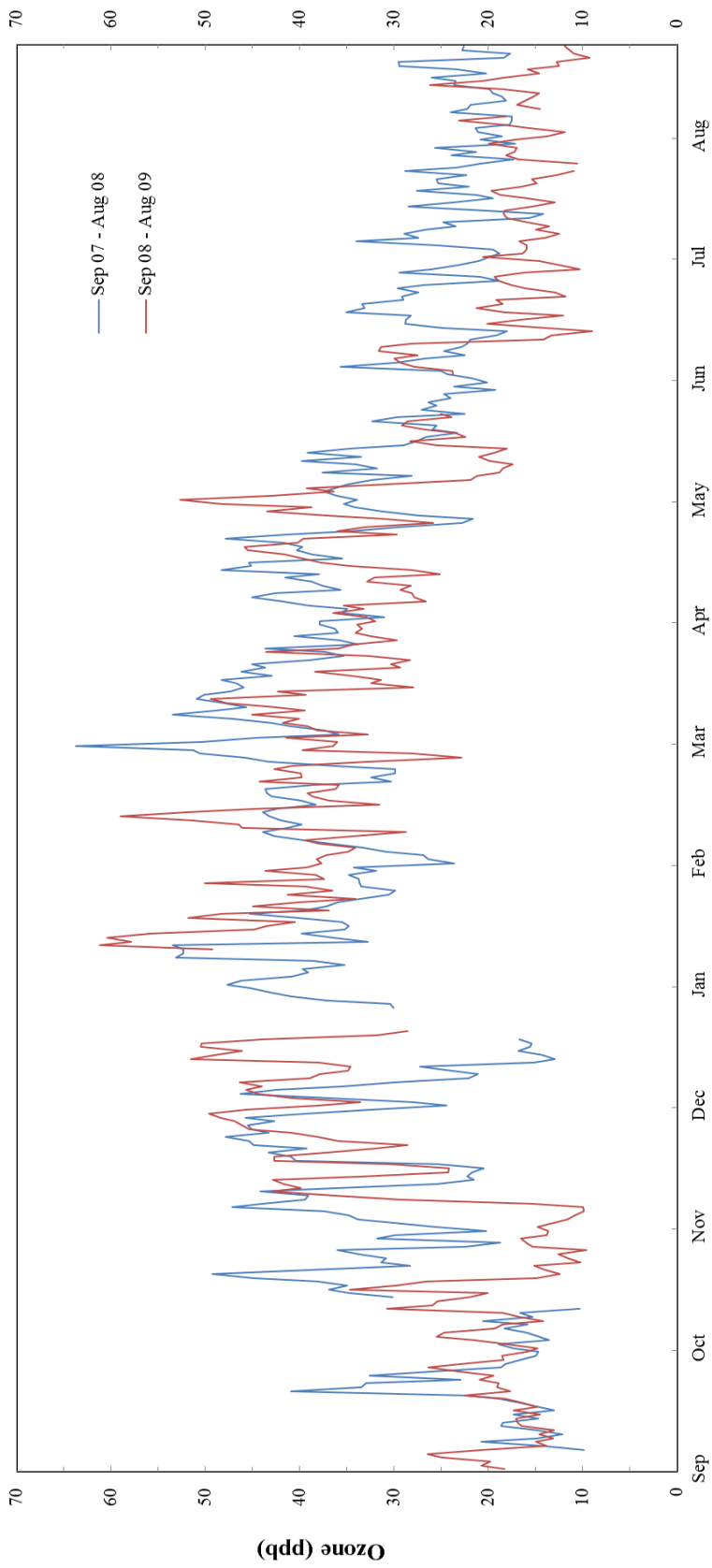

Figure 4.2 Seasonal variations of O_3 comparing between Sep 2007 to Aug 2008 and Sep 2008 to Aug 2009.

The monthly statistical data of O_3 at Phimai over 2 years periods during September 2007 to August 2009 are illustrated in Fig. 4.3 and the monthly average, the annual average, the observation time are also presented in table 4.1.

From table 4.1, the maximum monthly average is 45.7 ppb in January 2009 and the minimum is 15.8 ppb in July 2009. However, it can be seen that monthly averages of O_3 concentration approximate to the same month in different year and the annual averages of both periods were similar. Excepting for December, it should be noted that there were very different, monthly average of O_3 were 27.6 and 42.1 ppb in 2007 and 2008 respectively. Moreover, monthly average of O_3 in December 2007 also lowered than other months in dry season at the same annual period. It was shown clearly in Fig. 4.3 that the monthly boxplot in December 2007 dropped when compare to other months. This uncommon phenomenon will be investigated with trajectory analysis and discussed again in Chapter V.

Table 4.1 Statistical result of O_3 monthly average ± 1 standard deviation in ppb unit and the numbers in parenthesis are measurement hours.

Sep 2007 – Aug 2008		Sep 2008 – Sep 2009	
Month	Ozone (ppb)	Month	Ozone (ppb)
Sep-07	20.0 ± 12.4 (599.5)	Sep-08	18.7 ± 8.5 (719.5)
Oct-07	26.4 ± 13.2 (694)	Oct-08	18.9 ± 10.2 (743.5)
Nov-07	36.5 ± 13.2 (719.5)	Nov-08	31.0 ± 14.6 (719.5)
Dec-07	27.6 ± 11.6 (584.5)	Dec-08	42.1 ± 11.9 (526.5)
Jan-08	39.7 ± 13.7 (743.5)	Jan-09	45.7 ± 13.8 (480)
Feb-08	36.9 ± 11.0 (695.5)	Feb-09	40.4 ± 14.8 (671.5)
Mar-08	45.4 ± 16.0 (743.5)	Mar-09	36.6 ± 15.9 (743.5)
Apr-08	39.1 ± 14.2 (719.5)	Apr-09	33.9 ± 11.8 (719.5)
May-08	30.9 ± 9.9 (743.5)	May-09	28.9 ± 12.9 (681.5)
Jun-08	26.0 ± 10.4 (719.5)	Jun-09	20.9 ± 10.4 (518)
Jul-08	23.7 ± 9.1 (738.5)	Jul-09	15.8 ± 6.8 (685.5)
Aug-08	21.4 ± 9.4 (743.5)	Aug-09	15.9 ± 8.5 (711)
Annual	31.4 ± 14.5 (8444.5)	Annual	28.4 ± 15.6 (7919.5)

In this topic, we have discussed only the seasonal variation which is the broad view of long term change. In order to understand the variations in the short term change of daily variation, results of diurnal variation will be shown in the next topic.

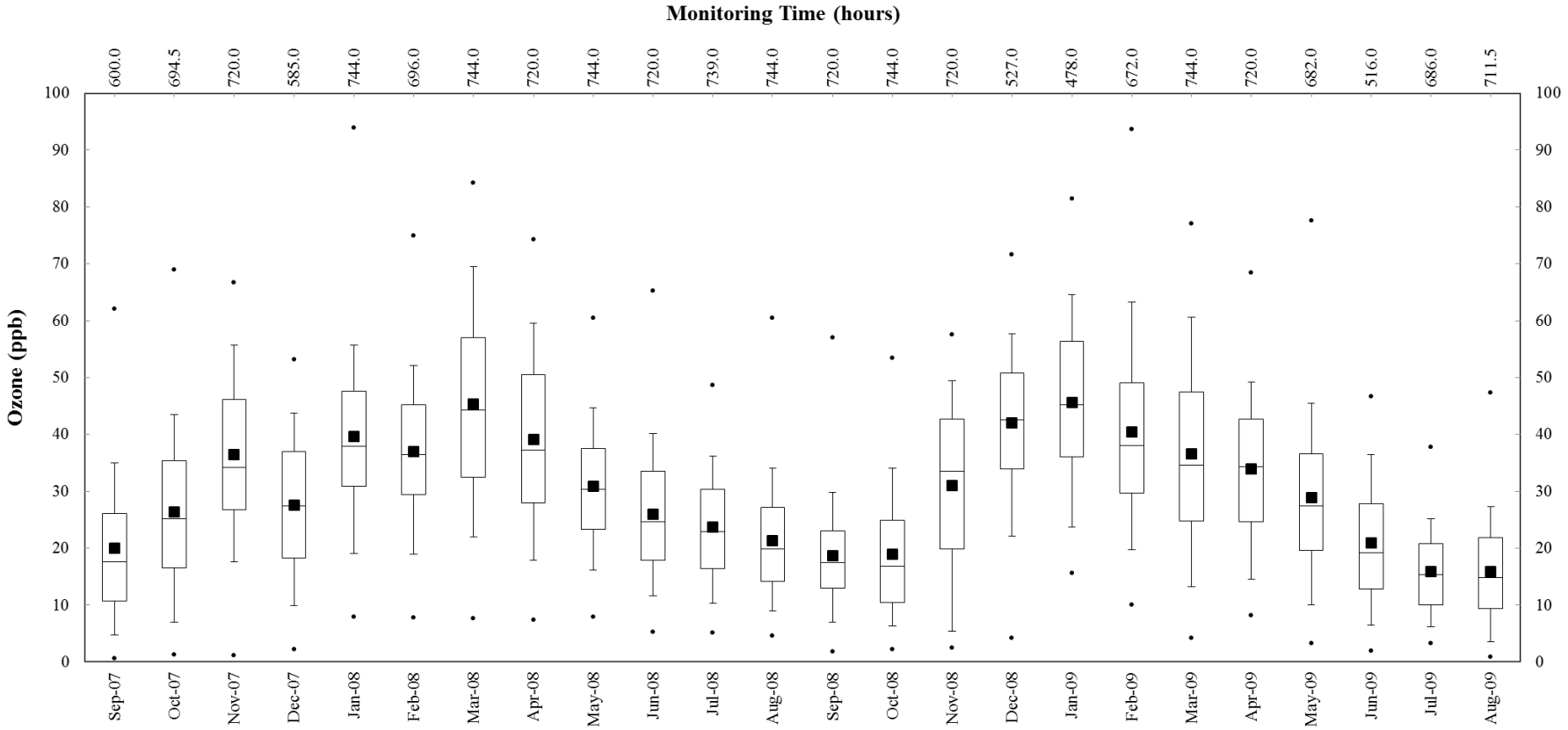

Figure 4.3 Monthly statistical boxplots of O_3 during September, 2007 – August, 2009 base on half-hourly data.The down cap, bottom of the box, middle line of the box, top of the box, and upper cap represent 5th, 25th, 50th (median), 75th, 95th percentile, respectively. The solid square in the middle of the box represent the monthly average. The bottom dot and top dot are the lowest and the highest half-hourly in that month.

4.2 Diurnal Variations of O_3

4.2.1 Averaged all diurnal variation of O_3

The overall average of diurnal variation of O_3 is plotted in Fig. 4.5 below.

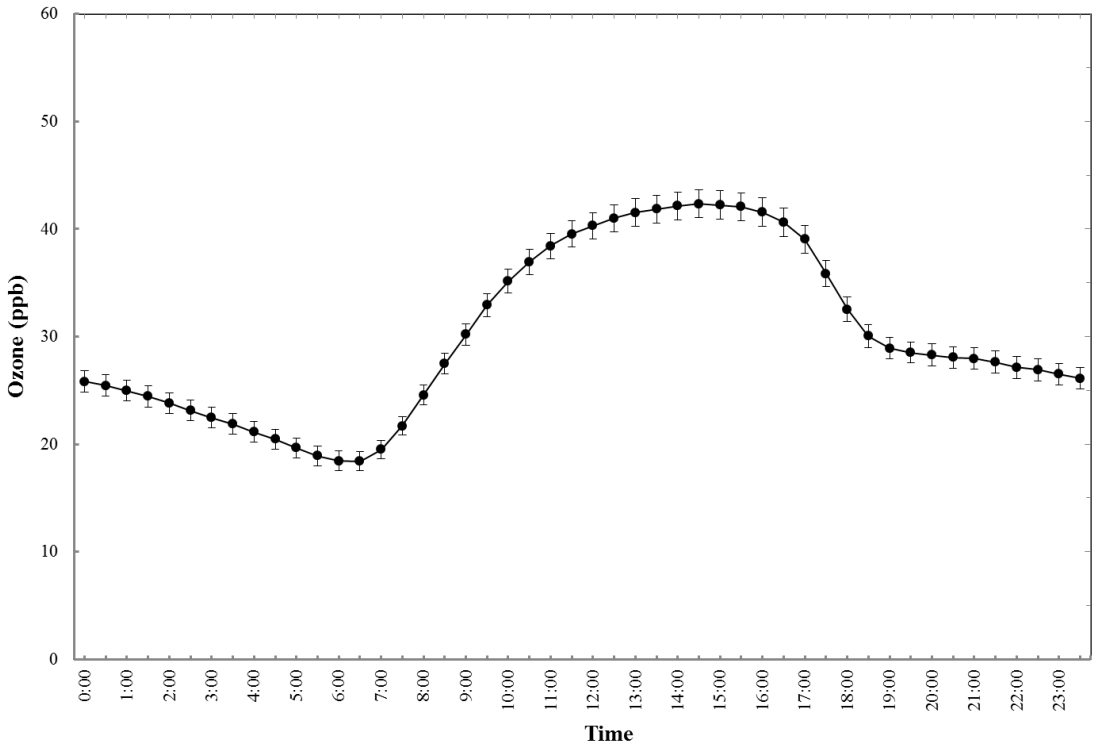

Figure 4.4 Average of all diurnal variation of O_3 during Sep 07 to Aug 09. The solid dot and bar represents half hourly average and ± 1 standard deviation, respectively.

From Fig. 4.4 the O_3 variations during a day are depend on time of the day, lowest concentration of O_3 starts in the early morning around 6 AM, where absent sunlight inhibits the photochemical process and led to O_3 destruction. After sunrise and presence of sunlight, O_3 concentration increases rapidly around 7 to 12 AM and reaches maximum concentration around afternoon (14 – 15 PM). During the day time, production of O_3 occurred by photochemical reaction, O_3 concentration rises together with increasing of radiation intensity. In the late afternoon to early night, O_3 concentration decreases rapidly around 16 PM to 19 PM, implies to the destruction rate of O_3 which is greater than production rate because of the decreasing of

radiation. Finally, with the absence of sunlight condition, O_3 decreases slightly during night time until before 6 AM.

4.2.2 Diurnal variation in wet and dry season

Phimai site is located at 212 m. above mean sea level in boundary layer. This is agreeable with diurnal variations that were observed with high during daytime and low during nighttime. To demonstrate the diurnal variations associated with season, the figure below (Fig. 4.5) illustrates the diurnal variations that were separated into dry and wet season; December, January, February, March, and April for dry season, June, July, August, September, and October for wet season months.

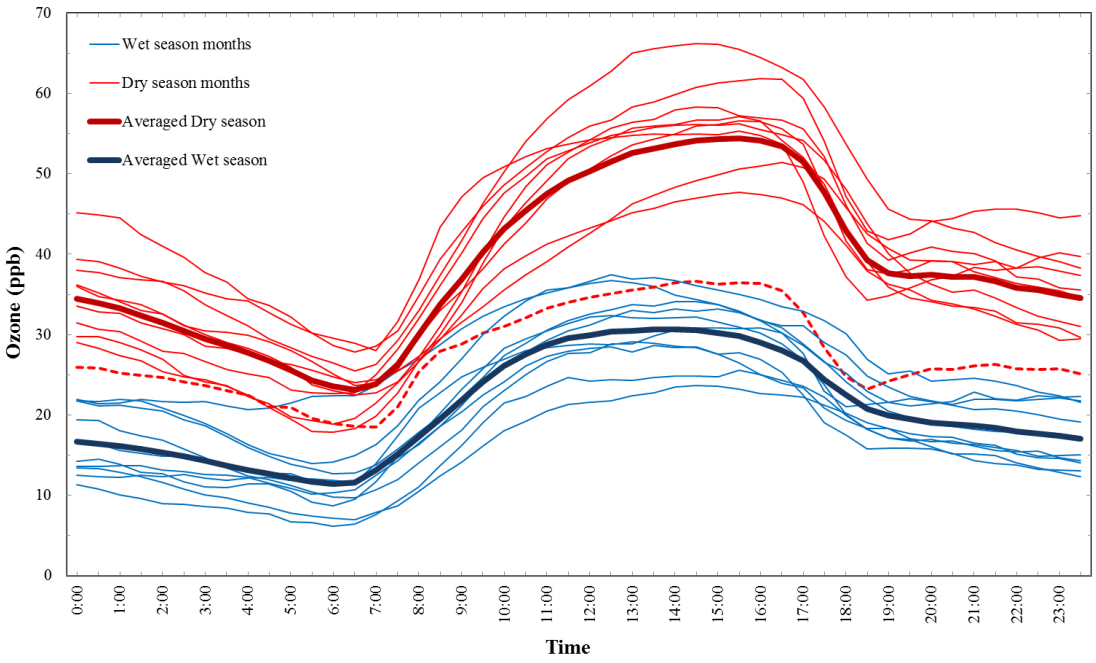

Figure 4.5 Diurnal variations of O_3 based on averaged dry and wet season months and averaged dry and wet season.

It can be seen from Fig. 4.5 that all months shows diurnal maximum in afternoon whereas diurnal minimum occurred in early morning. This figure also shows the differences between dry and wet season in diurnal variation. The higher diurnal cycle around 20 to over 60 ppb ranges were observed in dry season. It can be seen that most of those the red lines are higher than the blue lines except red dot line which is the uncommon phenomenon in December 2007 as mentioned in

previous topic 4.1. Wet season was observed to have low diurnal cycle with range 10 to below 40 ppb. However, the averages of dry and wet season months (red thick line for dry season and blue thick line for wet season) show explicitly that those two seasons were different in level of O_3 concentration but have the same pattern of diurnal variation of O_3.

4.3 O_3 behavior associated to backward trajectory analysis

Long-range transport of air mass influences on O_3 behavior. In order to investigate this effect, backward trajectory was employed. In this topic, O_3 characteristics at Phimai will be illustrated with classified air masses. Moreover, the hot spot fire maps were used to trace sources of CO as well.

4.3.1 Air mass categorization by backward trajectory analysis

In Chapter III, we had explained an overview of HYSPLIT model and trajectory analysis including steps of primary setting in model. Daily trajectories during September 2007 to August 2009 were set the starting point at the exact location of the observatory for atmospheric research at Phimai. And four others point displaced ± 0.5 longitude and latitude from exact location in order to investigate a homogeneous trajectory. The starting time at 0000 UTC or 7 AM local time for Thailand, starting 1,000 meters over mean sea level, and 10 days long of backward.

The results from backward trajectory analysis were categorized into six groups which are illustrated in Fig. 4.6.; Northeast Continental air mass (NE-C), Northeast/East Continental and Marine air mass (NEE-CM), Northeast/East/South Marine air mass (NEES-M), and Southwest Marine air mass (SW-M), these main four groups for investigation with O_3, others; Multiple, and Unclassified.

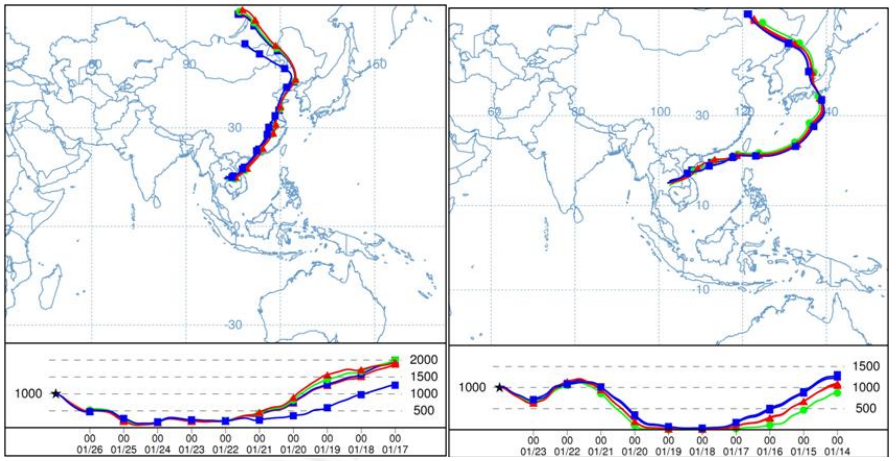

(a) NE Continental air mass (b) NE/E Continental & Marine air mass

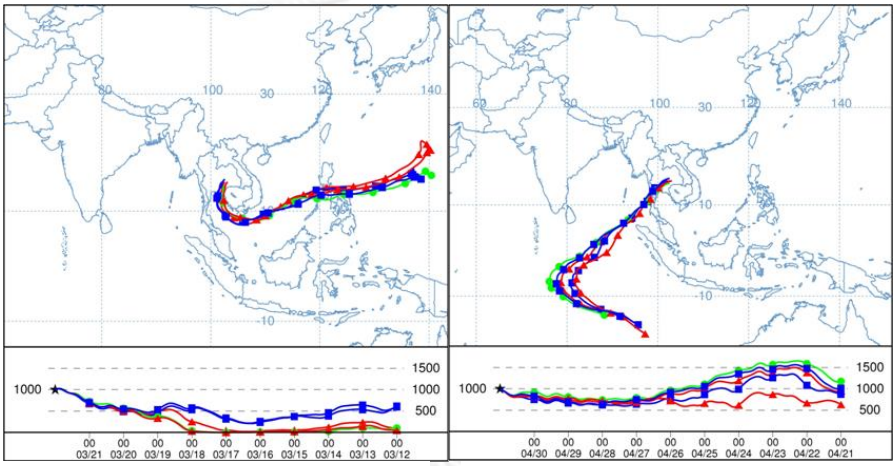

(c) NE/E/S Marine air mass (d) SW Marine air mass

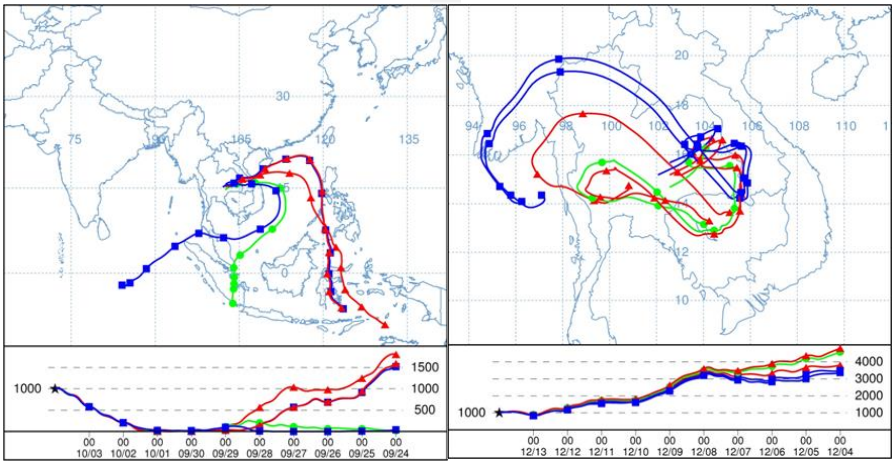

(e) Multiple (f) Unclassified

Figure 4.6 The types of air masses reaching at Phimai are classified by backward trajectory analysis starting point at 1,000 m asl. The symbols represent 24 hours

All types of air masses were classified with two conditions; 1) origination area of air mass, 2) transport time duration on continental and maritime areas. Explanations of each air mass are illustrated following below.

1). Northeast Continental air mass (NE-C)

NE-C is illustrated as sample in Figure 4.6 (a). This air mass originated on continent over North Asia and flows along this area to the Phimai site. The route of this air mass probably passed over maritime area of Pacific Ocean but less than 50% of total transportation time. Generally, NE-C air mass reached to Phimai site with north to east direction (0 – 90 degree). The condition of this air mass is thought to be dry and polluted due to it passed over the area in which low humidity and high anthropogenic emission such as eastern part of China. O_3 and precursors are assumed to be high with this air mass.

2). Northeast/East Continental and Marine air mass (NEE-CM)

NEE-CM type (Fig. 4.6 (b)) originated on continent as NE-C, but it passed over maritime area in Pacific Ocean more than 50% of total transport time. During it passing maritime area, by assumption, even it originated over high emission areas and carrying pollutants, but these pollutants might be washed by high humidity or precipitation, diluted by clean air, and reaction with OH. Therefore, O_3 and precursors that were carried to Phimai site by this air mass will be observed with lower concentration than those in NE-C type together with higher humidity. Normally, NEE-CM reaches to Phimai site with northeast to east direction (45 – 90 degree).

3). Northeast/East/South Marine air mass (NEES-M)

This NEES-M type (Fig. 4.6 (c)) originated on maritime area in Pacific Ocean. Most of transport time is on Pacific Ocean. However, this air mass type involves with NE-C and NEE-CM types which these 3 types often occur in the same period. Due to we have examined backward only 10 days long, NEES-M probably originated on continent if backward more than 10 days. This air mass mostly moves in maritime area, then, O_3 and precursors are observed with lower concentration than NE-C and

NEE-CM. NEES-M reaches to Phimai site with broad direction, northeast to south (45 – 180 degree).

4). Southwest Marine air mass (SW-M)

This air mass related to southwest monsoon that mainly occurs during wet season in Thailand. It originated in maritime area of Indian Ocean as shown in Fig. 4.6 (d). Most of total trajectory time passed over clean area in which very low emission activities in Indian Ocean before reaching to Phimai, therefore, SW-M is thought to be moist and cleanest air mass among all types of air mass. For these reasons, O_3 and precursors are lowest when compared to other types. However, due to Phimai site is located in the central of Indochina peninsula, SW-M possibly passed over Bangkok metropolis which is the mega city in central part of Thailand which is the high emission area, these may affects to O_3 at Phimai site.

5). Multiple air mass

Multiple air masses occurred with low frequencies. It is results from many air masses are convergent from difference directions as shown in Fig. 4.6 (e). There were no significant variations of O_3 with this type.

6). Unclassified air mass

The type of air mass that cannot be categorized, formless route, different from all 5 types of air masses.

4.3.2 Frequency for each type of backward trajectory

Monthly frequencies of backward trajectories are illustrated in Table 4.2.

Table 4.2 Monthly frequencies for each type of backward trajectory that reached to Phimai site during September 2007 to August 2009.

Month	Frequency (%) in a month					
	NE-C	NEE-CM	NEES-M	SW-M	Multiple	Unclassified
Sep-07	20	—	—	76	—	4
Oct-07	26	16	16	39	3	—
Nov-07	47	27	17	—	—	10
Dec-07	19	10	61	—	—	10
Jan-08	52	35	6	—	—	6
Feb-08	69	24	3	—	—	3
Mar-08	29	13	58	—	—	—
Apr-08	10	—	87	—	—	3
May-08	—	—	—	87	13	—
Jun-08	—	—	—	100	—	—
Jul-08	—	—	—	100	—	—
Aug-08	—	—	—	100	—	—
Annual	22	11	21	42	1	3
Sep-08	—	—	20	77	3	—
Oct-08	19	23	29	19	3	6
Nov-08	50	13	20	7	—	10
Dec-08	53	17	3	—	—	27
Jan-09	70	—	17	—	—	13
Feb-09	32	—	46	—	—	21
Mar-09	13	—	71	—	—	16
Apr-09	—	20	37	40	3	—
May-09	6	6	23	65	—	—
Jun-09	—	—	—	100	—	—
Jul-09	—	—	—	100	—	—
Aug-09	—	—-	3	87	—	10
Annual	20	7	22	42	1	9

As showed in Table 4.2, annual frequencies in both periods were prevailed by SW-M with 42%, followed by NE-C, NEES-M and NEE-CM. SW-M influenced on Phimai site in wet season especially in June, July, August, and September. NE-C influenced

around in January which is mid dry season, while, NEES-M influenced in late dry season or local summer in Thailand during March to April. NEE-CM occurred with lower frequency and sparse pattern during dry season.

The 2 years (September 2007 to August 2009) averaged frequencies for each type of backward trajectory reaching to Phimai is shown in Fig. 4.7. It can be seen that the air mass that originated on continent particularly NE-C type, starting in late wet season during September – October and then predominantly in mid-dry season or local winter during November to February and declined in late dry season or local summer. Another continental originated, NEE-CM, it is sparse with low frequencies during the same period as NE-C. Maritime origin type, NEES-M rather differs from the continental originated types, it also occurred in the same period as NE-C and NEE-CM but with moderate frequencies during early to mid-dry season and predominantly in late dry season especially in March and April. SW-M type totally differs from the first 3 types, it occurred in late dry season and completely influences during mid-dry season as can be seen that 100% in June and July.

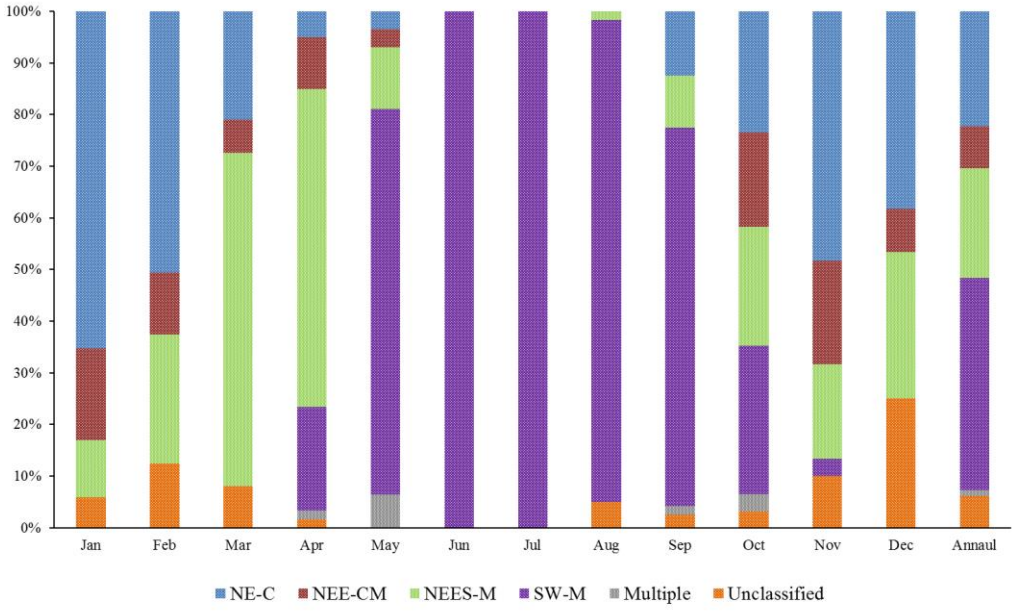

Figure 4.7 2 years frequencies average for each type of backward trajectory

4.3.3 O_3 variations based on air mass trajectories

Monthly averages of O_3 for each type of trajectories are shown in Table 4.3. It can be seen from this table that the annual average of O_3 in both years were highest in NE-C type and following by NEE-CM, NEES-M and lowest in SW-M. This reflects that the distinctions of O_3 between such four air mass types were results from singularity characteristic of each air mass.

Besides O_3, CO and humidity also shows different variations with air mass type. Therefore, in this topic, in order to thoroughly investigate about O_3 behavior, O_3 and other factors will be separately explained based on air mass type from categorization by backward trajectory analysis.

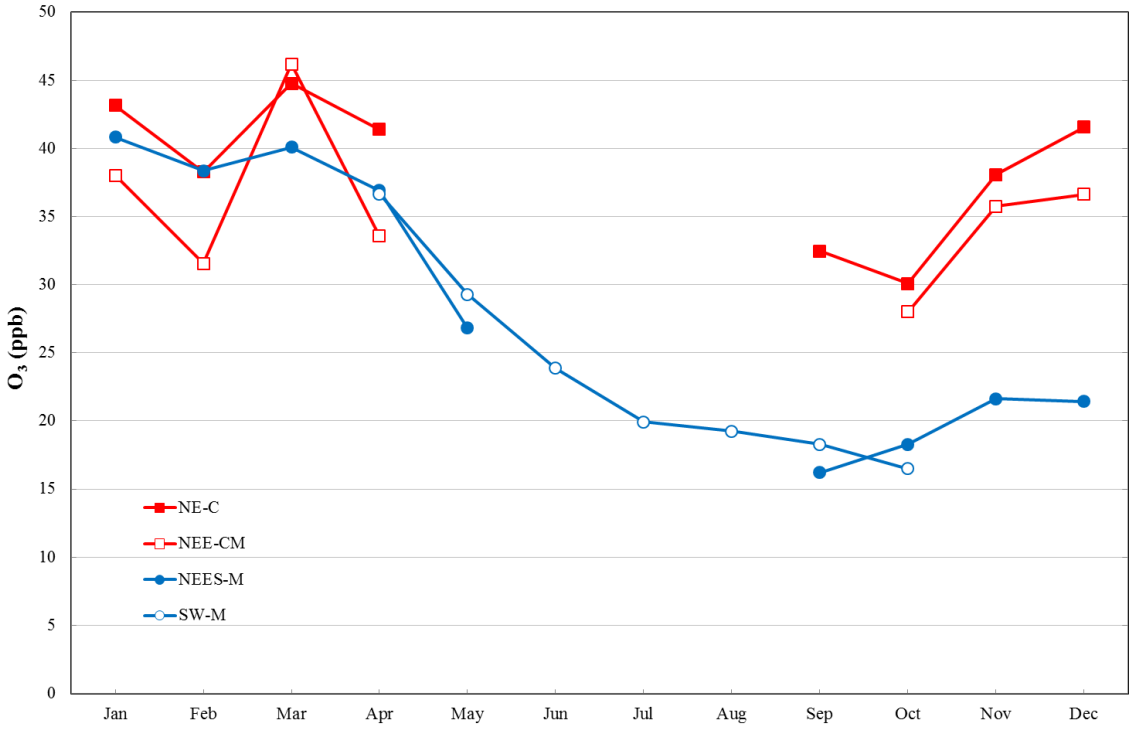

Figure 4.8 Monthly averages of O_3 during September 2007 to August 2009 categorized with backward trajectory.

Table 4.3 Monthly averages of O_3 ± 1 standard deviation in ppb unit based on backward trajectories.

Month	NE-C	NEE-CM	NEES-M	SW-M
Sep-07	32.6 ± 16.0	—	—	17.0 ± 9.0
Oct-07	36.9 ± 11.2	34.4 ± 8.5	27.8 ± 10.3	15.8 ± 8.2
Nov-07	29.8 ± 11.1	36.1 ± 13.1	31.2 ± 13.3	—
Dec-07	36.7 ± 9.4	31.7 ± 7.7	20.1 ± 8.8	—
Jan-08	39.8 ± 11.0	38.0 ± 15.9	44.4 ± 16.7	—
Feb-08	38.8 ± 10.6	31.6 ± 10.6	29.9 ± 7.1	—
Mar-08	47.0 ± 11.7	46.2 ± 14.3	44.4 ± 18.0	—
Apr-08	41.4 ± 14.3	—	39.3 ± 14.3	
May-08	—	—	—	30.7 ± 10.4
Jun-08	—	—	—	26.0 ± 10.4
Jul-08	—	—	—	23.7 ± 9.1
Aug-08	—	—	—	21.4 ± 9.4
Annual	38.5 ± 12.3	36.3 ± 13.6	35.8 ± 16.7	23.5 ± 10.7
Sep-08	—	—	16.2 ± 9.2	19.3 ± 8.2
Oct-08	21.0 ± 9.6	24.4 ± 11.0	13.2 ± 6.4	17.8 ± 8.5
Nov-08	38.1 ± 9.9	35.1 ± 10.1	13.7 ± 7.8	13.9 ± 8.4
Dec-08	44.2 ± 11.3	51.6 ± 11.8	37.9 ± 11.5	—
Jan-09	46.8 ± 13.8	—	38.5 ± 10.6	—
Feb-09	37.3 ± 10.6	—	39.0 ± 15.9	—
Mar-09	—	—	36.6 ± 15.9	—
Apr-09	—	33.6 ± 10.5	31.4 ± 10.8	36.7 ± 12.8
May-09	37.4 ± 9.9	41.4 ± 11.0	24.8 ± 16.0	27.1 ± 10.4
Jun-09	—	—	—	20.9 ± 10.4
Jul-09	—	—	—	15.8 ± 6.8
Aug-09	—	—	9.3 ± 5.0	16.4 ± 8.9
Annual	39.4 ± 13.4	32.8 ± 12.9	29.0 ± 16.6	20.7 ± 11.1

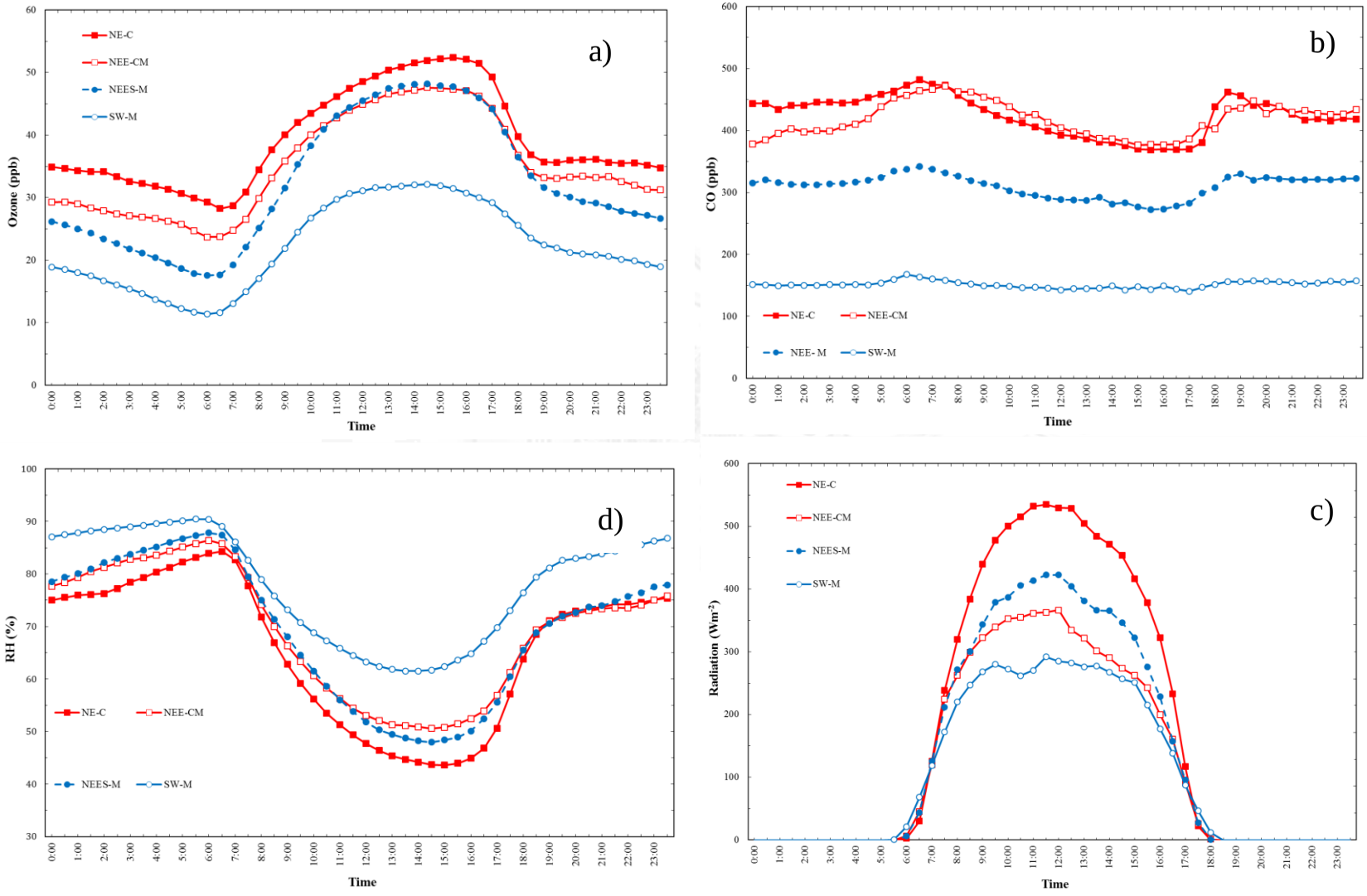

Figure 4.9 Diurnal variations of a) O_3, b) CO, c) RH, and d) direct radiation categorized by

1). O_3 with Northeast continental air mass (NE-C)

O_3 associated with this air mass type is thought to be highest concentration. Table 4.3 shows the highest O_3 concentration in both annual periods (38.5 and 39.5 ppb). Because this air mass type transported over Northern Asian continent more than 50% of total transportation time. Northern part of Asia especially east China, this area is knew that its anthropogenic emission is high.

The Northeast continental air mass mostly occurred in dry season or local winter in Thailand during November to February. O_3 concentration at Phimai site during these months were observed with high level by associated with NE-C air mass as shown in Fig. 4.8.

Fig. 4.9 a) illustrates diurnal variations of O_3 at Phimai site categorized by air mass trajectories. It can be seen that O_3 variation in NE-C air mass is highest for the whole day. This is agreeable with diurnal variations of CO, RH, and direct radiation. NE-C originated on a dry and cold area of continental North Asia and travelled across anthropogenic emission areas on East Asia and Southeast Asia continental, therefore, diurnal variations of CO, RH, and direct radiation in Fig. 4.9 b), c), and d) are the results from this air mass characteristic.

2). O_3 with Northeast/East Continental and Marine air mass (NEE-CM)

Second group of air mass that closely associated with NE-C air mass is the Northeast/East Continental and Marine air mass (NEE-CM). NEE-CM sparsely occurred with low frequency in the same period with NE-C. However, NEE-CM has different characteristic from NE-C, even NEE-CM has an origin on continent as NE-C, but it has transported more than 50% of total transportation time over maritime area of Pacific Ocean. Therefore, NEE-CM will be influenced by two environments of Northern Asian continent and Pacific Ocean.

From Fig. 4.8, the monthly average of O_3 concentration shows significant lower than NE-C except for March. And 4.9 a), O_3 diurnal variation in NEE-CM is significantly lower than NE-C (36.2 and 32.1 ppb for annual average from Table 4.3).

Even if CO diurnal variation in NEE-CM is not different from NE-C (Fig. 4.9 b)), but the diurnal variations of RH and direct radiation (Fig. 4.9 c) and d)) are different from NE-C; RH shows higher and direct radiation shows lower diurnal cycle.

3). O_3 with Northeast/East/South Marine air mass (NEES-M)

Marine originated air mass that reached to Phimai site during dry season especially in local summer months (March and April) is Northeast/East/South Marine air mass (NEES-M). It originated on maritime area of Pacific Ocean and transported mainly on Pacific before reaching onshore.

O_3 associated with NEES-M shows lower concentrations than NE-C and NEE-CM types (35.8 and 29.0 ppb for annual average from Table 4.3). However, it can be noted from Fig. 4.9 a) that O_3 diurnal variation in NEES-M is adjacent to O_3 diurnal variation in NEE-CM during 11AM to 18PM. This indicates that the amplitude (maximum – minimum) of O_3 variation in NEES-M is higher than NEE-CM. Higher O_3 variation during daytime in NEES-M implies to the strong photochemical production of O_3 in NEES-M air mass which will be discussed again in Chapter V.

In addition, due to NEES-M type originated on maritime area as Southwest Marine air mass (SW-M), O_3 and CO concentrations in NEES-M and SW-M should be similar to each other. However, in fact, O_3 and CO concentrations in NEES-M were found significantly higher than in SW-M as seen obviously in Fig. 4.8, 4.9 a) and Table 4.3. It can be assumed that NEES-M is observed with high frequencies during March and April which is local summer of Thailand and neighboring countries (Cambodia, Laos, Myanmar, and Vietnam). During this period, anthropogenic activities are very strong especially biomass burning.

4). O_3 with Southwest Marine air mass (SW-M)

O_3 associated with Southwest Marine air mass (SW-M) is thought to be lowest concentration (23.5 and 20.7 ppb for annual average from Table 4.3). SW-M is dominant in wet season during May to September and occurred with highest frequencies when compared to other air mass types (Fig. 4.7). SW-M originated on

remote maritime area of Indian Ocean and most of total transport time over Indian Ocean before reaching onshore.

Even SW-M transported over remote clean area of Indian Ocean but when it reaches onshore of continental Southeast Asia it may blows across Bangkok metropolis mega city before arriving to Phimai site. However, O_3 diurnal variation (Fig. 4.9 a)) and O_3 monthly average (Fig. 4.8) in SW-M are lowest when compared to all of air mass types. The characteristics of SW-M are shown as evidence in Fig. 4.9, due to clean and moist condition, therefore, CO diurnal variation and direct radiation are lowest and RH shows highest variations. These conditions provided the lower O_3 concentrations in this air mass.

4.4 Relations between O_3 and its factors.

To investigate the relation between O_3 and its factors i.e. CO, RH, and direct radiation, correlation analysis is used. Daily average of each parameter was calculated by SPSS program. As O_3 and other parameters are not normally distributed. Therefore, a non-parametric statistical test, the Spearman's rank correlation analysis, is chosen to analyze the relationship between O_3 and others factors.

Table 4.4 Correlation coefficients between O_3 and its factors calculated using daily average from September 2007 to August 2009. Numbers in parenthesis represent daily average days.

	All	NE-C	NEE-CM	NEES-M	SW-M
CO	0.763 (486)	0.530 (112)	0.536 (40)	0.560 (114)	0.382 (176)
RH	-0.764 (600)	-0.469 (141)	-0.623 (57)	-0.734 (144)	-0.684 (212)
Direct radiation	0.188 (678)	0.009 (141)	0.122 (57)	-0.093 (145)	0.265 (286)

Correlations coefficients are shown in Table 4.4 by based on type of air masses. It can be seen that the strongest correlation are O_3/CO and O_3/RH with R^2 = 0.763 and -0.764, respectively, followed by O_3/Direct radiation with R^2 = -0.675 and 0.188, respectively.

Based on air mass type, relation between O_3 and CO is highest with R^2 of 0.560 in NEES-M follows by NE-C and NEE-CM with R^2 of 0.530 and 0.536, respectively. While, SW-M shows the lowest relation with R^2 = 0.382.

Correlation coefficients between O_3 and RH are high negative relation in both two types of marine originated air mass, R^2 = -0.734 and -0.684 for NEES-M and SW-M, respectively. Moderate negative correlation is found with R^2 = -0.623 in the air mass that involved with continental and maritime area, NEE-CM. And lowest negative correlation is found in continental originated air mass, NE-C, with R^2 = -0.469.

The correlation between O_3 and direct radiation shows weak or no correlation at Phimai site due to the lag of maximum peaks between O_3 and direct radiation.

Relations between O_3 and factors will be discussed again in Chapter V.

CHAPTER V
DISCUSSIONS AND CONCLUSIONS

In this Chapter, the results from Chapter IV will be discussed with further information such as the results from previous studies, and fire map from remote sensing.

5.1 Discussions

5.1.1 Seasonal variations of O_3

As mentioned in Topic 4.1, seasonal variations of O_3 shows high variation during dry season and low variations in wet season. These behaviors are agreeable to previous studies either in Thailand and other sites in Asia.

The previous study at two remote sites in Thailand (Inthanon and Srinakarin) by Pochanart et al. (2001) was reported that the seasonal variations of O_3 has high variability during dry season typically in March at both sites and low variability occurred during in mid wet season (August – September). Such results show the consonances with the seasonal variations of O_3 at Phimai site. The O_3 high variability in dry season and low variability in wet season are the normally characteristics of O_3 in the remote site of Thailand. However, such variability can be observed at other tropical areas, for examples, at Ahmedabad, India. O_3 concentrations were observed to be maximum during autumn and winter months and higher than those observed during summer months (Lal et al., 2000). From the study of Latif et al. (2012), at Klang Valley, Malaysia, which observed O_3 concentrations at nine stations, their report showed that there were distinct seasonal pattern in the surface O_3 across the Klang Valley: high O_3 concentration was usually observed during January to April, while low O_3 concentrations were observed during June to August.

Such tropical seasonal variations of O_3 are the results from prevailing monsoon winds on those areas. The monsoon winds carries an air mass from different sources (oceanic or continent) to the downwind areas. However, there are some tropical areas in which the different characteristics of seasonal variation of O_3 occurred. For instance, at Watukosek (Eastern area of Java island in Southern

hemisphere), Indonesia, the seasonal variations of O_3 in the lower and middle troposphere increased in September and October and decreased in November. Such O_3 enhancement related to the surface activities in Indonesia such as biomass burning. It is noted that September and October are the end of dry season in East Java which is the time of biomass burning is active (Komala et al., 1996). In addition, the study in Tanah Rata, Malaysia, Toh et al. (2013) found that the highest O_3 mixing ratios occurred in the southwest (SW) monsoon period which was coincident with the regional biomass burning season that normally starts around May to September or October. The SW monsoon wind passed Sumatra Island before reaching to Tanah Rata, therefore, the wind may carried the emitted pollutants or precursors of O_3 to the site. While, the lowest O_3 mixing ratios were observed during the spring intermonsoon.

Example studies firmly show that the seasonal variations of O_3 are different depending on area and monsoon time. Variations of O_3 in this study are low in wet season (SW monsoon) during June to October, but in the previous study in Tanah Rata, Malaysia O_3 concentration were high during the same period because of burning activities in Sumatra Island, Indonesia. Although this period is the wet season in the tropics in Northern hemisphere, but it is dry season in the Southern hemisphere such as in Watukosek, Indonesia. Therefore, the regional burning season gives the high variations of O_3 around downwind area. For these reasons, the route or trajectory of monsoon wind is necessary for interpretation and illustration the variations of O_3. In this study, the trajectory is also employed to investigate and explain why the variations of O_3 are different in each season.

As mentioned, the fluctuations of O_3 between dry and wet season were significantly different: high during December to April (dry season) and low during June to October (wet season). It is shown in Fig. 4.3 by percentile, the high fluctuations in dry season months shows longer percentile bar than those in wet season months. Moreover, Table 4.1 shows the highest standard deviation occurred in March at both annual periods with 16.0 and 15.9 ppb, in contrast, the lowest standard deviation occurred in July at both annual periods with 9.1 and 6.8 ppb. These indicate that the data in dry season were more dispersion than wet season and also imply that the

factors which are the independent variables that control O_3 concentration were different in each season.

To understand the seasonal variations of O_3 and other parameters during September 2007 to August 2009, Fig. 5.1 illustrates to compare O_3 and a) relative humidity (RH), b) wind direction, and c) direct radiation. The figure shows;

i) Seasonal variations of O_3 were adversative to RH, in dry season RH were low while O_3 were high, but it converse in wet season with high RH and low O_3,

ii) Wind directions with 50 – 100 degree or northeast to east wind were observed during dry season with high O_3 and the wind direction with 150 – 250 degree or south or southwest wind were observed during wet season with low O_3. Wind directions indicate that the monsoon wind influenced on observed site. It corresponds to seasonal variations of RH, high RH occurred during southwest monsoon or wet season, whereas, low RH occurred during northeast monsoon or dry season. However, the seasonal variations of direct radiation (Fig. 4.4 c) were not clear.

The seasonal characteristics of O_3 are the results from the composite of the regional scale, the long range transport, and the local dynamic or photochemical effect (Pochanart et al., 2001). From Fig. 4.1, it can be seen that variations of O_3 have changed day-by-day. Because of Phimai site located at area which is under the influence of monsoon, therefore, the days with high O_3 concentration during dry season are thought to be result from north east monsoon that transports the continental air mass from the northern part of Asia, conversely, the days with low O_3 concentration during wet season are result from southwest monsoon that transports the maritime air mass from the Indian Ocean. However, these conceptions will be thoroughly investigated by using the air mass classification based on trajectory analysis.

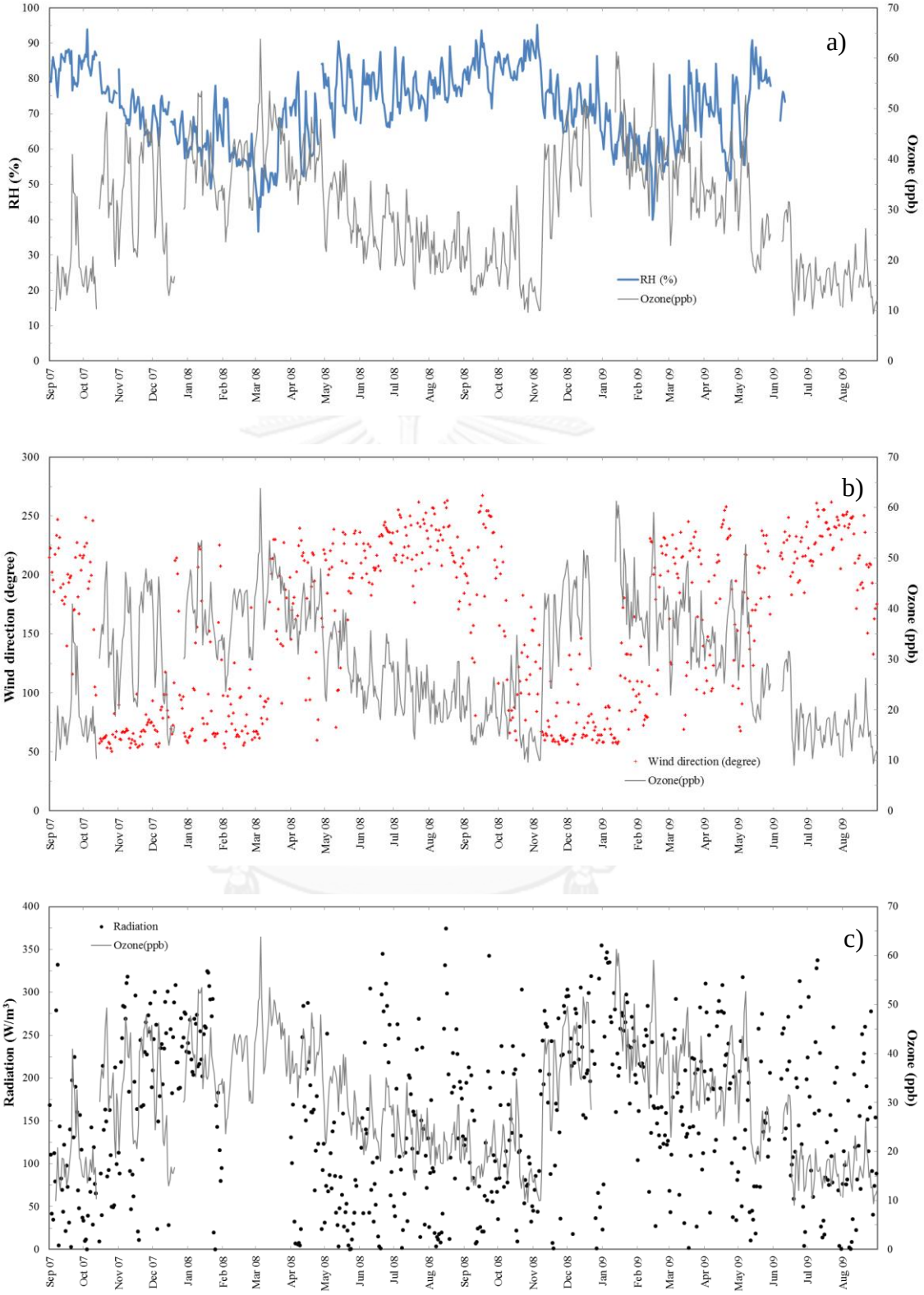

Figure 5.1 Seasonal variations of O_3 compared with a) Relative humidity (RH), b) Wind direction, and c) Direct radiation.

5.1.2 Diurnal variations of O_3

Pattern of diurnal variation of O_3 depends on areas and local weather condition, for example, diurnal variations of O_3 at Inthanon and Srinakarin, Thailand, shown in Fig. 5.2. It shows variations that were different by seasons and areas. There were constant or low variation in wet season at both sites due to vertical well mixed of the lower troposphere in this season. While strong diurnal variations in dry season were observed at both sites. However, 2,560 m. site at Inthanon shows no diurnal variation because this site is located higher than the boundary layer in which no effect from vertical mixing of air mass, while another sites are located in boundary layer (Pochanart et al., 2001).

However, diurnal variations in wet season at Phimai (Fig. 4.5) were higher than those variations in wet season at Inthanon and Srinakarin (Fig. 5.2), it can be assumed that the position of Phimai site are different from Inthanon and Srinakarin. Phimai site is located at the central of Indochina peninsular among agricultural areas, whereas Inthanon and Srinakarin sites are located at western part area near the Indian Ocean in which less anthropogenic activity. This assumption is related to the route of southwest monsoon wind which is originated in Indian Ocean. In wet season period, all sites are affected by southwest monsoon but the route of air mass that passed over continent to Phimai are longer than Inthanon and Srinakarin. Therefore, the air mass that reached to Phimai probably cumulating pollutants on continent more than the air mass that reached to Inthanon and Srinakarin. Moreover, the route of air mass to Phimai may passed Bangkok metropolis, the mega city in the central of Thailand which is a high anthropogenic emission area especially vehicles biomass burning. The example for air mass trajectory of southwest monsoon for Phimai and Inthanon sites are shown in Fig. 5.3.

Study of O_3 and other precursors in Bangkok metropolis was reported in 2002, the results revealed that O_3 concentrations were high especially in the downwind areas. Maximum hourly average of 370 ppb was observed in 1997 and the total hours exceeding the national hourly O_3 standard (100 ppb) for 314 hours (Zhang & Kim Oanh, 2002).

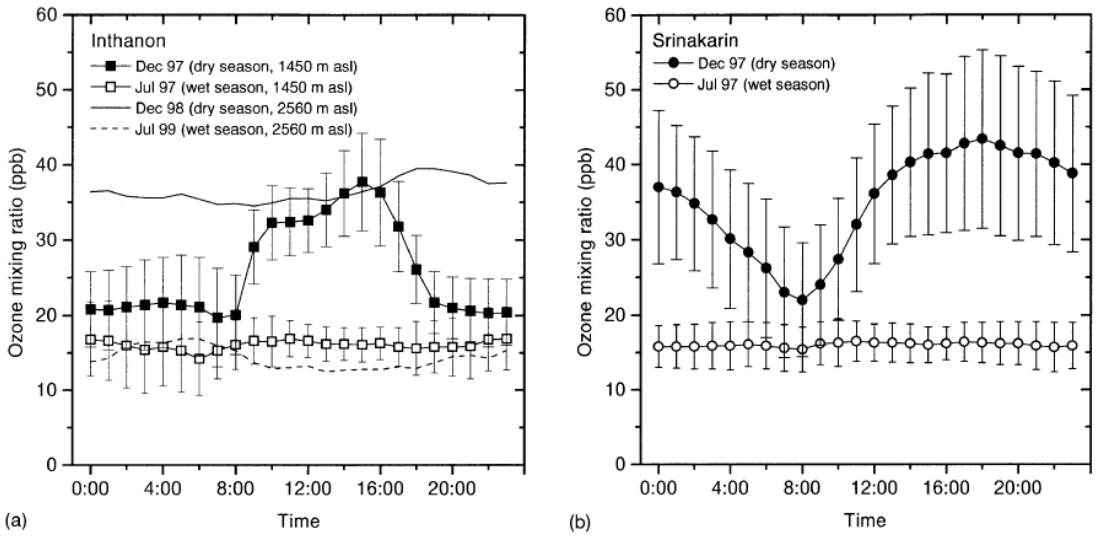

Figure 5.2 Diurnal variation of O_3 at (a) Inthanon and (b) Srinakarin (Pochanart et al., 2001).

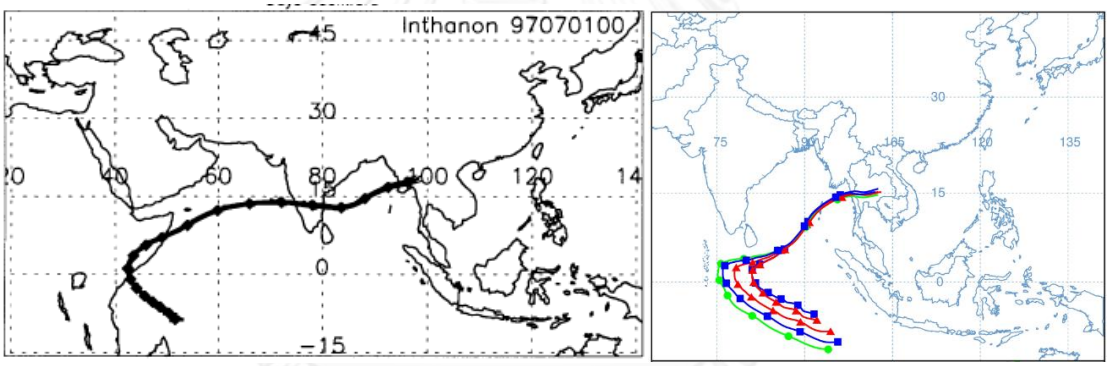

Figure 5.3 Air mass trajectory of southwest monsoon reached to Inthanon (left) (Pochanart et al., 2001) and Phimai sites (right).

The higher dry season and lower wet season in diurnal variations imply the influence of monsoon. As mentioned in the first part, northeast monsoon prevails in dry season and brings the continental air mass from northern Asia to Phimai site, while southwest monsoon prevails in wet season and brings the maritime air mass from Indian Ocean to Phimai site. Distinction in sources of air masses affect to chemical and physical characteristics in those air masses. Figure 5.4 and 5.5 show the evidence of monsoon effects, the prevailing northeast monsoon in dry season causes the high CO concentrations and low RH (red line) while the prevailing southwest monsoon in wet season causes the low CO concentrations and high RH (blue line).

In addition, Fig. 5.6 shows diurnal variations of direct radiation that were high in dry season and low in wet season. The radiation directly related to photochemical reaction. Strong direct radiation in dry season (red line) can enhances the rate of photochemical production of O_3 in sufficient condition of O_3 precursor, whereas, weak direct radiation in wet season (blue line) is inefficient to provide the strong photochemical reaction.

Lastly, the strong radiation together with high CO concentration and low relative humidity in dry season promote to O_3 photochemical production. However, in wet season, the condition of weak radiation, low CO concentration and high relative humidity are unsuitable for driving the O_3 photochemical production. Therefore, O_3 diurnal variation shows obvious high cycle during dry season and low cycle during wet season.

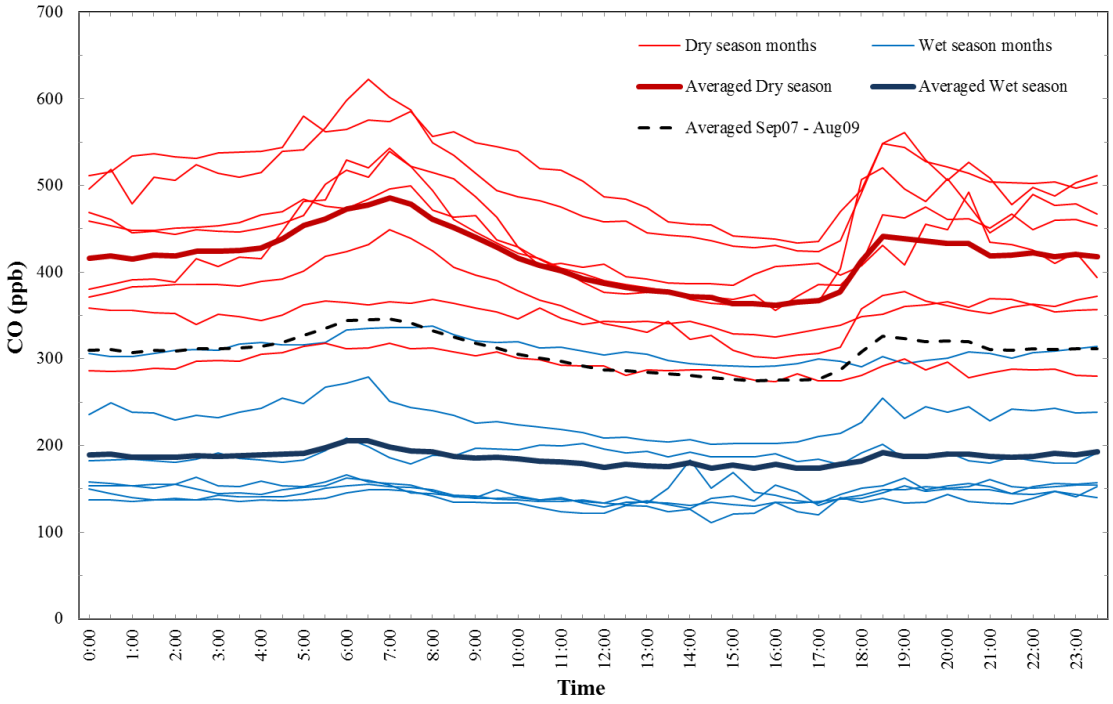

Figure 5.4 Diurnal variations of CO based on averaged dry and wet season months and averaged dry and wet season.

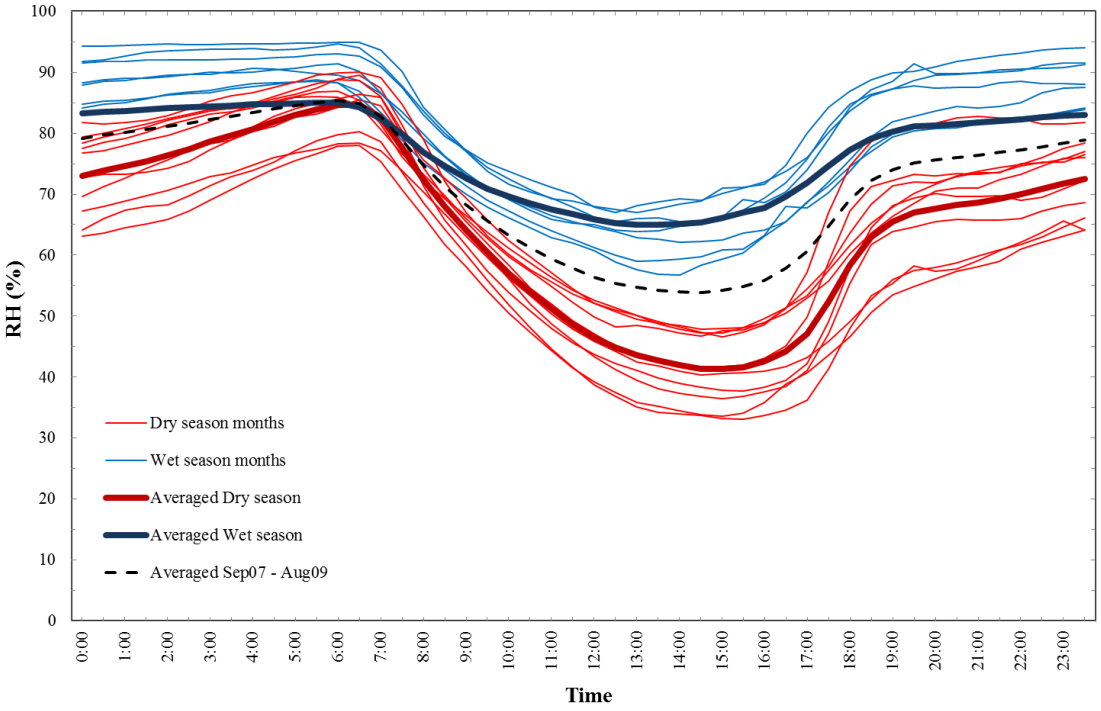

Figure 5.5 Diurnal variations of relative humidity (RH) based on averaged dry and wet season months and averaged dry and wet season.

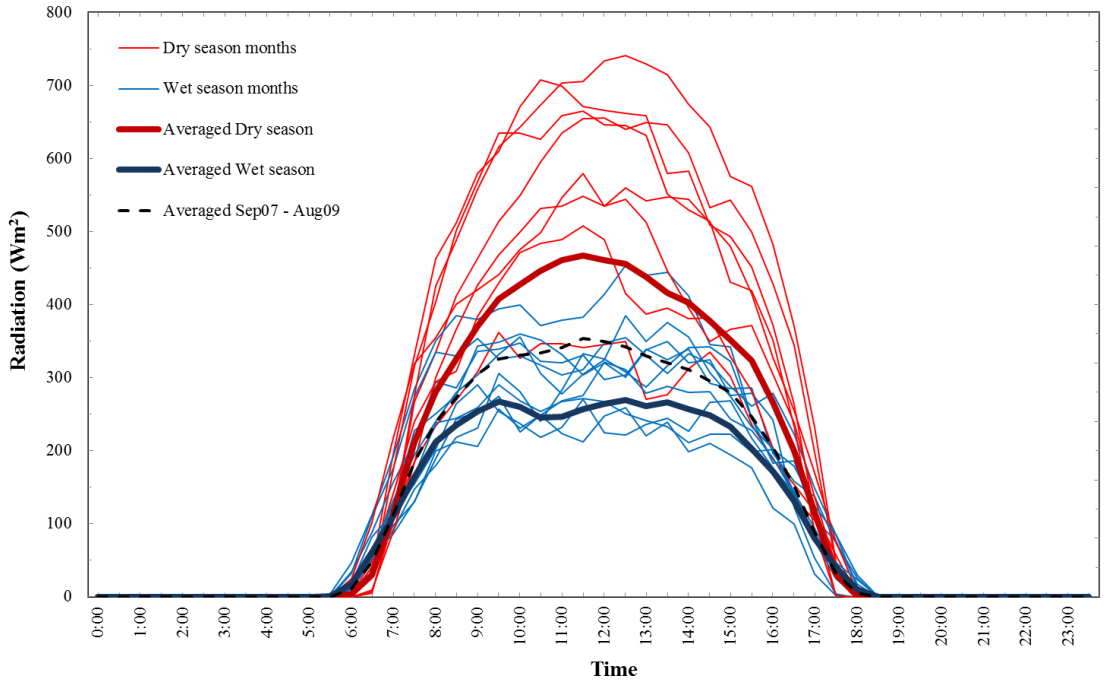

Figure 5.6 Diurnal variations of direct radiation based on averaged dry and wet season months and averaged dry and wet season.

5.1.3 Relations between diurnal variations of O_3 with CO, RH, and direct radiation

To considering the relation between O_3 – CO, O_3 – RH, and O_3 – direct radiation in a day, Fig. 5.7 and 5.8 are illustrated with averaged all diurnal variations of O_3, CO, RH, and direct radiation during September 2007 to August 2009.

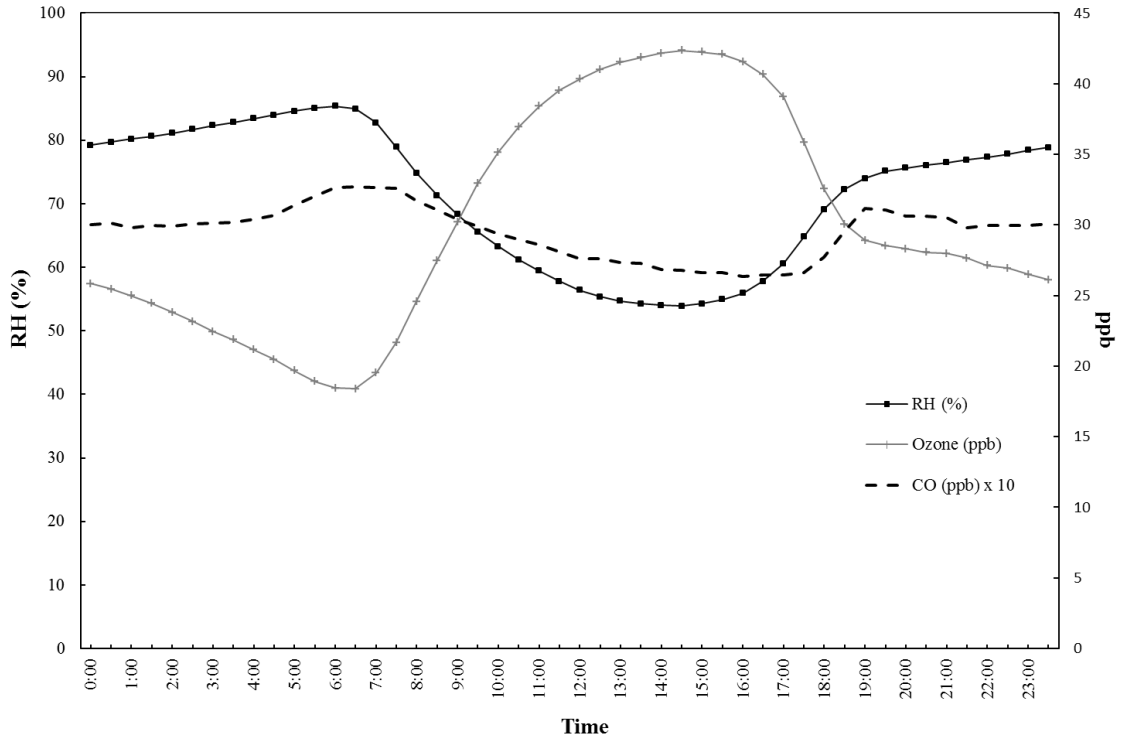

Figure 5.7 Comparison between diurnal variations of O_3, CO, and RH.

1. O_3 and CO

The diurnal variation of O_3 and CO in Fig. 5.7 reveals that CO has opposite cycle with O_3. At morning time which sunlight presents, CO decreases along with the increase of O_3. These are resulted from photochemical reaction, CO reacts with exiting OH radical (Lal et al., 2000; Sillman, 2003; Tsutsumi & Matsueda, 2000).

$$CO + OH + O_2 \longrightarrow HO_2 + CO_2 \qquad \text{(i)}$$

and followed by reactions of HO_2 with existing NO

$$HO_2 + NO \longrightarrow OH + NO_2 \qquad \text{(ii)}$$

photolysis of NO_2 results in the formation of atomic oxygen (O)

$$NO_2 + h\nu\ (\lambda\ 300\text{-}400\ nm) \longrightarrow NO + O(^3P) \quad \text{(iii)}$$

and then O_3 is formed by the association reaction of ground state O atoms with O_2.

$$O(^3P) + O_2 + M \longrightarrow O_3 + M \quad \text{(iv)}$$

As a result of photochemical reaction to produces O_3, CO is destroyed to support this process. Therefore, normally, in the clear sky day, CO will gradually decreases with the increase of O_3.

In the late afternoon when O_3 is decreasing rapidly, CO starts increasing simultaneously. In this time the O_3 production still forms O_3 but with lower rate than the O_3 destruction rate, therefore, these led CO to increase because CO is not necessary for produces O_3.

In the night time with absence of sunlight, O_3 decreases gradually. However, such decreasing rate in night time is slower than decreasing rate in late afternoon. This condition can be explained by this following reaction

$$O_3 + h\nu\ (\lambda<320\ nm) \longrightarrow O(^1D) + O_2 \quad \text{(v)}$$

In the late afternoon the primary loss of O_3 is the photochemical reaction the O_3 molecule disassociates by the absorption the sunlight. While in the night time with absence of sunlight, O_3 is destroyed by this following reaction

$$NO_2 + O_3 \longrightarrow NO_3 + O_2 \quad \text{(vi)}$$

NO_2 is slowly converted to NO_3 by reaction with O_3.

For this reason the rate of O_3 destruction in daytime by photochemical reaction is faster than in nighttime by reaction with NO_2.

The absence of sunlight in the nighttime led OH radical to be suppressed because OH radical is formed by the photolysis reaction of stable molecules in the presence sunlight condition. Therefore, NO_2 cannot regenerates NO for re-cyclic the

O_3 formation process. For this reason, O_3 concentration decreases continuously during the nighttime.

2. O_3 and Relative humidity (RH)

O_3 and RH in Fig. 5.7 also show the different diurnal variations, RH starts decreasing when sunlight presents together with the increase of O_3. The primary cause of decrease of RH during daytime is the increase of air temperature. It increases the air capacity for the saturated water vapor.

Water vapor in the atmosphere reacts with O radical ($O(^1D)$) from photo disassociation of O_3 to forms OH.

$$O_3 + h\nu\ (\lambda<320\ nm) \longrightarrow O(^1D) + O_2 \qquad (v)$$

$$O(^1D) + H_2O \longrightarrow 2OH \qquad (vii)$$

OH radical is necessary for re-cyclic NO to NO_2 by reacts with O_3 or CO to forms HO_2

$$OH + O_3 \longrightarrow HO_2 + O_2 \qquad (viii)$$

$$CO + OH + O_2 \longrightarrow HO_2 + CO_2 \qquad (ix)$$

$$HO_2 + NO \longrightarrow OH + NO_2 \qquad (ii)$$

Then NO_2 provides atomic oxygen ($O(^3P)$) by reaction (iii) for the production of O_3 in reaction (iv).

Moreover, the decrease of RH reflects in the energy from sunlight. As illustrated in Fig. 5.5, it can be seen that diurnal variations of RH in dry season decreased greater than in wet season because of strong radiation. Evidence of radiation for dry and wet seasons is shown in Fig. 5.6. The stronger direct radiation mostly occurred in dry season and can be seen clearly that the averaged line in dry season (red thick line) was significantly higher than the averaged line in wet season. In addition, the strong direct radiation also led to the higher photochemical activity in dry season.

RH increases rapidly in the late afternoon with the decrease of O_3, it implies the decrease of air temperature and radiation which led to the inhibition of photochemical reaction. However, RH increases continuously and increases gradually through the nighttime until maximum before morning.

However, because of the daily change of RH clearly related to air temperature and sunlight more than O_3. Therefore, the relation between O_3 and RH cannot be explained obviously.

3. O_3 and direct radiation

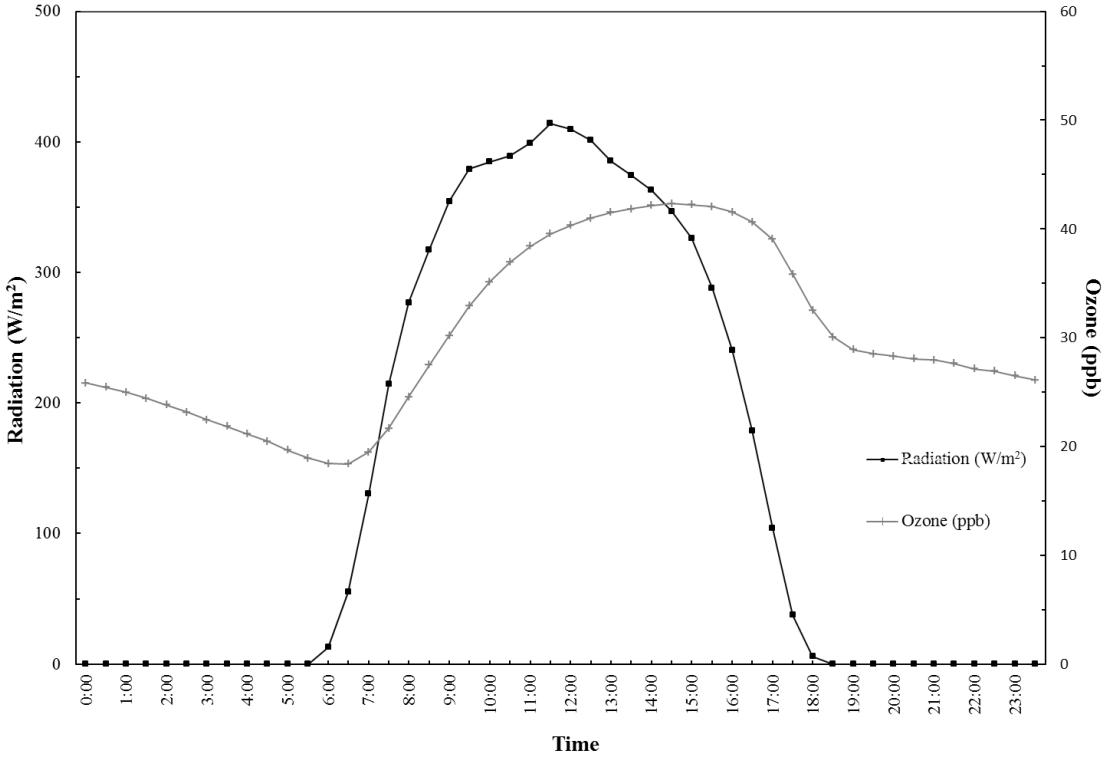

Figure 5.8 Comparing between diurnal variation of O_3 and direct radiation

UV Radiation is the energy source of a photochemical reaction. NO_2 absorbs 300-400 nm UV radiation to produces oxygen atom for O_3 production process. Therefore, generally the cycle of diurnal variation of O_3 will change in the same direction with radiation. Strong radiation (especially in dry season) induces much O_3 production in the condition that precursors are sufficient, whereas, weak radiation (in wet season) induces less O_3 production as showed in Fig. 4.5 and 5.6.

Figure 5.8 shows the diurnal variation between O_3 and direct radiation, it can be seen that O_3 begins coincide with the time which direct radiation can be observed. During morning period, direct radiation occurs immediately at 5-6 AM and increases rapidly after 6 AM. After direct radiation occurred, O_3 has rapid increasing. O_3 continues increasing with rapid rate and then the increasing rate slows down together with the direct radiation reached nearly maximum at noon. However, O_3 rises continuously and reaches maximum in afternoon even direct radiation already begins to decline. This indicates that although radiation decreases, it remains effective level to forces O_3 production rate exceeds O_3 destruction rate. At the late afternoon, O_3 decreases rapidly. It should be noted that the approximately 150 W/m^2 of direct radiation that is observed when O_3 starts decreasing in the late afternoon, it is the same level that is observed together with starting O_3 production in morning. This indicates that direct radiation of 150 W/m^2 might be the level that O_3 production rate balances with O_3 destruction rate for Phimai site for annual average.

At early nighttime, because of absence of sunlight, direct radiation cannot be observed. However, O_3 still decreases but with slower rate than decreasing in late afternoon. As mentioned, not only UV radiation can causes O_3 production, it also causes O_3 destruction. UV radiation drives O_3 destruction only in daytime which sunlight presents, while O_3 destruction in nighttime is driven by NO_2 as showed in reaction (vi). Therefore, responsibility of UV radiation on O_3 is effective only in the presence of sunlight condition.

5.1.4 O_3 variations based on air mass trajectories

The variations of O_3 that associated with air mass will be discussed in this topic with others effective factors. Moreover, the data of precipitation during air mass transportation from trajectory and the 10-days hot spot fire map from MODIS satellite by NASA will be employed for discussion in this topic.

Table 5.1 Percentage of precipitation hour during air mass transportation categorized by backward trajectory.

	NE-C	NEE-CM	NEES-M	SW-M
% of Precipitation	16	27	40	62

Table 5.2 Averaged all daily averages ± 1 standard deviation of O_3, CO, direct radiation, and RH, classified by air mass types.

	O_3 (ppb)	CO (ppb)	Radiation (Wm^{-2})	RH (%)
NE-C	39.3 ± 8.5	426.0 ± 116.4	178.2 ± 100.2	66.0 ± 9.5
NEE-CM	35.0 ± 8.5	418.3 ± 169.5	120.1 ± 109.4	69.5 ± 9.8
NEES-M	32.2 ± 11.5	310.0 ± 106.4	141.1 ± 94.9	69.5 ± 10.4
SW-M	22.1 ± 7.1	151.3 ± 33.0	123.1 ± 89.1	78.0 ± 7.4

1). O_3 with Northeast continental air mass (NE-C)

NE-C mostly occurred in dry season especially in local winter (November to February). It is the same period of burning season in East China and Southeast Asia. The hot spot fire maps are shown in Fig. 5.9 reveals the heavy burning area on East China during 27 November 2007 – 6 December 2007 and heavy burning with both areas of East China and Southeast Asia during 1-10 January 2008. These burning area are important sources of primary pollutants particularly O_3 precursors.

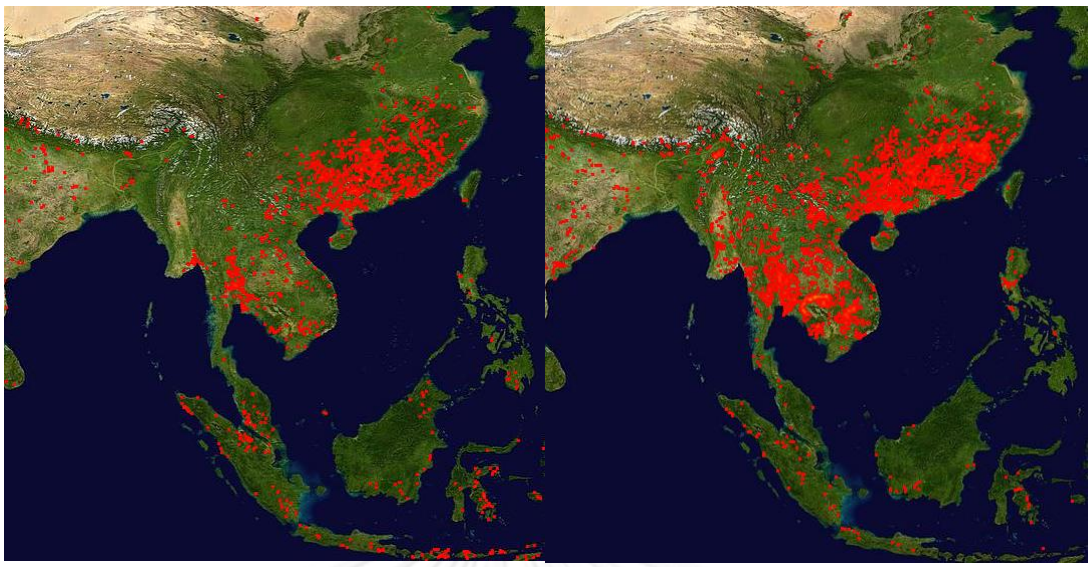

Figure 5.9 Fire map during 27 November 2007 – 6 December 2007 (left), and during 1 – 10 January 2008 (right) (NASA).

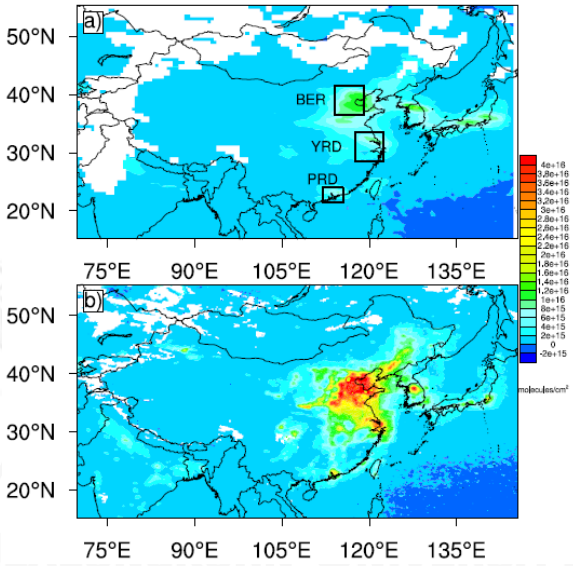

Figure 5.10 Yearly mean tropospheric excess columns of nitrogen dioxide over China in a) 1996 and b) 2011. Boxes PRD, YRD, and BER represent the three studied subregions: the Pearl River Delta, the Yangtze River Delta, and the Bohai Economic Rim (Huang et al., 2013).

Study of Huang et al. (2013) revealed that the past few decades, China urbanization increased rapidly. The built-up areas in Beijing, Shanghai, and Guangzhou increased by 197%, 148%, and 273%, respectively, and population grew with 87%, 65%, and 25%, respectively, from 1996 to 2011. Moreover, the satellite data of NO_2

over East China were reported that increased by 82%, 292%, and 307% in Guangzhou, Shanghai, and Beijing, respectively, during 1996 to 2011 (Fig. 5.10). For this reason, China is a dominant source of anthropogenic emission in Asia.

Many previous studies have reported that the high O_3 concentration during this period has associated with air mass that originated from East Asia continent. For examples, various studies at Hong Kong (Chan et al., 1998; Lam et al., 2001; Wang et al., 2001) and at coastal South China (Zhou et al., 2013). Such studies have reported agreeable results that high O_3 concentration frequently occurred with the Northeast wind that blows across East China before reaching to observed sites during autumn to spring. In addition, study at Cape Hedo, Japan, Suthawaree et al. (2008) reported that the O_3 and CO concentrations showed maximum values during winter – spring with 52 and 280 ppb, respectively. The 5-days backward trajectories of air masses from China and Korea have associated to such maximum O_3 and CO. Another study in Japan, at the summit of mountain Fuji, Tsutsumi and Matsueda (2000) also observed O_3 and CO with backward trajectory analysis, they found that both of O_3 and CO showed maximum concentrations in the air mass originated in Northeast Asia, whereas, O_3 and CO exhibited minimum in the air mass originated in Southeast Asia.

Moreover, Model of Ozone and Related Tracers version 1 (MOZART 1) was performed by Mauzerall et al. (2000) to investigate regional and seasonal characteristics of O_3 production and mixing ratio over East Asia. They found spring-summer maximum of O_3 production in East Asia with rate 117 Tg/yr.

One important factor that reduces primary pollutants especially O_3 precursors is precipitation. Once an air mass transports, it probably encounters precipitation and O_3 precursors could be washed. Table 5.1 shows the percent of precipitation hour during air mass transportation. From this table, NE-C air mass has lowest percent of precipitation hour of 16%. It implies that O_3 precursors which are carried by this air mass have lowest probability to be washed out. For this reason, CO shows significantly high concentration with prevailing NE-C air mass as shown in Table 5.2 with 426 ± 116.4 ppb and high O_3 concentration of 39.3 ± 8.5 ppb.

2). O_3 with Northeast/East Continental and Marine air mass (NEE-CM)

Due to NEE-CM transported over Pacific Ocean over 50% of total transport time. These indicate that during NEE-CM air mass transporting across maritime area of Pacific Ocean, the clean and moist air in such area will be mixed with NEE-CM air mass before reaching to Phimai site. O_3 in NEE-CM which is observed with lower concentration than in NE-C can be explained by following reasons:

- High water vapor might led to cloud formation, and cloud covering acts as the filter reduces the direct radiation, then, direct radiation are observed with lower than as observed in NE-C as can be seen in Fig. 4.9 d) and 120.1 Wm^{-2} from Table 5.2. In the condition of which UV radiation is scant, O_3 photochemical production will be reduced, therefore, O_3 in NEE-CM is also reduced.
- The percentage of precipitation hour (Table 5.1) in NEE-CM that higher than NE-C (27%) also repeats the effect from moist environment in maritime air mass. It implies to the probability that O_3 precursors will be washed out from this air mass and inhibits the O_3 photochemical production.
- Once the NEE-CM mixing with the clean Pacific air mass, O_3 and other precursors are diluted. Therefore, the concentration of O_3 shows lower value than NE-C.

The results of NEE-CM indicates that the resident time of NEE-CM on maritime area of Pacific Ocean more than 50% of total transportation time is the key for distinction between NEE-CM and NE-C. It encourages a clean environment in NEE-CM air mass. Even the CO diurnal variations between NEE-CM and NE-C were approximate, but RH is higher and direct radiation in NEE-CM is lower. These could cause the decrease of O_3 photochemical production. The averaged of all daily averages of O_3 and CO in NEE-CM (Table 5.2) are observed with significantly lower than NE-C with value of 35.0 ± 8.5 and 418.3 ± 169.5 ppb, respectively.

3). O_3 with Northeast/East/South Marine air mass (NEES-M)

As mentioned in Chapter IV, NEES-M occurred with high frequencies during late dry season or local summer (March – April) in Thailand. The local summer in Thailand is the period of burning season in Southeast Asia especially on the continental countries such as Thailand, Cambodia, Laos, Myanmar, and Vietnam. The evidences of biomass burning area from fire maps are shown in Fig. 5.11.

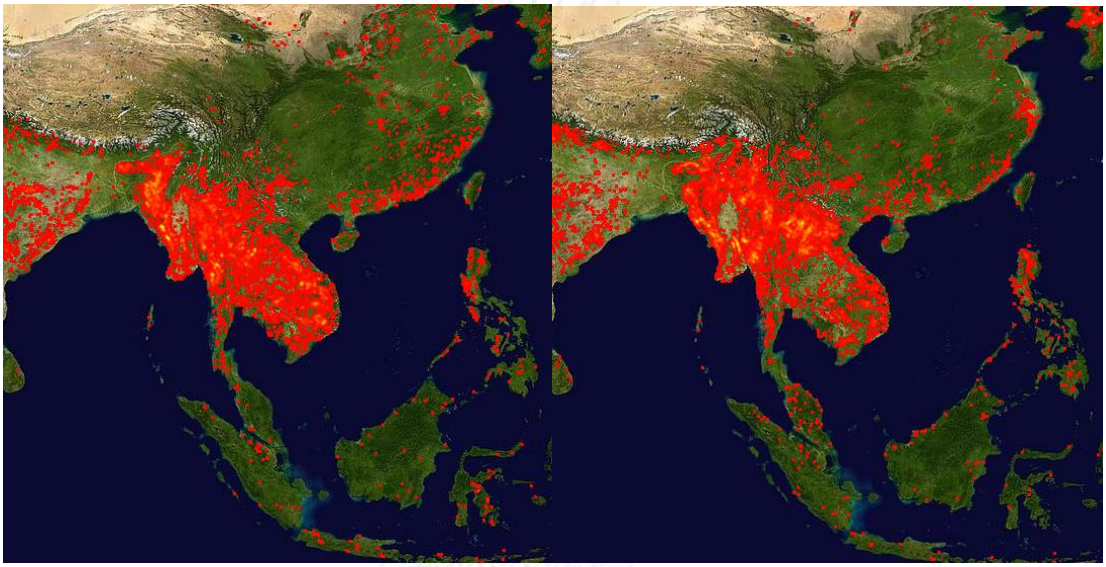

Figure 5. 11 Fire map during 11-20 March 2008 (left), and during 10-19 April 2008 (right).

From Fig. 5.11, it can be seen clearly that intense burnings were over an area of mainland countries in Southeast Asia. Previous study of Pochanart et al. (2003) had investigated CO seasonal behavior in rural site Srinakarin, Thailand. They found that the CO seasonal cycle showed a maximum during the late dry season (February – March) and minimum during mid-wet season (June – August). Moreover, the long-range transport of air mass showed that biomass burning activity in continental Southeast Asia were the main factors that controlling CO variation in Thailand. And analysis of fire hot spots indicated that the seasonal cycle of biomass burning in continental Southeast Asia was regular and maximum in March coincide with the CO maximum. Kondo et al. (2004) have investigated impacts of biomass burning in Southeast Asia on O_3 over the western Pacific in spring season. They found that biomass burning activity was high over SEA (Thailand, Myanmar, Laos, Cambodia, and Vietnam) during the dry season of February–April 2001. And convective activity on

Southeast Asia frequently transported boundary layer air which is impacted by biomass burning to free troposphere, followed by eastward transport to observed site.

As mentioned above, regional biomass burning in the continental Southeast Asia is the important factor that led to strong photochemical production of O_3 during prevailing NEES-M air mass in March to April at Phimai site. CO diurnal variation in Fig. 4.9 b) for NEES-M shows approximately 2 times higher than CO in SW-M which is supporting evidence to such regional emission.

To investigate the results from regional biomass burning on O_3 photochemical production, the O_3 diurnal variation in SW-M is considered to be O_3 that is the result from minimally anthropogenic emission affects. The differences between NE-C/SW-M, NEE-CM/SW-M, and NEES-M/SW-M diurnal variations can reveal the effects from either long range transport of O_3 precursors or regional biomass burning.

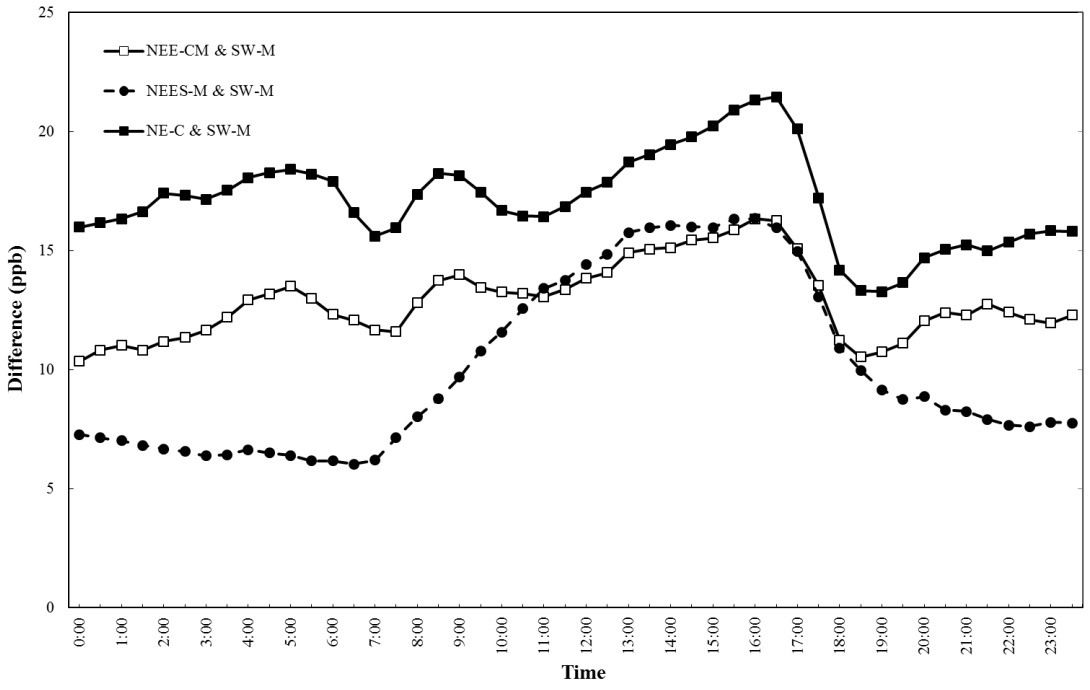

Figure 5.12 Difference diurnal variations between NE-C/SW-M, NEE-CM/SW-M, and NEES-M/SW-M.

Figure 5.12 shows the differences of O_3 diurnal variations between NE-C/SW-M, NEE-CM/SW-M, and NEES-M/SW-M, it can be seen that the results can be divided into two groups; i). low daytime fluctuations and ii) high daytime fluctuations.

NE-C/SW-M and NEE-CM/SW-M are classified as i) group, it show similar variation patterns with low fluctuation during daytime (but higher cycle in NE-C/SW-M), these patterns imply that the effect of long range transport of O_3 precursors in NE-C and NEE-CM air masses predominate the effect of regional emission. While, NEES-M/SW-M is classified as ii) group, it can be seen the broadly high amplitude during daytime, this indicates the effect of regional emission in continental Southeast Asia on O_3 photochemical production during daytime is dominant in NEES-M air mass.

High regional anthropogenic biomass burning in continental Southeast Asia and strong direct radiation (as shows in Fig. 4.9 c) and 141.1 ± 94.9 Wm^{-2} in Table 5.2 during prevailing NEES-M period (March to April) can leads to intense O_3 photochemical production during daytime. However, O_3 and CO concentrations in NEES-M air mass are lower than NE-C and NEE-CM air masses as shown in Table 5.2 with 32.2 ± 11.5 and 310.0 ± 106.4 ppb, respectively.

As mentioned in previous topic, the uncommon phenomenon of low O_3 in December 2007. The seasonal and diurnal variations of O_3 in such month shows significant decrease. The frequency of air mass as showed in Table 4.2 is the key of this phenomenon, it can be seen that the prevailing air mass in December 2007 was NEES-M with highest frequency of 61%, whereas, in December 2008, NE-C was the prevailing type by 53%. Generally, during dry season in Thailand, the NE-C is major type that influences in this period. NE-C originated on continental Northern Asia and passed over high anthropogenic emission areas and carried pollutants to Phimai site, therefore, high O_3 variations were normally found during this season. While, the NEES-M type originated on maritime area of Pacific Ocean and passed over clean area of Pacific, therefore, significant low variations of O_3 were observed in December 2007.

4). O_3 with Southwest Marine air mass (SW-M)

Since SW-M prevailed during wet season, the conditions of high humidity and low O_3 precursors inhibit the photochemical production of O_3. In contrast, it leads to O_3 destruction instead.

The low O_3 concentrations observed in SW-M air mass during wet season are thought to be the result from the O_3 destruction processes by OH radicals in the extremely low NO_x condition in the maritime area of Indian Ocean by following reaction

$$OH + O_3 \longrightarrow HO_2 + O_2$$

$$HO_2 + O_3 \longrightarrow OH + 2O_2$$

In addition, Table 5.1 shows the high percentage of precipitation hour with 62% for SW-M. It implies to high probability that primary pollutants especially O_3 precursors will be washed out from SW-M air mass. Therefore, even SW-M may carry O_3 precursors from Bangkok metropolis but it could be eliminated by precipitation. Moreover, as high humidity in wet season can effectively induce cloud formation, thus, cloud covering inhibits the sunlight penetration to the lower troposphere and led to decreasing O_3 photochemical production.

Study of Lam et al. (2001) reported that O_3 associated with southwest marine air mass reaching to Hong Kong was low with 18 ppbv. Lal et al. (2000) found that the annual variation in average O_3 concentration at Ahmedabad, India, was minimum value of 12±2 ppbv during August. The wind patterns are mainly southwesterly (180-270 degree) during June-August, bringing cleaner air from the Arabian Sea and the Indian Ocean. In Tanah, Malaysia, Toh et al. (2013) reported the highest O_3 mixing ratio (average 19.1 ppb) during Southwest monsoon which is local burning season in Sumatra Island. At Inthanon, Thailand, (Pochanart et al., 2001) found that O_3 lowest mixing ratio of 13 ppb associated with the long-range transport of southwest monsoon. However, in this study, O_3 associated with SW-M shows concentration of 22.1 ± 7.1ppb (Table 5.2) which is higher than previous studies. It can be assumed

that Phimai site is located in the center of continental Southeast Asia, therefore, SW-M probably passed over Bangkok metropolis and carried O_3 precursors to Phimai site.

5.1.5 Relations between O_3 and its factors

In this topic, the correlation coefficients from Topic 4.4 will be discussed with other results from this study and previous studies to reveal the relations between O_3 and other effective factors.

The correlation analysis is one of the often used methods in previous studies (Badarinath et al., 2007; Chin et al., 1994; Mauzerall et al., 2000; Pochanart et al., 2003; Sikder et al., 2011; Suthawaree et al., 2008; Toh et al., 2013; Tsutsumi & Matsueda, 2000). The correlation coefficient between O_3 and factors (CO, RH, and direct radiation) are discussed below.

1. *Relation between O_3 and CO* is highest with R^2 of 0.560 in NEES-M type. This confirm again to the strong O_3 photochemical production in such air mass. NEES-M is predominant during regional burning season in March to April. NE-C and NEE-CM show R^2 of 0.530 and 0.536, respectively, which are lower than NEES-M due to weaker photochemical reaction. While, SW-M shows the lowest relation with 0.382, this indicates obviously that photochemical production of O_3 is weak in this air mass during wet season because of clean and moist conditions. However, the relation between O_3 and CO in Phimai is agreeable with other sites especially during dry season, such as at Oki, Japan, highest correlation R^2 = 0.79 was found associated with regionally polluted continental air mass from East Asia in summer, lowest correlation was found with marine air masses (Sikder et al., 2011).
2. *Relation between O_3 and Relative humidity (RH)* are high negative relation in both two types of marine originated air mass, R^2 = -0.734 and -0.684 for NEES-M and SW-M, respectively. Because of clean and moist environment of maritime air mass, therefore, O_3 will be destroyed in three ways: i) the extremely low NO_x condition, ii) high water vapor probably wash out the O_3 precursors, and iii) polluted air mass from continent is dilute by clean

marine air mass. Moderate negative correlation is found with R^2 = -0.623 in the air mass that involved with continental and maritime area, NEE-CM. And lowest negative correlation is found in continental originated air mass, NE-C, with R^2 = -0.469. However, previous study at Tanah Rata, Malaysia, showed different relation. It was reported that lowest correlation (R^2 = -0.32) between O_3 and RH occurred with southwest monsoon, due to the impact of air pollutants from Indonesia during the burning season from May to late September that could lead to enhanced O_3 photochemical production (Toh et al., 2013).

3. *Relation between O_3 and direct radiation.* Even O_3 photochemical production occurs during daytime which follows solar radiation intensity, the correlation between O_3 and direct radiation shows weak or no correlation at Phimai site. Due to maximum direct radiation is observed around 11AM – 12PM, whereas, maximum O_3 is observed around 14PM – 16PM as shown in Fig. 5.8. This means that there is a lag of 3 – 5 hours between the peak of O_3 and direct radiation. The maximum O_3 concentration occurs when direct radiation decreases, therefore, leading to weak or no correlation. Moreover, could cover, precipitation and aerosol matters could decrease large amount of solar radiation (Toh et al., 2013).

5.2 Conclusions

The tropospheric ozone (O_3) has been observed by UV-photometric continuous ozone monitor (model 1006-AHJ) together with others parameters, i.e. carbon monoxide (CO), relative humidity (RH), and direct radiation during September 2007 to August 2009 at the observatory for atmospheric research at Phimai, Chang wat Nakhon Ratchasima, Thailand, to investigate seasonal behavior of O_3 and relations between O_3 and factors.

Seasonal variations of O_3 show dry season maximum (December to April) especially in local summer of Thailand (March to April) and wet season minimum (June to October). Seasonal variations of O_3 and CO show a good correlation. The highest daily O_3 concentration was 63.8 ppb in 5 March 2008 and the lowest was 9.0 ppb in 19 June 2009. And the maximum and minimum of O_3 monthly average were 45.7 ppb in January 2009 and 15.8 in July 2009, respectively. Seasonal characteristics of O_3 at Phimai were controlled by long-range transport of air mass by monsoon. Northeast monsoon prevailed in dry season was observed with high O_3 variations, whereas, low O_3 variations were observed with the southwest monsoon.

Diurnal variations of O_3, show the increase during day time and reached to maximum in afternoon, and show the rapid decrease during late afternoon following by the slight decreasing over nighttime until reached to minimum in early morning. However, there were different between O_3 diurnal variations in wet and dry season; higher diurnal variations were found in dry season, while, lower diurnal variations were found in wet season. Higher O_3 diurnal variations in dry season indicate the strong O_3 photochemical production during Northeast monsoon predominated, this corresponding to the high diurnal variations of CO and direct radiation and low diurnal variation of RH. Prevailing southwest monsoon during wet season leads to the low diurnal variations of CO and direct radiation and the high diurnal variation of RH, these were causes of lower O_3 diurnal variations in wet season.

To examine the influences of the long-range transport of air masses on O_3, the backward trajectory analysis in HYSPLIT model was performed. Air masses were categorized into four types, i.e. i) Northeast Continental (NE-C), ii) Northeast/East

Continental and Marine (NEE-CM), iii) Northeast/East/South Marine (NEES-M), and iv) Southeast Marine (SW-M). The examination showed that;

1. NE-C predominated during dry season especially in November to February (local winter), and associated with highest O_3 concentration of 39.3 ± 8.5 ppb and variation because this air mass originated on Northern Asian continent and blew over the burning areas of East China. It carried O_3 precursors and other primary pollutants to observed site along with the dry and strong radiation conditions. Therefore, these lead to enhancement of O_3 production.
2. NEE-CM was observed in the same period as NE-C but with lower frequencies. This type also originated on Northern Asian continent but transported over maritime area of Pacific Ocean more than 50% of total transport time. Therefore, O_3 is also influenced by clean and moist environment from Pacific. O_3 concentration in NEE-CM showed lower value than NE-C (35.0 ± 8.5 ppb). During NEE-CM passing over Pacific, higher precipitation may wash out the O_3 precursors, which is cause of the decrease of O_3.
3. NEES-M is a maritime originated air mass. It originated on Pacific Ocean and predominated in late dry season or local summer during March to April. This period is the regional burning season of Thailand and neighboring countries (Cambodia, Laos, Myanmar, and Vietnam). O_3 concentration in NEES-M was found with lower value than continent originated air mass (32.2 ± 11.5 ppb). Nevertheless, O_3 diurnal variation in NEES-M showed higher amplitude during daytime. It implies to the effect of regional emission on O_3 photochemical production predominates the effect of long-range transport of O_3 precursors.
4. SW-M is major maritime originated air mass during wet season in Thailand (May to September). It originated on clean and moist environment of Indian Ocean, therefore, O_3 in this air mass was found with lowest concentration of 22.1 ± 7.1 ppb. Low O_3 concentrations are the result from the O_3 destruction processes in the extremely low NO_x condition in

the maritime area of Indian Ocean. In addition, higher percentage for precipitation hour implies that O_3 precursors will be washed out from SW-M air mass. However, O_3 in SW-M is higher than previous study in Thailand, it is assumed that this is the effect of high emission over Bangkok metropolis.

Correlation between daily averages of O_3 and factors i.e. CO, RH, and direct radiation showed high positive correlation with CO (R^2 = 0.763), high negative correlation with RH (R^2 = -0.764), and low positive correlation with direct radiation (R^2 = 0.188). With categorization by air mass type;

- Correlations between O_3 and CO were found highest in NEES-M (R^2 = 0.560), emphasizing the effect of regional emission on O_3 photochemical production. While, lowest correlation, R^2 = 0.382, was found in SW-M due to weak O_3 photochemical production.
- Correlations between O_3 and RH were found with high negative correlation in marine originated air mass; R^2 = -0.734, and 0.684 for NEES-M and SW-M, respectively. Clean and moist environment in maritime area led to O_3 destroying in the extremely low NO_x condition, moreover, high water vapor probably washed out the O_3 precursors.
- Correlations between O_3 and direct radiation were found with very low or no correlations. Because of the lag around 3 – 5 hours between the peak of O_3 and direct radiation.

5.3 Suggestions for further study.

1. Study should have measurement other parameters such as NO_x, VOCs, and OH radical for better investigation of the ozone production and destruction reactions.

2. The observation period of ozone and other parameters should be longer in order to reveals the actual annual variation and reaches to accurate inter-annual relation.

REFERENCES

Ajavon, A.N., Albritton, D.L., & Watson, R.T. (2007). Scientific Assessment of Ozone Depletion: 2006, Rep. 50, Global Ozone Res. and Monit. Project. World Meteorol. Organ. Geneva.

Andreae, M. O., Chapuis, A., Cros, B., Fontan, J., Helas, G., Justice, C., Kaufman, Y. J., Minga, A., & Nganga, D. (1992). Ozone and Aitken nuclei over equatorial Africa: Airborne observations during DECAFE 88. *Journal of Geophysical Research: Atmospheres, 97*(D6), 6137-6148.

Avnery, Shiri, Mauzerall, Denise L., Liu, Junfeng, & Horowitz, Larry W. (2011). Global crop yield reductions due to surface ozone exposure: 2. Year 2030 potential crop production losses and economic damage under two scenarios of O_3 pollution. *Atmospheric Environment, 45*(13), 2297-2309.

Badarinath, K. V. S., Kumar Kharol, Shailesh, Kiran Chand, T. R., Parvathi, Y. Ganga, Anasuya, T., & Jyothsna, A. Nirmala. (2007). Variations in black carbon aerosol, carbon monoxide and ozone over an urban area of Hyderabad, India, during the forest fire season. *Atmospheric Research, 85*(1), 18-26.

Chan, L. Y., Liu, H. Y., Lam, K. S., Wang, T., Oltmans, S. J., & Harris, J. M. (1998). Analysis of the seasonal behavior of tropospheric ozone at Hong Kong. *Atmospheric Environment, 32*(2), 159-168.

Chin, Mian, Jacob, Daniel J., Munger, J. William, Parrish, David D., & Doddridge, Bruce G. (1994). Relationship of ozone and carbon monoxide over North America. *Journal of Geophysical Research: Atmospheres, 99*(D7), 14565-14573.

Deng, Xuejiao, Tie, Xuexi, Zhou, Xiuji, Wu, Dui, Zhong, Liuju, Tan, Haobo, Li, Fei, Huang, Xiaoying, Bi, Xueyan, & Deng, Tao. (2008). Effects of Southeast Asia biomass burning on aerosols and ozone concentrations over the Pearl River Delta (PRD) region. *Atmospheric Environment, 42*(36), 8493-8501.

Dentener, F., Keating, T., & Akimoto, H. (2010). Part a: ozone and particulate matter. *Air pollution studies, 17*.

Finlayson-Pitts, B. J., & Pitts, J. N. (1993). Atmospheric Chemistry of Tropospheric Ozone Formation: Scientific and Regulatory Implications. *Air & Waste, 43*(8), 1091-1100.

Fishman, Jack. (1991). The global consequences of increasing tropospheric ozone concentrations. *Chemosphere, 22*(7), 685-695.

Fujiwara, M., Tomikawa, Y., Kita, K., Kondo, Y., Komala, N., Saraspriya, S., Manik, T., Suripto, A., Kawakami, S., Ogawa, T., Kelana, E., Suhardi, B., Harijono, S. W. B., Kudsy, M., Sribimawati, T., & Yamanaka, M. D. (2003). Ozonesonde observations in the Indonesian maritime continent: a case study on ozone rich layer in the equatorial upper troposphere. *Atmospheric Environment, 37*(3), 353-362.

Gauss, M., Myhre, G., Isaksen, I. S. A., Grewe, V., Pitari, G., Wild, O., Collins, W. J., Dentener, F. J., Ellingsen, K., Gohar, L. K., Hauglustaine, D. A., Iachetti, D., Lamarque, F., Mancini, E., Mickley, L. J., Prather, M. J., Pyle, J. A., Sanderson, M. G., Shine, K. P., Stevenson, D. S., Sudo, K., Szopa, S., & Zeng, G. (2006). Radiative forcing since preindustrial times due to ozone change in the troposphere and the lower stratosphere. *Atmos. Chem. Phys., 6*(3), 575-599.

Guicherit, Robert, & Roemer, Michiel. (2000). Tropospheric ozone trends. *Chemosphere - Global Change Science, 2*(2), 167-183.

Huang, Jianping, Zhou, Chenhong, Lee, Xuhui, Bao, Yunxuan, Zhao, Xiaoyan, Fung, Jimmy, Richter, Andreas, Liu, Xiong, & Zheng, Yiqi. (2013). The effects of rapid urbanization on the levels in tropospheric nitrogen dioxide and ozone over East China. *Atmospheric Environment, 77*(0), 558-567.

IPCC. (2007). Climate changes 2007 - Synthesis Report.

Jacob, Daniel J. (2000). Heterogeneous chemistry and tropospheric ozone. *Atmospheric Environment, 34*(12–14), 2131-2159.

Jaeglé, Lyatt, Jacob, Daniel J., Brune, William H., & Wennberg, Paul O. (2001). Chemistry of HOx radicals in the upper troposphere. *Atmospheric Environment, 35*(3), 469-489.

Jenkin, Michael E., & Clemitshaw, Kevin C. (2000). Ozone and other secondary photochemical pollutants: chemical processes governing their formation in the planetary boundary layer. *Atmospheric Environment, 34*(16), 2499-2527.

Karnosky, David F., Skelly, John M., Percy, Kevin E., & Chappelka, Art H. (2007). Perspectives regarding 50 years of research on effects of tropospheric ozone air pollution on US forests. *Environmental Pollution, 147*(3), 489-506.

Kim, Y. K., Lee, H. W., Park, J. K., & Moon, Y. S. (2002). The stratosphere–troposphere exchange of ozone and aerosols over Korea. *Atmospheric Environment, 36*(3), 449-463.

Komala, Ninong, Saraspriya, Slamet, Kita, Kazuyuki, & Ogawa, Toshihiro. (1996). Tropospheric ozone behavior observed in Indonesia. *Atmospheric Environment, 30*(10–11), 1851-1856.

Kondo, Y., Morino, Y., Takegawa, N., Koike, M., Kita, K., Miyazaki, Y., Sachse, G. W., Vay, S. A., Avery, M. A., Flocke, F., Weinheimer, A. J., Eisele, F. L., Zondlo, M. A., Weber, R. J., Singh, H. B., Chen, G., Crawford, J., Blake, D. R., Fuelberg, H. E., Clarke, A. D., Talbot, R. W., Sandholm, S. T., Browell, E. V., Streets, D. G., & Liley, B. (2004). Impacts of biomass burning in Southeast Asia on ozone and reactive nitrogen over the western Pacific in spring. *Journal of Geophysical Research: Atmospheres, 109*(D15), D15S12.

Lal, Shyam, Naja, Manish, & Subbaraya, B. H. (2000). Seasonal variations in surface ozone and its precursors over an urban site in India. *Atmospheric Environment, 34*(17), 2713-2724.

Lam, K. S., Wang, T. J., Chan, L. Y., Wang, T., & Harris, J. (2001). Flow patterns influencing the seasonal behavior of surface ozone and carbon monoxide at a coastal site near Hong Kong. *Atmospheric Environment, 35*(18), 3121-3135.

Latha, K. Madhavi, & Badarinath, K. V. S. (2004). Correlation between black carbon aerosols, carbon monoxide and tropospheric ozone over a tropical urban site. *Atmospheric Research, 71*(4), 265-274.

Latif, Mohd Talib, Huey, Lim Shun, & Juneng, Liew. (2012). Variations of surface ozone concentration across the Klang Valley, Malaysia. *Atmospheric Environment, 61*(0), 434-445.

Lawrence, M. G., & Lelieveld, J. (2010). Atmospheric pollutant outflow from southern Asia: a review. *Atmos. Chem. Phys., 10*(22), 11017-11096.

Liu, Hongyu, Jacob, Daniel J., Chan, Lo Yin, Oltmans, Samuel J., Bey, Isabelle, Yantosca, Robert M., Harris, Joyce M., Duncan, Bryan N., & Martin, Randall V. (2002). Sources of tropospheric ozone along the Asian Pacific Rim: An analysis of ozonesonde observations. *Journal of Geophysical Research: Atmospheres, 107*(D21), 4573.

Liu, S. C., & Trainer, M. (1988). Responses of the tropospheric ozone and odd hydrogen radicals to column ozone change. *Journal of Atmospheric Chemistry, 6*(3), 221-233.

Mauzerall, Denise L., Narita, Daiju, Akimoto, Hajime, Horowitz, Larry, Walters, Stacy, Hauglustaine, Didier A., & Brasseur, Guy. (2000). Seasonal characteristics of tropospheric ozone production and mixing ratios over East Asia: A global three-dimensional chemical transport model analysis. *Journal of Geophysical Research: Atmospheres, 105*(D14), 17895-17910.

Milt, Austin, Milano, Aaron, Garivait, Savitri, & Kamens, Richard. (2009). Effects of 10% biofuel substitution on ground level ozone formation in Bangkok, Thailand. *Atmospheric Environment, 43*(37), 5962-5970.

Mohnen, V.A., Chameides, W., Demerjian, K.L., Lenschow, D.H., Logan, J.A., McNeal, R.J., Penkett, S.A., Platt, U., Schurath, U., & Silva Dias, P. (1985). Chapter 4 Tropospheric chemistry: processes controlling ozone and hydroxyl radical. *Atmospheric ozone 1985*, 117 – 147.

NOAA-Air-Resources-Laboratory (Producer). (2012). Retrieved from http://www.arl.noaa.gov/documents/Summaries/Dispersion_HYSPLIT.pdf

Oltmans, S. J., Lefohn, A. S., Shadwick, D., Harris, J. M., Scheel, H. E., Galbally, I., Tarasick, D. W., Johnson, B. J., Brunke, E. G., Claude, H., Zeng, G., Nichol, S., Schmidlin, F., Davies, J., Cuevas, E., Redondas, A., Naoe, H., Nakano, T., & Kawasato, T. (2013). Recent tropospheric ozone changes – A pattern dominated by slow or no growth. *Atmospheric Environment, 67*(0), 331-351.

Oltmans, Samuel J., & Levy Ii, Hiram. (1994). Surface ozone measurements from a global network. *Atmospheric Environment, 28*(1), 9-24.

Pochanart, Pakpong, Akimoto, Hajime, Kajii, Yoshizumi, & Sukasem, Phaka. (2003). Carbon monoxide, regional-scale transport, and biomass burning in tropical continental Southeast Asia: Observations in rural Thailand. *Journal of Geophysical Research: Atmospheres, 108*(D17), 4552.

Pochanart, Pakpong, Hirokawa, Jun, Kajii, Yoshizumi, Akimoto, Hajime, & Nakao, Makoto. (1999). Influence of regional-scale anthropogenic activity in northeast Asia on seasonal variations of surface ozone and carbon monoxide observed at Oki, Japan. *Journal of Geophysical Research: Atmospheres, 104*(D3), 3621-3631.

Pochanart, Pakpong, Kreasuwun, Jiemjai, Sukasem, Phaka, Geeratithadaniyom, Werathep, Tabucanon, Monthip S., Hirokawa, Jun, Kajii, Yoshizumi, & Akimoto, Hajime. (2001). Tropical tropospheric ozone observed in Thailand. *Atmospheric Environment, 35*(15), 2657-2668.

Sikder, Helena Akhter, Suthawaree, Jeeranut, Kato, Shungo, & Kajii, Yoshizumi. (2011). Surface ozone and carbon monoxide levels observed at Oki, Japan: Regional air pollution trends in East Asia. *Journal of Environmental Management, 92*(3), 953-959.

Sillman, S. (2003). 9.11 - Tropospheric Ozone and Photochemical Smog. In H. D. Holland & K. K. Turekian (Eds.), *Treatise on Geochemistry* (pp. 407-431). Oxford: Pergamon.

Suthawaree, Jeeranut, Kato, Shungo, Takami, Akinori, Kadena, Hisayoshi, Toguchi, Mikiko, Yogi, Kazuo, Hatakeyama, Shiro, & Kajii, Yoshizumi. (2008). Observation of ozone and carbon monoxide at Cape Hedo, Japan: Seasonal variation and influence of long-range transport. *Atmospheric Environment, 42*(13), 2971-2981.

Suthawaree, Jeeranut, Tajima, Yosuke, Khunchornyakong, Alisa, Kato, Shungo, Sharp, Alice, & Kajii, Yoshizumi. (2012). Identification of volatile organic compounds in suburban Bangkok, Thailand and their potential for ozone formation. *Atmospheric Research, 104–105*(0), 245-254.

Toh, Ying Ying, Lim, Sze Fook, & von Glasow, Roland. (2013). The influence of meteorological factors and biomass burning on surface ozone concentrations at Tanah Rata, Malaysia. *Atmospheric Environment, 70*(0), 435-446.

Tsutsumi, Yukitomo, & Matsueda, Hidekazu. (2000). Relationship of ozone and CO at the summit of Mt. Fuji (35.35°N, 138.73°E, 3776 m above sea level) in summer 1997. *Atmospheric Environment, 34*(4), 553-561.

U.S.-Environmental-Protection-Agency. Health Effects of Ozone in the General Population. http://www.epa.gov/apti/ozonehealth/population.html

Volz-Thomas, A., & Mihelic, D. (1990). Ozonproduktion in Reinluftgebieten. Einfluß von Schadstoff-Konzentrationen, Gesellschaft Österreichischer Chemiker (Hrsg.), Tagungsband zum Symposium "Bodennahes Ozon" in Salzburg, Bd. 11 der Schriftenreihe "Umweltschutz".

Voulgarakis, A., Hadjinicolaou, P., & Pyle, J. A. (2011). Increases in global tropospheric ozone following an El Niño event: examining stratospheric ozone variability as a potential driver. *Atmospheric Science Letters, 12*(2), 228-232.

Wang, T., Wu, Y. Y., Cheung, T. F., & Lam, K. S. (2001). A study of surface ozone and the relation to complex wind flow in Hong Kong. *Atmospheric Environment, 35*(18), 3203-3215.

West, J. Jason, Szopa, Sophie, & Hauglustaine, Didier A. (2007). Human mortality effects of future concentrations of tropospheric ozone. *Comptes Rendus Geoscience, 339*(11–12), 775-783.

WHO. (2006). Air quality guidelines: Global update 2005: Particulate matter, ozone, nitrogen dioxide, and sulfur dioxide, 22 pp, World Health Organization, Geneva. .

Yonemura, S., Tsuruta, H., Maeda, T., Kawashima, S., Sudo, S., & Hayashi, M. (2002). Tropospheric ozone variability over Singapore from August 1996 to December 1999. *Atmospheric Environment, 36*(12), 2061-2070.

Zhang, B. N., & Kim Oanh, N. T. (2002). Photochemical smog pollution in the Bangkok Metropolitan Region of Thailand in relation to O_3 precursor concentrations and meteorological conditions. *Atmospheric Environment, 36*(26), 4211-4222.

Zhou, D., Ding, A., Mao, H., Fu, C., Wang, T., Chan, L.Y., Ding, K., Zhang, Y., Liu, J., Lu, A., & Hao, N. (2013). Impacts of the East Asian monsoon on lower tropospheric ozone over coastal South China. *Environmental Research Letters, 8*, 044011.

APPENDIX

Day	Sep-07	Oct-07	Nov-07	Dec-07	Jan-08	Feb-08	Mar-08	Apr-08	May-08	Jun-08	Jul-08	Aug-08	Sep-08	Oct-08	Nov-08	Dec-08	Jan-09	Feb-09	Mar-09	Apr-09	May-09	Jun-09	Jul-09	Aug-09
1		14.74	20.22	39.34	43.21	31.95	43.28	35.81	22.82	26.38	26.87	20.78	18.33	15.85	13.70	49.63		43.69	32.80	29.69	25.83		17.58	10.64
2		17.34	25.72	32.25	45.22	34.25	45.89	40.56	21.65	24.01	18.82	17.38	20.77	14.80	14.81	45.63		39.31	22.88	32.57	31.25		18.91	16.85
3		18.90	30.19	24.42	47.74	23.65	50.63	35.92	27.45	24.76	20.96	23.92	19.81	18.08	13.09	37.95		37.71	28.04	34.09	37.15		19.40	18.12
4		13.60	33.81	28.05	46.25	26.43	51.30	36.32	31.29	19.32	29.43	21.30	25.02	21.59	11.69	33.58		38.26	39.75	33.38	43.52		16.26	17.23
5		14.60	34.77	36.99	40.87	26.95	63.77	37.89	34.19	23.66	26.01	25.65	26.50	25.56	10.85	40.86		37.15	36.47	33.96	38.79		10.36	17.04
6	9.91	15.98	37.41	46.27	39.09	30.90	50.35	37.89	35.36	20.13	23.22	17.17	20.66	24.71	9.94	44.47		34.86	36.07	31.97	48.30		12.49	20.00
7	14.36	18.33	47.14	42.46	39.76	33.33	44.55	31.01	33.90	21.73	21.05	20.90	13.81	19.41	10.01	45.71		34.10	41.47	32.98	52.70		14.63	17.11
8	20.81	15.85	43.90	35.55	35.27	36.92	35.86	35.53	36.12	24.39	19.90	18.55	14.98	18.46	15.39	44.01		38.04	32.78	36.46	42.84	23.72	20.56	13.75
9	14.89	20.63	39.45	29.93	38.59	39.59	37.48	34.94	37.44	25.12	18.86	21.11	13.11	14.23	29.26	46.38		39.48	38.13	33.23	36.41	23.82	16.36	11.88
10	12.20	15.35	39.12	22.08	53.10	42.67	41.05	39.11	36.29	35.67	19.51	21.44	14.64	16.73	36.45	38.90		34.16	39.17	35.33	39.31	27.89	15.95	15.81
11	14.93	16.69	44.22	21.16	52.32	43.91	43.10	41.83	34.84	29.71	25.48	17.78	13.08	18.46	43.00	37.91		28.75	41.84	26.66	30.47	29.42	15.98	18.49
12	18.66	10.37	36.03	23.91	52.35	41.26	47.17	45.11	32.34	26.73	33.99	17.49	16.47	30.81	39.94	34.92	49.28	46.14	40.11	27.89	21.95	30.03	16.78	23.17
13	18.48		25.42	27.30	53.51	39.77	53.46	42.62	28.13	22.57	27.42	17.54	16.94	26.00	41.77	34.68	61.22	46.47	45.05	28.12	21.19	27.57	13.99	18.14
14	14.77		21.59	15.15	32.78	41.99	48.84	35.69	37.61	24.68	28.90	24.00	17.08	25.46	42.88	38.06	57.90	51.45	39.45	29.40	18.84	31.64	12.50	
15	17.33	30.17	22.28	12.98	36.44	43.24	45.71	37.65	31.82	22.92	26.69	22.28	14.58	22.03	33.38	51.60	60.46	58.99	42.62	28.22	18.50	31.40	14.96	14.59
16	13.05	34.83	21.76	14.28	39.85	43.90	48.04	38.74	34.07	22.26	23.47	21.93	17.39	20.11	24.29	48.99	55.76	51.79	47.82	32.86	17.44	28.13	13.63	17.02
17	14.65	36.88	20.54	16.81	35.22	42.42	50.94	41.56	39.84	21.88	24.84	18.16	14.86	34.73	24.18	46.11	44.85	44.74	49.44	32.11	19.92	14.19	15.92	16.09
18	16.62	34.99	25.46	15.57	34.79	38.34	50.19	38.01	33.48	19.23	15.68	18.62	16.37	29.80	30.54	50.50	43.54	31.59	39.33	25.18	21.07	13.34	18.04	15.25
19	18.83	38.18	40.39	15.47	35.47	39.93	47.34	48.28	39.17	18.05	14.19	19.54	18.26	26.55	42.71	50.44	40.50	36.94	42.33	28.17	19.40	9.00	18.40	14.64
20	22.52	44.92	40.96	16.73	40.21	42.97	45.97	45.14	34.61	24.87	20.33	19.86	22.51	14.89	42.74	43.94	51.86	38.71	27.96	34.77	18.07	14.01	18.32	18.52
21	40.95	49.30	43.36		45.30	43.52	46.74	45.41	29.04	28.82	28.49	23.63	17.74	12.44	37.10	31.84	48.27	39.22	32.45	37.76	25.55	20.13	15.33	26.19
22	33.46	38.77	39.24		39.58	43.66	48.30	35.49	27.60	28.73	23.64	23.53	19.07	14.03	31.95	28.60	36.88	36.22	31.37	39.74	28.29	16.61	12.95	20.64
23	32.99	28.34	44.86		37.16	38.38	42.98	38.79	26.70	28.23	19.59	26.06	18.95	15.14	28.60		44.95	35.85	34.53	41.63	22.44	12.09	15.92	18.34
24	23.01	31.38	45.43		35.95	30.30	46.23	40.32	23.35	35.07	21.34	20.29	20.93	10.28	35.99		40.00	44.25	38.38	45.49	23.61	18.30	18.73	14.67
25	32.58	30.87	47.91	30.23	33.58	32.46	43.69	39.72	25.98	33.11	27.58	23.43	19.44	11.55	38.19		34.08	39.82	29.39	45.82	26.75	21.32	19.70	15.86
26	25.95	33.72	43.34		30.57	29.87	45.04	41.70	25.48	33.38	22.05	29.43	23.13	12.60	40.99		41.33	39.89	30.31	40.21	29.19	18.49	16.51	12.57
27	18.68	36.03	45.08		29.87	29.90	38.92	47.88	32.37	29.03	25.33	29.57	26.41	9.62	45.32		36.52	42.69	28.32	39.63	28.55	19.17	14.91	12.82
28	18.20	22.46	45.50	30.11	33.51	36.40	35.38	41.34	29.73	29.23	25.54	18.41	22.95	15.32	46.12		39.41	40.82	32.72	29.70	23.93	11.85	15.42	9.32
29	16.66	18.80	42.68	30.45	33.71	42.22	37.34	34.61	22.51	27.43	22.33	17.68	18.39	16.01	46.92		50.10		43.56	36.01	25.12	12.98	12.79	10.99
30	14.98	31.81	45.74	37.21	33.72		43.69	29.36	27.07	29.59	28.85	22.77	18.58	16.55	48.38		37.40		35.94	33.04		16.16	10.97	11.36
31		29.94		40.96	34.84		33.83		25.50		23.39	22.62		13.84			38.36		34.31					11.93

Daily averages of O_3 (ppb) during September 2007 to August 2009

	Mean	hrs
Sep-07	19.98	600.0
Oct-07	26.37	694.5
Nov-07	36.45	720.0
Dec-07	27.60	585.0
Jan-08	39.67	744.0
Feb-08	36.93	696.0
Mar-08	45.39	744.0
Apr-08	39.14	720.0
May-08	30.90	744.0
Jun-08	26.02	720.0
Jul-08	23.69	739.0
Aug-08	21.38	744.0
Sep-08	18.69	720.0
Oct-08	18.89	744.0
Nov-08	31.01	720.0
Dec-08	42.06	527.0
Jan-09	45.65	478.0
Feb-09	40.40	672.0
Mar-09	36.61	744.0
Apr-09	33.87	720.0
May-09	28.88	682.0
Jun-09	20.87	516.0
Jul-09	15.85	686.0
Aug-09	15.94	711.5
Sep-09	15.31	645.0
Oct-09	14.67	683.5
Nov-09	25.78	711.0
Dec-09	32.09	744.0

Monthly averages of O_3 (ppb) and measurement hours.

Time	Sep-07	Oct-07	Nov-07	Dec-07	Jan-08	Feb-08	Mar-08	Apr-08	May-08	Jun-08	Jul-08	Aug-08	Sep-08	Oct-08	Nov-08	Dec-08	Jan-09	Feb-09	Mar-09	Apr-09	May-09	Jun-09	Jul-09	Aug-09	Dry season	Wet season	All
0:00	14.2	21.9	29.2	25.9	36.2	33.5	38.0	31.4	29.5	21.8	21.8	16.9	13.6	12.5	25.9	39.4	45.2	36.0	29.0	29.8	24.3	19.4	13.4	11.3	34.4	16.7	25.8
0:30	14.5	21.4	28.9	25.9	35.2	32.8	37.8	30.6	28.9	21.7	21.1	16.4	13.6	12.4	26.0	39.1	44.9	34.8	28.3	29.7	23.8	19.3	13.3	10.8	33.9	16.4	25.5
1:00	13.9	21.5	28.5	25.2	34.1	32.7	37.1	30.3	27.7	21.9	21.2	15.6	13.7	12.3	26.2	38.3	44.6	34.3	27.3	29.1	23.2	18.0	12.8	10.1	33.3	16.1	25.0
1:30	12.9	22.0	28.8	24.9	33.0	31.4	36.8	29.2	26.7	21.8	20.9	15.2	13.7	12.5	26.2	37.3	42.5	33.7	26.8	28.1	23.0	17.4	12.3	9.6	32.4	15.8	24.4
2:00	12.7	21.6	29.1	24.7	32.5	30.8	36.6	27.9	25.6	20.9	20.5	14.9	13.1	12.4	26.3	36.6	41.0	32.6	25.4	26.9	22.0	16.9	11.6	9.0	31.5	15.3	23.8
2:30	11.7	21.6	29.6	24.1	31.1	30.0	35.4	27.7	24.6	19.9	19.4	14.8	13.0	12.6	26.6	36.1	39.7	31.2	24.7	24.9	21.2	15.8	10.8	8.9	30.5	14.8	23.1
3:00	11.1	21.7	30.3	23.6	30.4	28.6	33.8	26.6	23.9	19.0	18.7	14.3	12.6	12.1	26.5	35.2	37.8	30.0	24.3	24.1	21.0	14.7	10.1	8.6	29.4	14.3	22.5
3:30	10.9	21.1	30.5	23.0	30.3	28.3	32.4	25.7	22.6	17.7	17.3	13.7	12.5	11.9	27.0	34.5	36.6	29.0	23.6	23.6	20.9	13.4	9.7	8.5	28.7	13.7	21.9
4:00	11.4	20.7	30.7	22.5	29.9	27.6	31.1	25.1	21.5	16.3	16.0	13.0	12.2	12.1	27.2	34.2	34.5	28.3	22.5	22.3	19.4	12.4	9.1	7.9	27.8	13.1	21.1
4:30	11.4	20.8	30.5	21.1	29.1	26.7	29.5	24.7	20.9	15.3	14.8	12.8	11.5	12.2	27.0	32.8	33.6	27.3	20.9	21.4	18.7	11.9	8.5	7.7	26.7	12.7	20.5
5:00	10.5	21.5	30.0	20.9	28.0	26.3	28.4	23.1	20.0	14.6	13.9	12.7	10.9	11.9	26.6	31.3	32.2	25.9	19.5	19.7	18.2	11.2	7.8	6.7	25.5	12.2	19.7
5:30	9.2	22.3	30.2	19.6	26.7	25.5	27.3	22.8	19.3	14.0	13.3	11.8	10.1	12.0	26.6	30.2	30.2	23.7	17.9	19.3	17.6	10.4	7.4	6.6	24.3	11.7	18.9
6:00	8.7	22.4	29.7	19.0	25.2	24.7	26.5	22.6	18.7	14.1	12.7	11.2	10.3	11.9	26.5	29.6	28.7	23.0	17.8	18.9	17.6	9.8	7.1	6.2	23.6	11.4	18.4
6:30	9.5	22.4	29.1	18.6	23.6	24.0	25.5	22.7	18.8	15.0	12.8	11.3	10.7	11.6	26.6	28.9	27.9	22.5	18.3	19.6	19.0	9.7	7.0	6.4	23.2	11.6	18.4
7:00	11.7	23.7	30.2	18.5	24.0	24.4	26.3	25.0	20.5	16.3	13.8	13.0	12.5	14.0	26.5	28.1	28.5	22.8	19.9	21.5	20.7	10.7	7.8	7.6	23.9	13.1	19.5
7:30	14.9	25.5	32.6	21.0	25.7	25.5	29.3	28.2	22.6	18.6	15.8	14.6	14.3	17.4	28.3	31.7	30.5	24.1	22.7	24.0	23.0	12.0	8.7	9.3	26.3	15.1	21.7
8:00	17.4	26.9	36.5	25.3	29.8	27.3	33.1	32.0	25.0	21.8	17.8	16.3	16.5	20.9	30.6	36.8	34.9	27.2	26.7	26.7	24.7	14.0	10.5	11.1	30.0	17.3	24.6
8:30	20.2	28.8	40.1	27.9	33.0	29.5	37.3	36.1	27.8	24.1	19.8	18.6	18.6	22.8	32.3	43.3	39.4	31.0	30.0	29.4	27.4	16.0	12.4	13.7	33.7	19.5	27.5
9:00	23.2	30.7	42.6	28.8	35.4	31.6	41.7	40.2	30.6	27.0	22.2	21.2	20.4	24.8	33.9	47.1	42.8	35.4	34.0	32.5	30.0	18.2	14.1	16.3	37.0	21.8	30.2
9:30	25.8	32.3	44.4	30.2	38.2	33.5	46.4	44.5	33.2	30.0	24.6	24.1	22.5	25.9	35.3	49.5	46.0	40.2	38.9	35.7	32.8	21.1	16.2	19.0	40.3	24.1	32.9
10:00	28.3	33.5	45.5	31.0	41.3	35.5	50.3	47.6	34.9	32.3	27.4	26.1	24.1	26.9	36.3	50.9	48.6	44.6	43.3	38.2	34.4	23.0	18.0	21.5	43.1	26.1	35.2
10:30	29.5	34.5	46.2	32.1	43.9	37.4	54.0	49.7	36.7	34.2	29.0	27.9	26.2	28.0	37.5	52.1	50.8	48.4	46.4	39.8	35.6	25.0	19.2	22.3	45.5	27.6	36.9
11:00	30.4	35.2	46.8	33.2	46.9	39.1	56.8	51.9	37.5	35.6	30.6	29.3	27.3	28.4	38.2	53.2	52.8	51.2	49.2	41.3	36.2	26.7	20.5	23.6	47.6	28.8	38.4
11:30	31.4	35.8	47.2	34.0	49.0	40.9	59.2	52.9	38.6	35.8	31.7	30.5	27.9	28.6	39.1	53.7	54.5	52.7	51.9	42.3	37.4	27.7	21.3	24.7	49.1	29.5	39.5
12:00	32.2	36.4	47.4	34.6	50.7	42.6	61.0	53.9	38.7	36.6	32.5	31.2	28.3	28.8	39.3	54.3	56.0	54.2	53.4	43.2	38.6	27.8	21.6	24.2	50.4	30.0	40.3
12:30	32.4	36.7	47.5	35.1	52.2	44.4	62.8	54.8	38.9	37.5	33.1	32.2	28.5	28.7	39.2	54.6	56.7	55.7	54.4	44.2	39.4	28.8	21.7	24.4	51.5	30.4	41.0
13:00	32.1	36.5	47.9	35.6	53.6	46.3	65.0	55.3	39.4	36.9	33.7	33.0	27.8	29.1	39.6	54.8	58.3	56.4	55.7	45.2	39.2	28.8	22.4	24.3	52.6	30.5	41.5
13:30	32.1	36.0	48.1	35.9	54.4	47.4	65.6	55.8	39.6	37.1	33.5	32.7	28.6	28.9	39.8	54.9	59.0	56.8	55.9	45.8	39.2	29.8	22.7	24.6	53.2	30.6	41.8
14:00	32.1	35.0	48.4	36.5	55.0	48.3	65.9	56.0	39.8	36.7	34.1	33.2	28.4	28.6	40.0	54.8	59.9	57.9	56.2	46.6	39.3	30.6	23.5	24.8	53.7	30.7	42.2
14:30	32.2	34.3	48.5	36.6	55.9	49.2	66.2	56.2	39.7	36.1	34.1	32.9	28.5	28.4	40.2	54.9	60.8	58.4	56.7	47.0	40.1	30.8	23.6	24.8	54.2	30.6	42.3
15:00	31.6	33.7	48.5	36.3	56.2	49.8	66.1	56.0	39.7	35.6	33.7	33.2	27.6	27.6	40.3	54.9	61.4	58.2	56.7	47.4	40.1	30.9	23.6	24.8	54.3	30.2	42.2
15:30	31.0	32.9	48.2	36.4	56.6	50.6	65.5	56.2	39.8	35.0	32.9	32.7	26.5	27.7	39.8	55.3	61.6	57.3	57.2	47.8	38.9	30.8	23.2	25.6	54.4	29.8	42.1
16:00	30.2	31.7	47.7	36.4	56.5	51.0	64.5	55.5	39.9	34.4	31.7	31.8	25.0	26.9	39.4	54.8	61.8	57.0	56.6	47.5	38.6	30.8	22.7	25.0	54.2	29.0	41.6
16:30	28.9	30.2	46.0	35.5	55.6	51.4	63.3	54.8	39.2	33.5	31.1	30.8	23.9	25.3	38.3	53.7	61.8	56.7	54.2	47.0	37.6	30.2	22.5	24.3	53.4	28.1	40.7
17:00	26.8	27.7	42.1	32.8	53.7	50.8	61.7	54.2	39.5	32.9	31.1	28.9	23.4	22.5	35.6	49.0	59.4	55.6	52.1	46.2	37.2	28.7	22.2	23.6	51.5	26.8	39.1
17:30	23.8	23.0	36.4	28.4	48.0	49.3	58.3	51.7	37.7	31.7	29.0	26.7	20.9	19.0	30.0	42.2	54.1	52.1	48.7	44.1	35.4	26.6	21.3	22.2	47.7	24.4	35.9
18:00	20.1	21.0	32.2	24.7	41.6	45.8	53.7	48.1	36.0	30.1	27.5	24.1	19.3	17.5	26.6	37.2	47.1	46.1	43.2	41.1	32.8	25.2	20.2	19.9	42.9	22.5	32.5
18:30	18.2	21.3	31.6	23.2	38.1	42.5	49.4	43.8	33.6	26.9	24.9	22.2	18.3	15.8	26.6	34.3	42.9	41.4	39.1	37.9	29.4	22.9	19.0	18.2	39.3	20.8	30.1
19:00	17.2	21.6	31.5	24.2	37.5	40.8	45.7	40.1	32.5	25.1	23.5	20.5	18.3	15.8	26.2	34.8	41.8	39.3	35.9	36.3	28.3	21.6	18.3	17.1	37.6	19.9	28.9
19:30	16.7	21.1	31.0	25.1	38.1	39.2	44.4	37.7	31.1	25.4	22.3	19.7	17.1	15.8	26.6	35.8	42.5	40.1	34.6	35.6	27.8	22.1	17.7	17.0	37.3	19.5	28.5
20:00	17.0	21.4	30.5	25.8	39.2	39.2	44.1	36.3	30.5	24.2	21.7	18.8	16.7	15.8	26.2	36.8	44.1	40.9	34.1	34.3	26.7	21.7	17.3	16.1	37.5	19.1	28.3
20:30	16.5	21.7	30.3	25.7	39.1	39.1	43.3	35.3	30.3	24.4	21.3	18.6	16.8	15.3	26.4	37.3	44.5	40.4	33.5	33.9	26.2	21.2	17.2	15.1	37.2	18.8	28.1
21:00	16.3	22.9	29.9	26.1	38.7	37.9	42.7	35.6	29.9	24.6	21.9	18.2	16.2	14.3	26.4	38.4	45.4	40.1	33.4	33.2	26.8	20.7	16.5	15.1	37.1	18.7	28.0
21:30	15.9	22.1	30.1	26.3	39.0	37.1	41.4	34.6	30.6	24.2	21.9	18.0	15.6	14.0	26.1	38.0	45.6	39.2	32.9	32.3	26.3	20.8	16.2	14.9	36.7	18.4	27.6
22:00	15.5	21.9	30.3	25.7	38.3	36.3	40.5	33.4	30.3	23.6	21.7	17.9	15.4	13.8	26.0	38.3	45.7	37.2	31.5	31.3	26.7	20.5	15.1	14.1	35.8	18.0	27.1
22:30	14.9	22.4	30.1	25.7	38.5	35.9	39.7	32.3	30.8	22.9	22.0	17.9	15.5	13.3	26.8	39.5	45.2	36.9	31.3	30.6	26.0	20.0	14.7	13.4	35.6	17.7	26.9
23:00	14.9	22.2	29.4	25.8	37.9	35.4	39.1	31.6	29.9	22.4	22.1	17.7	14.7	13.2	26.7	40.2	44.5	35.8	30.8	29.3	25.5	19.5	14.6	12.9	35.0	17.4	26.5
23:30	15.0	22.3	28.9	25.2	37.4	34.7	38.2	31.0	29.3	21.6	21.8	17.2	14.4	13.0	26.7	39.8	44.8	35.6	29.6	29.5	25.1	19.1	14.0	12.3	34.6	17.1	26.1

Half-hourly averages of O_3 (ppb) by months and seasons during September 2007 to August

	NE-C	NEE-CM	NEES-M	SW-M	Multiple	Unclassified
Jan	65	18	11	0	0	6
Feb	51	12	25	0	0	12
Mar	21	6	65	0	0	8
Apr	5	10	62	20	2	2
May	3	3	12	75	6	0
Jun	0	0	0	100	0	0
Jul	0	0	0	100	0	0
Aug	0	0	2	93	0	5
Sep	13	0	10	73	2	3
Oct	23	18	23	29	3	3
Nov	48	20	18	3	0	10
Dec	38	8	28	0	0	25
Annual	22	8	21	41	1	6

Monthly and annual averages frequencies by air mass types.

	NE-C		NEE-CM		NEES-M		SW-M	
	Average	SD	Average	SD	Average	SD	Average	SD
Jan	43.1	12.9	38.0	16.0	40.8	13.9		
Feb	38.3	10.3	31.6	10.8	38.4	15.6		
Mar	44.8	13.6	46.2	14.7	40.1	17.3		
Apr	41.4	14.7	33.6	10.6	36.9	13.8	36.7	12.9
May					26.8	16.1	29.3	10.5
Jun							23.9	10.7
Jul							19.9	9.0
Aug							19.2	9.4
Sep	32.5	16.2			16.2	9.2	18.3	8.7
Oct	30.1	13.1	28.0	11.3	18.3	10.7	16.5	8.3
Nov	38.1	11.7	35.8	12.2	21.6	13.8		
Dec	41.6	11.4	36.6	12.6	21.4	10.2		

Monthly averages of O_3 (ppb) and standard deviations by air mass types.

	NE-C		NEE-CM		NEES-M		SW-M	
	Average	SD	Average	SD	Average	SD	Average	SD
0:00	34.9	10.2	29.3	9.9	26.2	11.3	18.9	9.0
0:30	34.7	10.2	29.3	9.8	25.6	10.9	18.5	8.9
1:00	34.3	10.2	29.0	9.6	25.0	10.9	18.0	8.8
1:30	34.2	10.3	28.3	9.0	24.3	10.5	17.5	8.8
2:00	34.1	10.2	27.9	9.7	23.4	10.1	16.7	8.6
2:30	33.4	10.3	27.4	9.5	22.7	9.8	16.1	8.3
3:00	32.6	10.6	27.1	9.5	21.8	9.4	15.4	8.1
3:30	32.2	10.5	26.9	9.3	21.1	8.8	14.7	7.5
4:00	31.8	10.3	26.7	9.3	20.4	8.9	13.8	6.9
4:30	31.3	10.4	26.3	9.1	19.6	8.5	13.1	6.5
5:00	30.7	10.3	25.8	8.9	18.7	8.1	12.3	6.3
5:30	29.9	10.2	24.7	9.2	17.9	8.3	11.7	5.9
6:00	29.3	10.1	23.7	9.4	17.6	8.6	11.4	5.6
6:30	28.3	10.6	23.7	9.4	17.7	8.5	11.7	5.5
7:00	28.7	9.8	24.8	8.8	19.3	8.5	13.1	5.5
7:30	30.9	9.6	26.6	8.6	22.1	8.7	15.0	6.0
8:00	34.5	9.5	29.9	9.3	25.1	9.1	17.1	6.5
8:30	37.7	10.0	33.2	10.1	28.2	10.1	19.4	7.1
9:00	40.0	10.4	35.9	10.8	31.6	11.4	21.9	7.9
9:30	42.0	10.5	38.0	11.0	35.3	13.1	24.5	8.5
10:00	43.5	10.6	40.0	11.4	38.4	14.7	26.8	9.1
10:30	44.8	10.6	41.6	11.3	40.9	15.9	28.4	9.4
11:00	46.1	10.6	42.8	11.8	43.1	16.6	29.7	9.6
11:30	47.5	10.5	44.0	11.8	44.4	17.2	30.7	9.6
12:00	48.6	10.5	44.9	12.1	45.5	17.4	31.1	9.7
12:30	49.5	10.4	45.7	12.4	46.4	17.7	31.6	9.8
13:00	50.4	10.4	46.6	12.7	47.4	18.1	31.7	9.8
13:30	50.9	10.5	46.9	12.7	47.8	17.9	31.9	9.8
14:00	51.5	10.4	47.2	12.8	48.1	18.2	32.1	9.5
14:30	51.9	10.6	47.6	13.2	48.2	18.3	32.2	9.8
15:00	52.2	10.7	47.5	13.5	47.9	18.5	32.0	9.9
15:30	52.4	10.7	47.3	13.9	47.8	18.3	31.5	10.1
16:00	52.1	10.8	47.1	13.9	47.1	18.2	30.8	10.1
16:30	51.5	10.9	46.3	13.8	46.0	18.0	30.0	10.2
17:00	49.3	11.0	44.3	13.4	44.2	18.0	29.2	10.3
17:30	44.6	11.7	41.0	12.6	40.5	17.9	27.4	10.2
18:00	39.7	11.8	36.8	12.1	36.5	16.5	25.6	10.0
18:30	36.9	11.1	34.1	10.5	33.5	15.0	23.5	9.3
19:00	35.7	10.1	33.2	9.9	31.6	13.6	22.5	9.1
19:30	35.6	9.8	33.1	10.9	30.7	12.8	22.0	8.7
20:00	36.0	9.8	33.3	11.2	30.1	12.7	21.3	8.5
20:30	36.1	10.0	33.4	10.8	29.3	12.7	21.0	8.5
21:00	36.1	10.1	33.2	11.2	29.1	12.2	20.9	8.6
21:30	35.6	10.2	33.4	11.7	28.6	11.8	20.6	8.9
22:00	35.5	10.1	32.6	11.1	27.8	11.6	20.2	9.0
22:30	35.6	10.1	32.0	11.3	27.5	11.8	19.9	9.1
23:00	35.2	10.0	31.3	10.6	27.2	11.7	19.4	8.8
23:30	34.8	10.2	31.2	10.4	26.7	11.3	18.9	8.9

Half-hourly averages and standard deviations of O_3 (ppb) by air mass types

VITA

Mr. Supattarachai Saksakulkrai was born in Bangkok, Thailand on 9 February 1988. In 2010 he received a Bachelor of Science degree in Marine science (Oceanography), Department of Marine science, Faculty of Science, Chulalongkorn University. After then he entered the Earth Sciences program, Department of Geology, Faculty of Science, Chulalongkorn University for a Master of Science degree.